Adiabatic quantum computing from an eigenvalue dynamics point of view

by Richard D. Wilson

A Doctoral Thesis submitted in partial fulfillment of the requirements
for the award of
Doctor of Philosophy
of
Loughborough University

July 2011

Abstract

We investigate the effects of a generic noise source on a prototypical adiabatic quantum algorithm. We take an alternative eigenvalue dynamics viewpoint and derive a generalised, stochastic form of the Pechukas-Yukawa model. The distribution of avoided crossings in the energy spectra is then analysed in order to estimate the probability of level occupation.

We find that the probability of successfully finding the system in the solution state decreases polynomially with the computation speed and that this relationship is independent of the noise amplitude. The overall regularity of the eigenvalue dynamics is shown to be relatively unaffected by noise perturbations. These results imply that adiabatic quantum computation is a relatively stable process and possesses a degree of resistance against the effects of noise. We also show that generic noise will inherently break any symmetries, and therefore remove degeneracies, in the energy spectrum that might otherwise have impeded the computation process. This suggests that the conventional stipulation that the initial and final Hamiltonians do not commute is unnecessary in realistic physical systems. We explore the effects of an artificial noise source with a specifically engineered time-dependent amplitude and show that such a scheme could provide a significant enhancement to the performance of the computation.

Finally, we formulate an extended version of the Pechukas-Yukawa formalism. This provides a complete description of the dynamics of a quantum system by way of an exact mapping to a system of classical equations of motion.

Contents

List of Figures

Acknowledgements

I would like to sincerely thank my supervisors; Dr Alexandre Zagoskin and Dr Sergey Savel'ev, for their support and guidance over the course of my PhD, it has been invaluable. I would also like to thank my friends and family for their continual support and encouragement along the way. Finally, I would like to thank Loughborough University for my studentship and support for various conferences.

Chapter 1

Introduction

> "And therefore, the problem is, how can we simulate the quantum mechanics? There are two ways that we can go about it. We can give up on our rule about what the computer was, we can say: Let the computer itself be built of quantum mechanical elements which obey quantum mechanical laws. Or we can turn the other way and say: Let the computer still be the same kind that we thought of before–a logical, universal automaton; can we imitate this situation?" - R.P. Feynman [1]

Interest and research in the field of quantum engineering has steadily grown over recent years. This is because it offers a direct opportunity to experiment with and even utilise the very phenomena that differentiate the quantum mechanical picture of the universe from that of the classical one.

Quantum computing is one area of quantum engineering in particular that has received a lot of attention since the discoveries of Shor's factoring algorithm [2], and Grover's search algorithm [3] during the 1990's. Both of these algorithms demonstrate the power of harnessing explicitly quantum mechanical processes to perform a computational process. This allows them to perform in a more efficient manner than is possible using classical resources. The idea of storing and processing information quantum mechanically was first proposed by Feynman in 1981, [1], while discussing the problems of simulating physics with computers. Simulating quantum mechanical systems on a classical computer is a computationally demanding task as the number of dimensions of the phase space needed to describe the state of the quantum system scales exponentially with its size. Hence, Feynman proposed the idea of building a computer that works and stores information on a quantum mechanical level so it can inherently work with the high dimensional phase spaces needed to describe these quantum systems. The concept of a quantum computer was later solidified by Deutsch in 1985 [4] when he defined a quantum generalisation of the classical uni-

versal Turing machine. Deutsch, in conjunction with Jozsa, then went on to develop one of the first quantum algorithms that could be shown to be exponentially faster than any possible classical deterministic counterpart [5]. Although the Deutsch-Jozsa algorithm is of little practical use, it paved the way for further research in to whether quantum mechanical information processing techniques could be used to solve other computational problems. The discovery of Shor's aforementioned factoring algorithm [2], which offers an exponential speedup in time over its classical counterparts, and Grover's search [3], which offers a polynomial speedup, showed that quantum computing could offer significant improvements in computational efficiency for practical real world problems. Since then a number of other quantum algorithms have been discovered for a wide variety of different problems (an up to date list of which can be found at http://www.its.caltech.edu/ sjordan/zoo.html).

The standard paradigm of quantum computing that has developed over recent years is analogous to a classical digital computer, as a register of qubits (quantum bits) are manipulated using a universal set of quantum logic gates. However, this approach requires a delicate balance between attempting to isolate the system from its environment but at the same time maintaining precise control over individual qubits, which unfortunately appears as though it may not be experimentally achievable in the near future. In light of this realisation a number of alternative approaches have been proposed; one of which is adiabatic quantum computing (AQC) [6]. AQC involves slow adiabatic evolution from a configuration with an easily reachable ground state to one where the ground state encodes the solution to the problem in hand. In this scheme precise time-dependent control of individual qubits is no longer required and it benefits from an inherent robustness against some of the effects of decoherence by remaining in the instantaneous ground state at all times [7, 8, 9]. Crucially, it has also been shown to be polynomially equivalent to the standard gate model of quantum computing in [10, 11]. There have also been some results that suggest that noise may actually have some positive effects on an AQC process, which is an interesting and counter-intuitive prospect [7, 12].

In this thesis we aim to further explore the role and effects of noise in the paradigm of adiabatic quantum computing. This is clearly an important consideration as all realistic physical systems will be subject to some form of noise. To do this we will make use of a novel eigenvalue dynamics based approach. It is felt that this approach is worth exploring as it offers an alternative viewpoint to the standard Schrödinger picture which may provide some extra insight.

1.1 Thesis overview

The remainder of this chapter will be devoted to a review of the field of AQC and some theoretical tools that will be of use in the following chapters. In chapter 2, we derive a generalised form of the Pechukas-Yukawa model of eigenvalue dynamics that incorporates a generic noise model. Appropriate numerical methods for solving this system of equations are also discussed.

In chapter 3, we derive the problem Hamiltonian for the adiabatic equivalent of the CNOT gate as an example of a prototypical quantum algorithm. Then in the following chapters 4, 5 and 6, we go on to explore how the presence of noise affects the properties and performance of this example algorithm. In chapter 4, we study the energy spectra of the CNOT gate and look at the effects of noise on its statistical properties. We investigate the effects of noise on the statistics of level occupation and the success rate of the CNOT algorithm in chapter 5. Based on the previous results, in chapter 6 we envision a system where a specifically engineered noise signal is used to enhance the performance of our prototypical quantum algorithm.

Also, in chapter 7, we derive a novel extended version of the Pechukas-Yukawa model that provides a complete description of the dynamics of the quantum system.

Then in chapter 8 we draw together our results and make some final conclusions, as well as proposing a number of possible directions in which this work could be taken in the future.

1.2 Quantum information processing devices

1.2.1 Basic postulates and notation

In this section we will briefly review the basic postulates of quantum mechanics, mainly as a way of codifying the notation used throughout this thesis. The four basic postulates of quantum mechanics that can be used to describe any closed system are as follows;

1. **State:** The state of any closed quantum system at a particular point in time is completely described by the state vector, $|\psi(t)\rangle$, which is a unit vector in the Hilbert space associated with the system's degrees of freedom.

2. **Evolution:** The evolution of a closed quantum system is described by a unitary transformation, *i.e.* the state $|\psi(t_1)\rangle$ is related to the state $|\psi'(t_2)\rangle$ by $|\psi'(t_2)\rangle = U(t_1, t_2)|\psi(t_1)\rangle$, where $U(t_1, t_2)$ is a unitary operator (*i.e.* one that obeys $UU^\dagger = U^\dagger U = I$) that depends only on the times t_1 and t_2. In

terms of continuous time, the unitary evolution of a closed quantum system is generated by the Schrödinger equation

$$i\hbar\frac{d}{dt}\left|\psi(t)\right\rangle = \mathcal{H}(t)\left|\psi(t)\right\rangle, \tag{1.2.1}$$

where $\hbar$ is Planck's constant (taken as 1 from herein) and $\mathcal{H}(t)$ is the Hermitian operator (*i.e.* one that obeys $H = H^\dagger$)known as the Hamiltonian.

3. **Measurement:** Quantum measurements are described by a set of measurement operators, $\{\mathrm{M}_m\}$, that act on the state space of the system and satisfy the completeness relation $\sum_m \mathrm{M}_m^\dagger \mathrm{M}_m = 1$. If a measurement is performed on a system in state $|\psi(t)\rangle$, then the probability of result m occurring is given by

$$p(m) = \left\langle\psi(t)\right| \mathrm{M}_m^\dagger \mathrm{M}_m \left|\psi(t)\right\rangle \tag{1.2.2}$$

and after the measurement the state of the system "collapses" to

$$\frac{\mathrm{M}_m\left|\psi(t)\right\rangle}{\sqrt{\left\langle\psi(t)\right| \mathrm{M}_m^\dagger \mathrm{M}_m \left|\psi(t)\right\rangle}}. \tag{1.2.3}$$

4. **Composite systems:** Composite systems, made up of a number (n) of distinct physical systems, have a state space that is the tensor product of the state spaces of the constituent subsystems. A composite system is said to be in a product or separable state if its state be constructed from the tensor product of the subsystem's states, *i.e.*$|\psi_1(t)\rangle \otimes |\psi_2(t)\rangle \ldots |\psi_n(t)\rangle$. Whereas an entangled state is defined as one where the overall state of composite system cannot be described in terms of single qubit states.

The Hamiltonian operator, $\mathcal{H}(t)$, of a system is crucial, as if we have knowledge of this, then we can completely describe the dynamics of the system. In terms of this thesis, an important point to note is that because the Hamiltonian is a Hermitian operator it will have an instantaneous spectral decomposition of the form

$$\mathcal{H}(t) = \sum_n x_n(t)\left|n(t)\right\rangle\left\langle n(t)\right|, \tag{1.2.4}$$

where the $x_n(t)$ are the instantaneous eigenvalues describing the energy levels of the system at time t, and the $|n(t)\rangle$ are their corresponding normalised eigenvectors, known as the eigenstates. The collection of all n eigenstates forms the instantaneous energy eigenbasis of the Hamiltonian at time t. These energy levels and eigenstates

satisfy the following instantaneous eigenvalue equation;

$$\mathcal{H}(t)\left|n(t)\right\rangle = x_n(t)\left|n(t)\right\rangle, \tag{1.2.5}$$

which is simply the time-independent version of the Schrödinger equation.

In some situations it is often more convenient to work with the density matrix, or density operator, instead of the state vector. This is defined as

$$\rho = \sum_i p_i \left|i\right\rangle \left\langle i\right|, \tag{1.2.6}$$

where p_i is the probability of the system being found in a given pure state $|i\rangle$. This alternative formulation is particularly suited to dealing with statistical mixtures of states and is often used when dealing with dissipation and composite systems. The equation of motion for the density matrix is the Von Neumann equation,

$$i\hbar\frac{d}{dt}\rho(t) = \left[\mathcal{H}(t), \rho(t)\right]. \tag{1.2.7}$$

The density matrix formulation will be of particular use in chapter 7.

1.2.2 Quantum computing

In [4], Deutsch showed that the Church-Turing principle,

> "Every finitely realisable physical system can be perfectly simulated by a universal model computing machine operating by finite means".

(restated in a more physical way), is compatible with quantum mechanics and that any real (dissipative) finite system can be simulated by a universal quantum computer. As mentioned in section 1, he then went on to describe the first universal model of quantum computation, essentially a quantum generalisation of a Turing machine [13]. Unfortunately, like the Turing machine before it, this model of universal quantum computation proved unwieldy in practical situations. An equivalent model more akin to classical digital computation, where logic gates are applied to a register of quantum bits (qubits), was then developed. This is commonly known as the quantum circuit or gate model. In [14], DiVincenzo proposed a set of five requirements for a physical implementation of a gate model quantum computer. These criteria allow us to completely describe the operation of a gate model quantum computer;

1. *A scalable physical system with well characterized qubits*

2. *The ability to initialize the state of the qubits to a simple fiducial state, such as* $|0000...0\rangle$

3. *Long relevant decoherence times, much longer than the gate operation time*

4. *A "universal" set of quantum gates*

5. *A qubit-specific measurement capability*

The first DiVincenzo criterion calls for scalable, well characterised qubits. As a qubit is the quantum analogue of a bit, it is simply a two-level quantum system. The 0 and 1 states of a classical bit correspond to the computational basis states of a qubit,

$$|0\rangle = \begin{pmatrix} 1 \\ 0 \end{pmatrix} \text{ and } |1\rangle = \begin{pmatrix} 0 \\ 1 \end{pmatrix}, \tag{1.2.8}$$

therefore a qubit in an arbitrary state can be described by

$$|\psi\rangle = \alpha\,|0\rangle + \beta\,|1\rangle = \begin{pmatrix} \alpha \\ \beta \end{pmatrix} \text{ where } \langle\psi|\psi\rangle = |\alpha|^2 + |\beta|^2 = 1. \tag{1.2.9}$$

In the density matrix formulation, the state of a qubit can be expressed as follows;

$$\rho = \frac{I + r \cdot \sigma}{2}, \tag{1.2.10}$$

where $r = (x, y, z)$ is the Bloch vector which describes a point in the Bloch sphere and $\sigma = (\sigma_x, \sigma_y, \sigma_z)$ is a vector of the Pauli matrices;

$$\sigma_x = \begin{pmatrix} 0 & 1 \\ 1 & 0 \end{pmatrix}, \ \sigma_y = \begin{pmatrix} 0 & -i \\ i & 0 \end{pmatrix}, \ \sigma_z = \begin{pmatrix} 1 & 0 \\ 0 & -1 \end{pmatrix}. \tag{1.2.11}$$

The Bloch sphere is a unit sphere which provides a convenient geometrical representation of a qubit's state space. The Bloch vector of pure states will lie on the surface of the sphere, whereas the points representing mixed states will fall within it. There are a number of different candidates for physical realisations of qubits, e.g. single electrons, trapped ions, superconducting circuits and laser polarisation, these will be discussed in more detail in section 1.2.3.5.

The fourth criterion asks for a "universal" set of quantum gates, this is a set of gates with which any arbitrary quantum operation can be reproduced. A simple example of which would be the set of the Hadamard gate, the $\pi/8$ phase rotation

gate and the CNOT gate;

$$\text{HAD} = \frac{1}{\sqrt{2}}\begin{pmatrix}1 & 1\\ 1 & -1\end{pmatrix},\ \text{ROT} = \begin{pmatrix}1 & 0\\ 0 & e^{\frac{\pi}{4}i}\end{pmatrix}\ \text{and}\ \text{CNOT} = \begin{pmatrix}1 & 0 & 0 & 0\\ 0 & 1 & 0 & 0\\ 0 & 0 & 0 & 1\\ 0 & 0 & 1 & 0\end{pmatrix}, \tag{1.2.12}$$

a finite combination of these 3 gates can be used to construct any possible quantum circuit to any desired accuracy [15].

The third DiVincenzo criterion is generally considered to be the most difficult to meet experimentally. It involves finding a type of qubit that is sufficiently well isolated from noise sources in its environment to remain quantum coherent but is still readily controllable. This is a very difficult compromise to meet as all five DiVincenzo criteria must be kept in mind. Error-correcting codes could be used to protect the information stored in the register against the effects of decoherence by storing a single logical qubit across a number of physical qubits. They therefore require significantly larger physical systems, but simply adding more qubits requires more control lines and adds more potential noise sources, which in turn means more sophsticated error-correcting codes that require even more qubits. This leads to another difficult compromise that has to be met experimentally to find a system that satisfies all five of the DiVincenzo criteria.

The DiVincenzo criteria give us an excellent framework to use when considering potential realisations of a gate model quantum computer. They also serve to highlight the important balance between decoherence and controllability that must be met to build this type of device. In light of the difficulties of finding this balance, a number of alternatives to the gate model of quantum computation are being explored. Adiabatic quantum computing is a promising alternative paradigm to the gate model. It has been shown to be computationally equivalent to the gate model and also avoids some of the difficult experimental compromises that need to be met to build a gate model quantum computer.

1.2.3 Adiabatic quantum computing

1.2.3.1 Basic principles

AQC was first proposed as a method of solving the n-SAT satisfiability problem by Farhi *et al.* in [6]. In AQC an n-qubit quantum system (2^n dimensional Hilbert space) is prepared in an initial configuration with an easily reachable, non-degenerate ground state. The system is put in to the ground state of the initial configuration

(H_i) and then over time it evolves into a final configuration (H_f) that encodes the problem to be solved. The quantum adiabatic theorem states that if a Hamiltonian varies slowly the probability to excite the system out of its original state will be approximately equal to 0 [16]. Therefore, provided the evolution time (T) is long enough the quantum computer will remain in the instantaneous ground state at all times. The ground state at the end of the computation (at $t = T$) encodes the solution to the problem at hand and can then be read out. A diagram explaining this method is shown in Fig. 1.2.1.

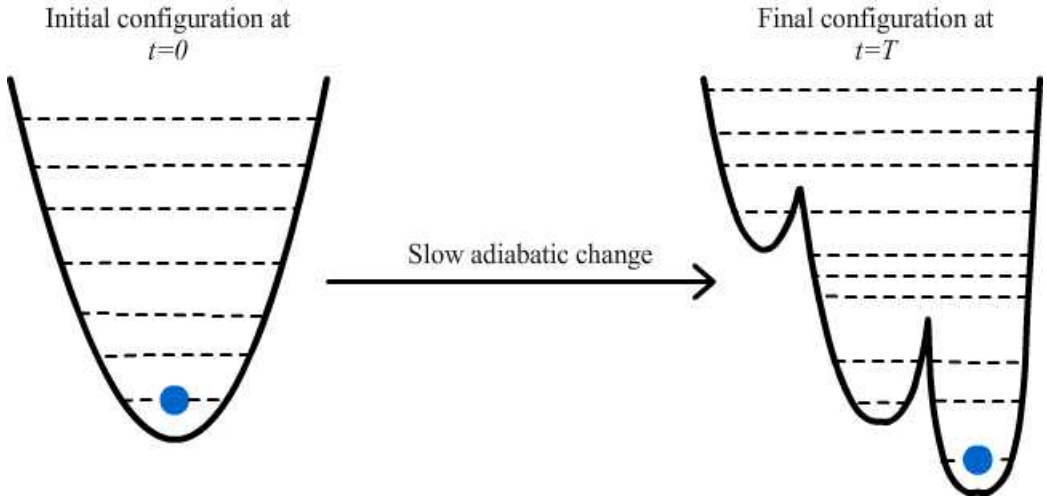

Figure 1.2.1: Schematic diagram of a generic adiabatic quantum computation where the system is prepared in the ground state of the initial Hamiltonian (H_i) and then evolves adiabatically slowly to a final Hamiltonian (H_f) that encodes the problem.

In the original paper by Farhi *et al.* in [6] they take the evolution of the system to be a smooth linear interpolation from H_i at time $t = 0$ to H_f at time $t = T$ at a rate of T^{-1};

$$\mathcal{H}(t) = \left(1 - \frac{t}{T}\right) H_i + \left(\frac{t}{T}\right) H_f. \tag{1.2.13}$$

The H_i and H_f are usually chosen such that they do not commute (*i.e.* $[H_i, H_f] \neq 0$), this is to avoid degeneracies that may obstruct the computation in a closed system. If we assume that the system is initially prepared in the ground state (*i.e.* $|\psi(0)\rangle = |0(t = 0)\rangle$) and that the ground state energy gap is finite throughout the computation (*i.e.* $x_1(t) - x_0(t) > 0$ for $0 \leq t \leq T$), the quantum adiabatic theorem can be defined as

$$\lim_{T\to\infty} P(n = 0; t = T | n = 0; t = 0) = \lim_{T\to\infty} |\langle 0(t = T)|\psi(T)\rangle|^2 = 1. \tag{1.2.14}$$

In the context of AQC $P(n = 0; t = T | n = 0; t = 0)$ is known as the success probability as it denotes the probability of the system being found in the eigenstate

that encodes the result of the algorithm at the end of the computation time. This implies that in practice if T is sufficiently long enough the probability of the system being excited out of the ground state is arbitrarily small, *i.e.* $P(n > 0; t = T | n = 0; t = 0) \ll 1$ and the condition for the validity of this statement can be shown to be

$$T \gg \frac{\alpha}{\Delta_{01}^2} \tag{1.2.15}$$

where

$$\alpha = \max_{0 \leq t \leq T} \left| \langle n = 1; t | \frac{d}{dt} \mathcal{H}(t) | n = 0; t \rangle \right| \text{ and } \Delta_{01} = \min_{0 \leq t \leq T} \left(x_1(t) - x_0(t) \right). \tag{1.2.16}$$

We expect the magnitude of the maximum matrix element of the change of $\mathcal{H}(t)$ during T (α) to be of the order of a typical eigenvalue. Thus, we expect the minimum ground state energy gap (Δ_{01}) to be the determining factor of the length of the computation time (T).

The DiVincenzo criteria set out in section 1.2.2 can be used to compare the adiabatic quantum computing paradigm to the standard gate model. Decoherence (the effects of a system's coupling to its environment) is a major issue in all physical realizations of quantum information processing systems. In the standard gate model of quantum computing, error correcting codes are used to fight the effects of decoherence by encoding a fault tolerant logical qubit into a number of noisy physical qubits, therefore a significant number of physical qubits will be necessary to perform computations involving only a few qubits of information. This affects the scalability of the system required by the first DiVincenzo criteria . However, AQC has an inherent robustness against the effects of decoherence and it is believed that error correcting schemes will not be necessary, therefore relatively few physical qubits will be needed to perform useful computations. The effects of noise and decoherence on AQC will be discussed in greater detail in section 1.2.3.4 and then throughout the rest of this work.

To fulfil the second, fourth and fifth DiVincenzo criteria, the precise control and measurement capability of individual qubits is required. To achieve this level of control experimentally it would require the use of a large number of external control lines which would be a major source of noise. However, in AQC we only require global control and measurement capability over the system which should limit the number of control lines, and therefore potential sources of decoherence, needed in physical realisations.

The fourth DiVincenzo criterion asks for a "universal" set of quantum logic gates; a universal set of gates is one that can be used to simulate any other combination

of gates and in principle allow any possible algorithm to be implemented on the computer. It has been proven that AQC is a universal model of computation as any universal quantum circuit can be encoded into an adiabatic quantum algorithm with at worst a polynomial time complexity overhead (as detailed in section 1.2.3.2).

1.2.3.2 Algorithms

Adiabatic quantum computing was first proposed as a method of solving the boolean satisfiability, or **SAT**, problem in [6]. In an n bit system an instance of the k-**SAT** problem is specified by a Boolean formula of the form

$$C_1 \wedge C_2 \wedge \ldots \wedge C_M, \tag{1.2.17}$$

where the Boolean clauses C_a are either True or False depending on the values of a subset of k bits. Solving the **SAT** problem involves testing all 2^n possible assignment combinations; which in the limit of large n, generally becomes intractable on a classical computer. Problems whose solution space grows exponentially with input size are usually hard to deal with on a classical computer as each potential solution has to be checked individually. These appear to be one of the main potential areas of application for quantum computing. Quantum computing aims to exploit quantum mechanical phenomenon to try to solve these types of problem in a more efficient manner than is possible classically; the superposition principle is particularly important when dealing with these types of problem as it allows the quantum computer to operate on the entire solution space.

To recast the k-**SAT** problem instance into the form of an adiabatic quantum algorithm, for each of the clauses we define a corresponding "energy" function (h_{C_a}) that applies an energy cost to any binary combination that satisfies it,e.g.

$$h_{C_a} = \begin{cases} 0, & \text{for any binary combination which satisfies clause } C_a \\ 1, & \text{for any binary combination which violates clause } C_a \end{cases} \tag{1.2.18}$$

and an associated operator (H_{C_a}) of the form

$$H_{C_a} |\psi\rangle = h_{C_a} |\psi\rangle \tag{1.2.19}$$

where $|\psi\rangle$ are the computational basis states of the n qubit system. The operator H_{C_a} only depends on the clause C_a and only acts on the subset of k qubits related to that clause. The problem Hamiltonian is therefore of the form

$$H_{k-\mathbf{SAT}} = H_{C_1} + H_{C_2} + \ldots + H_{C_M}. \tag{1.2.20}$$

The ground state of $H_{k-\mathbf{SAT}}$ encodes the binary combinations that minimise the total "energy" and therefore satisfy all of the clauses if the problem instance is solvable (*i.e.* the "energy" cost of the resulting combinations are zero).

The **SAT** problem is a type of combinatorial search problem, *i.e.* it involves finding the combinations of a discrete set of items that meet a set of specified requirements. AQC is particularly suited to solving problems of a combinatorial nature (search or optimisation) as a lot of them can be written in the form of an "energy" cost function that requires minimisation and hence recast as an adiabatic quantum algorithm using the method described above, e.g. MAXCUT, Exact Cover, The Traveling Salesman , Max Independent Set, n-queens, etc..

The **SAT** problem is often studied in the literature as a prototypical example of the type of problem that AQC will be applied to (e.g. as in [17, 18]). It belongs to the complexity class **NP-complete**, as do a number of the other combinatorial search and optimization problems mentioned above. **NP** problems are a class of problems whose solutions can be verified, but not necessarily calculated, efficiently in a time that scales polynomially with the input size. An **NP** problem belongs to the subset **NP-complete** if any other **NP** problem can be efficiently recast into the form of that problem, *i.e.* if that problem can be solved efficiently therefore so can any other **NP** problem. The question as to whether **NP-complete** problems can be solved efficiently using AQC is an open one and it is one of the main reasons that these types of problems are studied. In their original paper on AQC, Farhi *et al.* showed that certain "easy" instances of the **SAT** problem could be solved efficiently using AQC. Then in [19] Van Dam *et al.* then demonstrated that a family of "hard" search problems with a time complexity lower bound that scales exponentially with system size for AQC can be constructed. However, Farhi *et al.* subsequently showed that the exponential lower bound "hard" search problems could be overcome by choosing an alternate interpolation path between H_i and H_f in [20]. A recent paper, [21], conjectures that adiabatic quantum computing will fail to solve random instances of **NP-complete** problems because of the appearance of an exponentially small ground state energy gap (Δ_{min}) towards the end of the evolution. However, they estimate that this exponentially small gap only appears as the system size exceeds the bound of $n \gtrsim 86000$ qubits and a more recent paper, [22], shows analytically that there will always be an adiabatic path along which no such exponentially small gaps occur for another example of an **NP-hard** optimisation problem.

Two of the most famous quantum algorithms are Grover's search ([3]) and Shor's factoring algorithm ([2]) for the gate model. Shor's algorithm can be used to find the prime factors of a given N-bit integer in a time that scales $O((\log N)^3)$, which is exponentially faster than the best classical algorithm. A factoring algorithm for

adiabatic quantum computers was proposed in [23] and implemented experimentally with an NMR system to find the prime factors of 21. The adiabatic factoring algorithm described in [23] requires fewer qubits to factor an integer of a given length than Shor's algorithm. Numerical results appear to show that it also scales in polynomial time, however this has not been verified analytically like it has for Shor's algorithm. Grover's search algorithm allows a given item in an unstructured database of N items to be found in a time that scales proportionally to $O\left(\sqrt{N}\right)$, whereas a classical search would on average take a time that scales $O(N)$. An adiabatic version of Grover's algorithm was proposed in [6], however it was found to offer no advantage over a classical search when using AQC with a basic linear interpolation scheme (*i.e.* (1.2.13)). In [24], Roland and Cerf show that by locally adjusting the evolution rate to make sure adiabatic theorem is met for an infinitesimal time interval the polynomial speedup of Grover's search can be recovered for the adiabatic version. They then explored the use of the adiabatic quantum search further in [25] by showing that the nesting of one quantum search within another allows searches of structured databases to be performed in a manner more efficient than is possible classically.

The equivalence of adiabatic quantum computing and the gate model was first shown in 2004 by Aharonov *et al.*in [10], where they demonstrated that any quantum circuit can be efficiently simulated (*i.e.* with at worst a polynomial overhead) by an adiabatic quantum computer. A more intuitive proof of the equivalence of AQC and the cicuit model was then presented in [11] by Mizel, Lidar and Mitchell using an approach known as "ground state quantum computing" (GSQC).

1.2.3.3 The GSQC method

The GSQC method allows an arbitrary quantum circuit with N steps involving M qubits to be encoded into the form of a problem Hamiltonian suitable for AQC. In this method each of the M qubits in the circuit is pictured as a single electron that can occupy the states in an array of $2 \times (N+1)$ quantum dots; where the rows in the array represents either the $|0\rangle$ or $|1\rangle$ states of the qubit. The state of the mth qubit during the nth step of the algorithm is given by the probability amplitude of the electron being found on the quantum dots denoted by the indices $(m, n, 0)$ and $(m, n, 1)$. They then define fermionic creation (annihilation) operators, $c^{\dagger}_{mn0}$ (c_{mn0}) or $c^{\dagger}_{mn1}$ (c_{mn1}), that create (annihilate) an electron in the relevant dot. These operators can be used to construct the (unnormalised) ground state that contains

the results of the algorithm, for a single qubit ($m = 0$) we have

$$\left|\psi^N\right\rangle = \left(C_{00}^\dagger \begin{bmatrix} 1 \\ 0 \end{bmatrix} + C_{01}^\dagger U_{01} \begin{bmatrix} 1 \\ 0 \end{bmatrix} + \ldots + C_{0N}^\dagger U_{0N} \ldots U_{01} \begin{bmatrix} 1 \\ 0 \end{bmatrix} \right) |vac\rangle \,, \tag{1.2.21}$$

where the creation operators are grouped into the row vectors $C_{mn}^\dagger = \left[c_{mn0}^\dagger, c_{mn1}^\dagger\right]$, U_{mn} is the 2×2 unitary matrix that describes the n^{th} step of the algorithm acting on the m^{th} qubit and $|vac\rangle$ is the vacuum state. This ground state can also be constructed recursively in terms of the different steps of the algorithm,

$$\left|\psi^j\right\rangle = \left(1 + C_{0j}^\dagger U_{0j} C_{0(j-1)}\right) \left|\psi^{j-1}\right\rangle, \tag{1.2.22}$$

where $|\psi^0\rangle = C_{00}^\dagger |vac\rangle$. The state (1.2.22) can be easily generalised for the case of M non-interacting qubits,

$$\left|\psi^j\right\rangle = \prod_{i=0}^{M} \left(1 + C_{ij}^\dagger U_{ij} C_{i(j-1)}\right) \left|\psi^{j-1}\right\rangle, \tag{1.2.23}$$

where $|\psi^0\rangle = \prod_{i=0}^{M} C_{i0}^\dagger |vac\rangle$. To realise the state (1.2.23) they construct a Hamiltonian of the form

$$H = \sum_{i=0}^{M} \sum_{j=0}^{N} h_i^j(U_{ij}), \tag{1.2.24}$$

, where the single qubit, single step terms $h_i^j(U_{ij})$ are of the form

$$h_i^j = \epsilon \left(C_{ij}^\dagger - {C_{i(j-1)}}^\dagger {U_{ij}}^\dagger\right) \left(C_{ij} - C_{i(j-1)} U_{ij}\right), \tag{1.2.25}$$

where ϵ sets the energy scale. This basic non-interacting Hamiltonian, (1.2.24), can then be easily modified to account for the interaction required for multi-qubit gates. In section 3.1, the problem Hamiltonian for the adiabatic equivalent of a CNOT gate will be constructed explicitly as an example of the GSQC method.

1.2.3.4 Noise and decoherence

Noise is a general term that can be used to describe any uncontrolled artefacts that affect the evolution of a physical system. In the context of adiabatic quantum computing we can identify two main sources of noise; control errors and decoherence. Control errors will arise through imperfect implementation of the time-dependent Hamiltonian and are essentially uncontrolled deviations of the interpolation path from H_i to H_f. Decoherence or dissipation in a quantum mechanical system de-

scribes the quantum noise processes caused by the interaction of the system with its environment. In practice all quantum systems are open, as it is impossible to perfectly isolate one from its environment. This interaction of a quantum system with its environment leads to non-unitary, irreversible evolution of the system as they become entangled with each other and the system of interest therefore evolves into a mixed state. The effects of dissipation can be separated into two distinct types of process in a given basis of orthogonal eigenstates:

- **Relaxation or state-mixing:** When the Bloch vector describing the state of the system diffuses in the latitude direction, e.g. parallel to the z-axis of the Bloch sphere.
- **Dephasing or decoherence (when used in its narrower meaning):** When the Bloch vector diffuses in the longitude direction, e.g. the x-y plane of the Bloch sphere.

It is possible to make a number of intuitive arguments that suggest AQC will be intrinsically more resistant to the effects of noise than the gate model of quantum computing. We can first say that for the types of optimisation and search algorithms that AQC is applied to the phase of the ground state will have no effect on the result, therefore we can assume pure dephasing is not an issue. By evolving the system adiabatically slowly we aim to keep it in the ground state at all times, this will automatically protect it against the effects of relaxation. Also, by keeping the system at low temperatures where $k_B T < \Delta_{01}$ we can try to control the effect of interactions with the environment that cause transitions between eigenstates.

The natural fault tolerance of AQC was first studied by Childs, Farhi and Preskill in [7]. They numerically studied the effects of decoherence and unitary control errors on the adiabatic algorithm for the exact cover problem. They found that neither of the different types of error had a significant effect on the scaling of the success probability as a function of the computation time for the relatively small problem instances ($n \leq 4$ bits in the case of decoherence) they could simulate efficiently. These conclusions were later verified by more analytical means in the papers of Roland and Cerf: [9], and Ashhab *et al.*: [8].

A lot of analyses of the performance of AQC tend to neglect the effects of noise from their models because of AQC's apparent natural fault tolerance. However, some results have suggested that noise may play a subtle but important role in the performance of adiabatic quantum algorithms. Childs *et al.* noted that in some cases a unitary control error could increase the success probability of the computation by providing an alternate interpolation path between H_i and H_f. They also noted that relaxation caused by interaction with a low temperature environment can help keep

the system in the ground state and therefore also improve the success probability. A paper by Amin, Love and Truncik, [12], explored the idea that in some situations decoherence can enhance the performance of AQC in more detail. They showed that thermal mixing around the minimum ground state gap as well as relaxation after the avoided crossing could help improve performance.

1.2.3.5 Physical realisations

Adiabatic quantum computation was first demonstrated experimentally using nuclear magnetic resonance (NMR) by Steffen *et al.* in 2003 in[26]. They solved a three qubit instance of the **NP-complete** MAXCUT optimisation algorithm and showed that the results were in agreement with the predictions of a simple theoretical model that included decoherence. In NMR quantum computing, the nuclear spins of specific individual atoms in large molecules are identified and used as qubits. The molecules as a whole therefore represent individual quantum computers. Algorithms can then be implemented by performing operations on an ensemble of these molecular quantum computers using RF pulses that address the specific spins that represent qubits. NMR spectroscopy can then be used to readout the ensemble average of the solution state. Unfortunately, NMR implementations are not scalable because of the exponential decrease of the signal-to-noise ratio with the system size [27]. However, these results provided a good experimental proof of principle for AQC.

Currently, superconducting flux qubits are widely considered to be among the most promising candidates for the experimental implementation of an AQC system. These devices consist of small loops of superconducting metal interrupted by a number of weak links, which are known as Josephson junctions, as shown schematically in Fig. 1.2.2(a). They are designed such that when the loop is threaded by an external magnetic field, a persistent current will flow around the loop. The computational basis states are then defined as clockwise and anti-clockwise circulating currents. This device can be thought of as a double well potential with respect to the applied flux where the left and right hand wells correspond to the clockwise or anti-clockwise circulating currents that represent the computational basis states. This type of qubit can be readily coupled together and controlled inductively and readout can be performed by probing one of the qubit's macroscopic quantum variables; the circulating current ([28]), the flux within the loop ([29]) or the phase ([30]). These devices also have the advantage that they can be produced using similar fabrication techniques to those commonly used in the micro-electronics industry, which bodes well for the scalability. It is also possible to realise a degree of controllability over

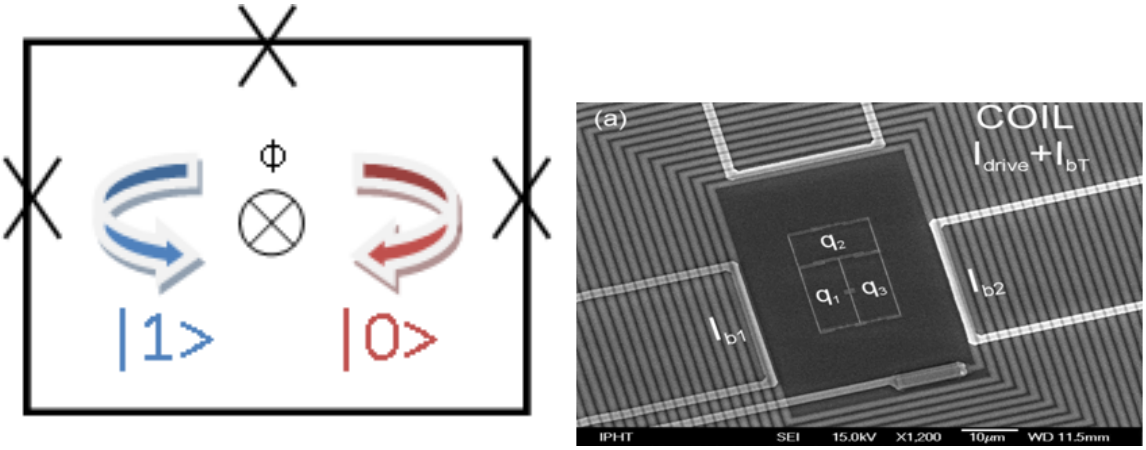

(a) (b)

Figure 1.2.2: (a) shows a schematic of a single persistent current qubit of the Delft type [32]. (b) shows the micrograph of a device consisting of three inductively coupled flux qubits in resonant tank readout circuit, reproduced from [33].

the inductive coupling elements which is required by the fourth DiVincenzo criterion for universal quantum computation [31].

This leaves us with the crucial third DiVincenzo criterion to consider; long decoherence times. By operating flux qubits at low temperatures they gain a degree of inherent protection against the effects of noise, as we can assume that the gap between the two lowest energy states (Δ_{01}) will be much larger than k_BT, therefore suppressing thermal excitation. The main sources of noise in flux qubit systems are therefore background magnetic fluctuations. These can be caused by impurities and defects in the substrate and superconducting wires, as well as circuit elements like control lines, coupling devices and readout probes. A number of systematic studies of the noise in flux qubits have found it to be characterised by a low frequency $1/f$ or coloured noise spectrum [34, 35]. Flux qubits with a decoherence time of the order of $10^{-5}s$ have been demonstrated, e.g. [36], but the question of whether a large number of them can remain quantum coherent long enough for an AQC operation to be performed remains open. Despite this, there have been a number of promising experimental results with flux qubit systems.

In 2006, van der Ploeg *et al.* demonstrated a system of three coupled flux qubits that could be used to encode a realisation of the MAXCUT problem in [33], as shown in Fig. 1.2.2(b). They then made use of a resonant tank circuit to measure the ground state susceptibility, it was then shown that this could be used to construct the ground state flux diagram and therefore the solution to the MAXCUT problem. These results demonstrated a number of the key elements needed to build an AQC system using flux qubits. Recently, in [37] D-Wave Systems

Inc. demonstrated a device consisting of 8 flux qubits with programmable couplings that can be used to solve adiabatic quantum algorithms which can be described by an Ising model problem Hamiltonian. They show that the results of an example computation are in agreement with an explicitly quantum mechanical theoretical model as oposed to a classical description of the system. Although this device is limited to solving a certain class of problems it represents an important step in the process of implementing a practical, large scale AQC system.

1.3 Eigenvalue dynamics

In the field of quantum chaos, which involves the study of the quantum mechanics of classically chaotic systems, a lot of information about the nature of a system can be determined by the analysis of the distribution of its energy spectrum. In a lot of the spectroscopic experiments used to measure this distribution, the energy levels are determined as a function of some external parameter, e.g. the distribution of the energy levels of a hydrogen atom in the presence of a strong magnetic field gradually become chaotic as the strength of the perturbing field is increased. Motivated by this, in [38] Pechukas derived a set of equations motion for the dynamics of the energy eigenvalues of a quantum system with a Hamiltonian of the form

$$\mathcal{H}(\lambda(t)) = H_0 + \lambda(t)V, \tag{1.3.1}$$

where H_0 is the Hamiltonian of the unperturbed system, V is the perturbation and the perturbation strength $\lambda(t)$ plays the role of "time" in the system. In [39], Yukawa simplified Pechukas's equations of motion to the form

$$\begin{aligned}
\frac{\partial}{\partial\lambda}x_n &= v_n, \\
\frac{\partial}{\partial\lambda}v_n &= \sum_{k\neq n}\frac{2\left|l_{nk}\right|^2}{(x_n - x_k)^3}, \\
\frac{\partial}{\partial\lambda}l_{nm} &= \sum_{k\neq m,n} l_{nk}l_{km}\left(\frac{1}{(x_n - x_k)^2} - \frac{1}{(x_m - x_k)^2}\right),
\end{aligned} \tag{1.3.2}$$

by introducing a new set of dynamical variables, where x_n are the instantaneous energy eigenvalues of the system that obey the standard relation (1.2.5), $v_n = V_{nn}$ are the diagonal matrix elements of the perturbation, $l_{nm} = (x_n - x_m)V_{nm}$ for $n \neq m$ and V_{nm} are the off-diagonal matrix elements of the perturbation. This system of equations motion (1.3.2) is now known as the Pechukas-Yukawa model. These equations of motion are analogous to those of a classical one-dimensional gas with

cubic repulsion where the x_n take the role of the positions of the gas particles, the v_n their velocity or momenta and the l_{nm} represent the strength of the interaction between particles n and m. In fact, as no assumptions or simplifications are made in the derivation of (1.3.2), the mapping of the dynamics of the eigenvalues of the quantum system to those of the classical 1D gas is exact. The initial conditions for the Pechukas gas will contain all the information about the Hamiltonian of the quantum system, (1.3.1), and this simple, generic form of Hamiltonian can be used to describe a wide range of physical systems.

In [40] Zagoskin, Savel'ev and Nori used the Pechukas-Yukawa equations to model an adiabatic quantum computer. The Hamiltonian (1.3.1) can be used to describe the operation of an adiabatic quantum computer by assuming the perturbation takes the form of a large bias, *i.e.* $V = ZH_b$ where $Z \gg 1$, and that $H_i = \mathcal{H}(\lambda = 1) = H_0 + ZH_b$ has a unique and easily achievable ground state. In this case the final Hamiltonian that encodes the algorithm will take the form of the unperturbed Hamiltonian, *i.e.* $H_f = \mathcal{H}(\lambda = 0) = H_0$. This scheme is sometimes referred to as "quantum annealing" (see [41]) because the perturbation term in the Hamiltonian (V) plays a similar role to the "temperature" in simulated annealing (*i.e.* it is a source of disorder that is gradually reduced to try to find a desired ground state), however it is essentially the same as the linear interpolation scheme of (1.2.13). Using an eigenvalue dynamics approach to model an adiabatic quantum computer is a particularly relevant and insightful method because knowledge of how the energy spectrum evolves as a function of time can provide a lot of information about the performance of the algorithm. For example, the minimum ground state energy gap width can be easily extracted. Also, being able to identify and analyse the distribution of avoided crossings between pairs of adjacent energy levels in the spectrum is advantageous because of Landau-Zener-Stückelberg tunneling. Landau-Zener-Stückelberg tunneling ([42, 43, 44]) is a mechanism by which there exists a finite probability of tunneling between the states of a quantum system as it moves through an avoided level crossing at a finite rate and in the absence of noise it is the sole factor that determines the success probability of an adiabatic quantum algorithm.

1.4 Random matrices

Random matrix theory was originally developed in the 1950's by Wigner as a way of trying to describe the energy spectra of complex nuclei and it has more recently been successfully applied in the field of quantum chaos. The main principle of random matrix theory is that the Hamiltonian is thought of as a large matrix with randomly

distributed elements which belongs to a large class or ensemble of matrices that have similar general properties and symmetries, *i.e.* that it is the properties of the matrix as a whole and not individual elements that determine the trends in the corresponding eigenspectrum. The individual matrix elements are often assumed to obey Gaussian distributions, which allows the definition of the three ensembles; the Gaussian orthogonal ensemble (GOE), the Gaussian unitary ensemble (GUE) and the Gaussian symplectic ensemble (GSE). These three ensembles are defined by the type of transformation the constituent matrices are invariant under and there properties are summarized in the table 1.1 ([45, 46]).

	GOE	GUE	GSE
Time-reversal symmetry	Yes	No	Yes
Spin-1/2 interaction	No	n/a	Yes
Matrix elements	real	complex	real-quaternionic
Transformation invariance	orthogonal	unitary	symplectic

Table 1.1: Summary of the properties and symmetries of the three Gaussian ensembles of random matrix theory [45, 46].

Throughout this work we will only be concerned with the GOE and GUE. They will be useful as a means of modeling different types of generic Hamiltonians. The probability distribution functions for the matrix elements of $N \times N$ random matrices drawn from the GOE and GUE are

$$p(H_{11}, \ldots, H_{NN}) = \left(\frac{A}{\pi}\right)^{N/2} \left(\frac{2A}{\pi}\right)^{N(N-1)/2} \exp\left(-A \sum_{n,m} H_{nm}^2\right) \text{ and} \tag{1.4.1}$$

$$p(H_{11}, \ldots, H_{NN}) = \left(\frac{A}{\pi}\right)^{N/2} \left(\frac{2A}{\pi}\right)^{N(N-1)} \exp\left(-A \sum_{n,m} \left[(\mathrm{Re}(H_{nm}))^2 + (\mathrm{Im}(H_{nm}))^2\right)\right] \tag{1.4.2}$$

respectively ([45, 46]), where A is determined by the variances $\langle H_{nn}^2 \rangle = 1/2A$ and $\langle H_{nm}^2 \rangle = 1/4A$. An interesting property of the Gaussian ensembles is that in all three cases the average density of states is described by Wigner's semicircle law; which is of the form

$$\langle \rho(E) \rangle = \begin{cases} \frac{A}{\pi}\sqrt{\frac{2N}{A} - E^2}, \text{ for } |E| < \sqrt{\frac{2N}{A}} \\ 0, \text{ for } |E| > \sqrt{\frac{2N}{A}} \end{cases} \tag{1.4.3}$$

([45, 46]).

In the papers [17] and [18] the authors attempted to determine whether the statistical properties of the energy spectra of adiabatic quantum computers can

be described using the predictions of random matrix theory and hence discover whether it is applicable to use random matrix theory to predict the behaviour of AQC for large problem instances. In general they found that for problem instances of increasing complexity the degree of regularity of the spectrum decreased meaning random matrix theory becomes more applicable. In particular, the bulk of the eigenspectrum (*i.e.* eigenstates from the centre of the spectrum) appear to be well described by random matrix theory. Whereas the properties of the top and bottom parts of the energy spectrum, the latter of which is of critical importance in AQC, do not appear to fit the predictions of random matrix theory quite as well, meaning it may not be applicable in those regions. Another way in which random matrices have been used in the study of adiabatic quantum computing is as a simple way of representing noise in the Hamiltonian; this was done by Roland and Cerf in [9].

Chapter 2

Generalised Pechukas-Yukawa model

2.1 Generalised Pechukas-Yukawa equations

As mentioned in section 1.3 the Pechukas-Yukawa model offers a method of exploring the dynamics of the energy eigenvalues of a quantum system. This model is particularly appropriate for studying an adiabatic quantum computer as it is based on a Hamiltonian of a similar form and knowledge about the behaviour of the lowest few energy levels is crucial when analysing the performance of adiabatic quantum algorithms. We aim to explore the effects of noise on an adiabatic quantum computer, therefore we need to generalise the Pechukas-Yukawa equations to the stochastic case. This can be done by including an additional term in the Hamiltonian, $\delta h(\lambda)$, which accounts for the effects of noise on the system. At this point we need not make any assumptions about the exact form of the stochastic variable $\delta h(\lambda)$. We follow the derivation of the standard Pechukas-Yukawa equations described in [46], except that we start with the following Hamiltonian;

$$\mathcal{H}(\lambda(t)) = \mathcal{H}_0 + \lambda(t)V + \delta h(\lambda(t)) \tag{2.1.1}$$

where the perturbation strength $\lambda(t)$ is interpreted as 'time'.

The instantaneous eigenvalues of $\mathcal{H}(\lambda)$ are denoted by $x_n(\lambda)$ and the corresponding eigenfunctions by $|n(\lambda)\rangle$;

$$\mathcal{H}(\lambda)\,|n(\lambda)\rangle = x_n(\lambda)\,|n(\lambda)\rangle\,. \tag{2.1.2}$$

The eigenfunctions obey the orthogonality relation

$$\langle n|m\rangle = \delta_{nm}, \tag{2.1.3}$$

which after differentiation with respect to 'time' (λ) gives

$$\left(\frac{\partial}{\partial\lambda}\langle n|\right)|m\rangle + \langle n|\left(\frac{\partial}{\partial\lambda}|m\rangle\right) = 0. \tag{2.1.4}$$

If we now introduce the operator

$$H = i\frac{\partial}{\partial\lambda}, \tag{2.1.5}$$

with matrix elements

$$H_{nm} = \langle n|\, H\, |m\rangle\,, \tag{2.1.6}$$

which allows (2.1.4) to be written as $H_{nm} = H^*_{mn}$, *i.e.* H is hermitian.

We can now derive an equation for the 'time' evolution of the matrix elements of an arbitrary operator A

$$\frac{d}{d\lambda}\langle n|\, A\, |m\rangle = \left(\frac{\partial}{\partial\lambda}\langle n|\right) A\, |m\rangle + \langle n|\,\frac{\partial A}{\partial\lambda}\,|m\rangle + \langle n|\, A\left(\frac{\partial}{\partial\lambda}|m\rangle\right), \tag{2.1.7}$$

using the completeness relation, $\sum_k |k\rangle\langle k| = 1$, we get

$$\frac{d}{d\lambda}\langle n|\, A\, |m\rangle = \sum_k\left[\left(\frac{\partial}{\partial\lambda}\langle n|\right)|k\rangle\langle k|\, A\, |m\rangle + \langle n|\, A\, |k\rangle\langle k|\left(\frac{\partial}{\partial\lambda}|m\rangle\right)\right] + \langle n|\,\frac{\partial A}{\partial\lambda}\,|m\rangle\,. \tag{2.1.8}$$

Using the definition (2.1.5) we have

$$\frac{dA_{nm}}{d\lambda} = i\sum_k\left(H_{nk}A_{km} - A_{nk}H_{km}\right) + \left(\frac{\partial A}{\partial\lambda}\right)_{nm}, \tag{2.1.9}$$

which, when written in matrix notation and H is interpreted as a Hamiltonian, is simply the equation of motion for an operator A in the Heisenberg picture

$$\frac{dA}{d\lambda} = i[H, A] + \frac{\partial A}{\partial\lambda}. \tag{2.1.10}$$

If we insert the Hamiltonian $\mathcal{H}(\lambda)$ for A in (2.1.9) we have

$$\dot{x}_n\delta_{nm} = iH_{nm}(x_m - x_n) + V_{nm} + \dot{\delta h}_{nm}, \tag{2.1.11}$$

where the dot denotes differentiation with respect to 'time' and $\dot{\delta h}_{nm}$ is the instan-

taneous 'time' derivative of an element of the noise matrix, which arises from the partial derivative term of (2.1.9). For $n = m$ (2.1.11) gives

$$\dot{x}_n = V_{nn} + \delta\dot{h}_{nn} \tag{2.1.12}$$

and for $n \neq m$ it gives

$$H_{nm} = \frac{V_{nm} + \delta\dot{h}_{nm}}{i(x_n - x_m)}. \tag{2.1.13}$$

Next we insert V for A in (2.1.9) to get

$$\dot{V}_{nm} = i\sum_k \left(H_{nk}V_{km} - V_{nk}H_{km}\right). \tag{2.1.14}$$

For $n = m$ in (2.1.14), using (2.1.13), we obtain

$$\dot{V}_{nn} = \sum_{k\neq n}\left[\frac{\left(V_{nk} + \delta\dot{h}_{nk}\right)V_{kn}}{x_n - x_k} - \frac{V_{nk}\left(V_{kn} + \delta\dot{h}_{kn}\right)}{x_k - x_n}\right] \tag{2.1.15}$$

$$= \sum_{k\neq n}\frac{2V_{nk}V_{kn} + \delta\dot{h}_{nk}V_{kn} + V_{nk}\delta\dot{h}_{kn}}{x_n - x_k} \tag{2.1.16}$$

as for $k = n$ the contribution to the sum is $H_{nn}V_{nn} - V_{nn}H_{nn} = 0$. For $n \neq m$ in (2.1.14) we get

$$\dot{V}_{nm} = \sum_{k\neq n,m}\left[\frac{\left(V_{nk} + \delta\dot{h}_{nk}\right)V_{km}}{x_n - x_k} - \frac{V_{nk}\left(V_{km} + \delta\dot{h}_{km}\right)}{x_k - x_m}\right] + i(H_{nn}V_{nm} - V_{nn}H_{nm}) + i(H_{nm}V_{mm} - V_{nm}H_{mm}) \tag{2.1.17}$$

where the second and third terms are the contributions to the sum for $k = n$ and $k = m$ respectively. This can be rearranged to give

$$\dot{V}_{nm} = \sum_{k\neq n,m}\left[\frac{V_{nk}V_{km} + \delta\dot{h}_{nk}V_{km}}{x_n - x_k} + \frac{V_{nk}V_{km} + V_{nk}\delta\dot{h}_{km}}{x_m - x_k}\right] + i(H_{nn} - H_{mm})V_{nm} + iH_{nm}(V_{mm} - V_{nn}). \tag{2.1.18}$$

The second term can be removed by the substitution

$$V_{nm} = \hat{V}_{nm}\exp\left[i\int(H_{nn} - H_{mm})dt\right]. \tag{2.1.19}$$

as the $\hat{V}_{nm}$ obey the same equation of motion as the V_{nm} but without the second term of (2.1.18); therefore we may assume that $H_{nn} = 0$ and write V_{nm} instead of $\hat{V}_{nm}$ without loss of generality. Using the identity (2.1.13), the third term in (2.1.18) can then be rearranged to give

$$\dot{V}_{nm} = \sum_{k\neq n,m} \left[\frac{V_{nk}V_{km} + \dot{\delta h}_{nk}V_{km}}{x_n - x_k} + \frac{V_{nk}V_{km} + V_{nk}\dot{\delta h}_{km}}{x_m - x_k} \right] - \frac{(V_{nm} + \dot{\delta h}_{nm})(V_{nn} - V_{mm})}{x_n - x_m} \quad (2.1.20)$$

$$\dot{V}_{nm} = \sum_{k\neq n,m} \left[\frac{V_{nk}V_{km} + \dot{\delta h}_{nk}V_{km}}{x_n - x_k} + \frac{V_{nk}V_{km} + V_{nk}\dot{\delta h}_{km}}{x_m - x_k} \right] - \frac{V_{nm}(V_{nn} - V_{mm})}{x_n - x_m} - \frac{\dot{\delta h}_{nm}(V_{nn} - V_{mm})}{x_n - x_m}. \quad (2.1.21)$$

Equations (2.1.12), (2.1.16) and (2.1.21) form a closed system of equations describing the dynamics of the energy eigenvalues of $\mathcal{H}(\lambda)$, similar to those originally derived by Pechukas in [38].

We can now introduce the new dynamical variables v_n and l_{mn} as done by Yukawa in [39].

$$v_n = V_{nn} \quad (2.1.22)$$

$$l_{nm} = (x_n - x_m)V_{nm}, \qquad n \neq m \quad (2.1.23)$$

If we imagine that the energy eigenvalues x_n take the role of the position of the n^{th} particle in a 1D classical gas, the new variables v_n and l_{mn} are analogous to the particle's velocity and the particle-particle repulsion strength respectively. The new variables v_n and l_{mn} can be substituted into equations (2.1.12), (2.1.16) and (2.1.21) to derive a system of equations describing the dynamics of the 1D classical gas. Substituting (2.1.22) into (2.1.12) gives the equation of motion for the n^{th} particle's position

$$\dot{x}_n = v_n + \dot{\delta h}_{nn}. \quad (2.1.24)$$

Substitution of (2.1.23) into (2.1.16) gives the equation of motion for the n^{th} particle's velocity

$$\dot{v}_n = \sum_{k\neq n} \left[\frac{2l_{nk}l_{kn}}{(x_n - x_k)^2(x_k - x_n)} + \frac{\dot{\delta h}_{nk}l_{kn}}{(x_n - x_k)(x_k - x_n)} + \frac{l_{nk}\dot{\delta h}_{kn}}{(x_n - x_k)^2} \right], \quad (2.1.25)$$

as V is a hermitian matrix $l_{nk} = -l^*_{kn}$ for $k \neq n$, therefore we can write

$$\dot{v}_n = \sum_{k\neq n} \left[\frac{2\left|l_{nk}\right|^2}{(x_n - x_k)^3} + \frac{l_{nk}\dot{\delta h}_{kn} - \dot{\delta h}_{nk} l_{kn}}{(x_n - x_k)^2} \right]. \tag{2.1.26}$$

If we then differentiate (2.1.23) with respect to 'time';

$$\begin{aligned} \dot{l}_{nm} &= \frac{d}{d\lambda}(x_n V_{nm} - x_m V_{nm}) && (2.1.27)\\ &= (x_n \dot{V}_{nm} + \dot{x}_n V_{nm}) - (x_m \dot{V}_{nm} + \dot{x}_m V_{nm}) && (2.1.28)\\ &= \dot{V}_{nm}(x_n - x_m) + V_{nm}(\dot{x}_n - \dot{x}_m). && (2.1.29) \end{aligned}$$

Then equation (2.1.24) and the identities (2.1.22) and (2.1.23) can be substituted into give;

$$\dot{l}_{nm} = \dot{V}_{nm}(x_n - x_m) + \frac{l_{nm}(v_n - v_m)}{(x_n - x_m)} + \frac{l_{nm}(\dot{\delta h}_{nn} - \dot{\delta h}_{mm})}{(x_n - x_m)}. \tag{2.1.30}$$

The new variable l_{nm} can then be substituted into (2.1.21);

$$\begin{aligned} \dot{V}_{nm} = \sum_{k\neq n,m} \Bigg[&\frac{l_{nk}l_{km}}{(x_n - x_k)^2(x_k - x_m)} - \frac{l_{nk}l_{km}}{(x_m - x_k)^2(x_n - x_k)} + \frac{\dot{\delta h}_{nk} l_{km}}{(x_n - x_k)(x_k - x_m)} \\ &+ \frac{l_{nk}\dot{\delta h}_{km}}{(x_n - x_k)(x_m - x_k)} \Bigg] + \frac{l_{nm}(v_m - v_n)}{(x_n - x_m)^2} + \frac{\dot{\delta h}_{nm}(v_m - v_n)}{(x_n - x_m)} \end{aligned} \tag{2.1.31}$$

Combining equations (2.1.30) and (2.1.31) we derive an equation of motion for the particle-particle repulsion strength in the eigenvalue gas (N.B. the second term in (2.1.30) will cancel the first term outside the sum in (2.1.31)),

$$\begin{aligned} \dot{l}_{nm} = (x_n - x_m) \sum_{k\neq m,n} \Bigg[&l_{nk}l_{km} \left(\frac{1}{(x_n - x_k)^2(x_k - x_m)} - \frac{1}{(x_m - x_k)^2(x_n - x_k)} \right) \\ &+ \frac{l_{nk}\dot{\delta h}_{km} - l_{km}\dot{\delta h}_{nk}}{(x_m - x_k)(x_n - x_k)} \Bigg] + \dot{\delta h}_{nm}(v_m - v_n) + \frac{l_{nm}(\dot{\delta h}_{nn} - \dot{\delta h}_{mm})}{(x_n - x_m)}. \end{aligned} \tag{2.1.32}$$

The $(x_n - x_m)$ can then be taken inside the sum to give

$$\begin{aligned} \dot{l}_{nm} = \sum_{k\neq m,n} \Bigg[&l_{nk}l_{km} \left(\frac{1}{(x_n - x_k)^2} - \frac{1}{(x_m - x_k)^2} \right) + \frac{(x_n - x_m)(l_{nk}\dot{\delta h}_{km} - l_{km}\dot{\delta h}_{nk})}{(x_m - x_k)(x_n - x_k)} \Bigg] \\ &+ \dot{\delta h}_{nm}(v_m - v_n) + \frac{l_{nm}(\dot{\delta h}_{nn} - \dot{\delta h}_{mm})}{(x_n - x_m)}. \end{aligned} \tag{2.1.33}$$

We now have the following dynamical equation system to describe the motion of the energy eigenvalues of the Hamiltonian $\mathcal{H}(\lambda(t)) = \mathcal{H}_0 + \lambda(t)V + \delta h(\lambda(t))$;

$$\begin{aligned}
\dot{x}_n =& v_n + \dot{\delta h}_{nn}, \\
\dot{v}_n =& \sum_{k\neq n}\left[\frac{2\left|l_{nk}\right|^2}{(x_n - x_k)^3} + \frac{l_{nk}\dot{\delta h}_{kn} - \dot{\delta h}_{nk}l_{kn}}{(x_n - x_k)^2}\right], \\
\dot{l}_{nm} =& \sum_{k\neq m,n}\left[l_{nk}l_{km}\left(\frac{1}{(x_n - x_k)^2} - \frac{1}{(x_m - x_k)^2}\right) + \frac{(x_n - x_m)(l_{nk}\dot{\delta h}_{km} - l_{km}\dot{\delta h}_{nk})}{(x_m - x_k)(x_n - x_k)}\right] \\
&+ \dot{\delta h}_{nm}(v_m - v_n) + \frac{l_{nm}(\dot{\delta h}_{nn} - \dot{\delta h}_{mm})}{(x_n - x_m)}.
\end{aligned} \tag{2.1.34}$$

When the noise term $\delta h(\lambda)$ equals zero at all times this simply reduces to the normal Pechukas-Yukawa system as expected.

We have derived a generalised stochastic form of the Pechukas-Yukawa model of eigenvalue dynamics. This retains the key feature of the standard Pechukas-Yukawa equations as it is also an exact mapping of the quantum eigenvalue dynamics to a classical gas. It is also done without making any assumptions about the nature of the noise source $\delta h(\lambda)$ and can therefore be used to model a wide range of different physical systems.

2.2 Random matrix Noise model

In order to close the generalised Pechukas-Yukawa system of dynamical equations (2.1.34) we need to consider the exact nature of the noise term $\delta h(\lambda)$. In reality, noise in most physical systems arises from a number of different sources via different mechanisms, because of this it seems reasonable to assume that, by the central limit theorem, the sum of their effects will be a random term in the Hamiltonian with independent Gaussian distributed elements. Therefore, we take the noise term $\delta h(\lambda)$ to be a random matrix drawn from the Gaussian ensembles of random matrix theory described in section 1.4; this is similar to the noise model used in [9].

The generalised Pechukas-Yukawa model depends on the derivative of the noise term, $\dot{\delta h}(\lambda)$, because of this we require a noise source which obeys a simple stochastic differential equation. As mentioned in section 1.2.3.5, some of the most promising physical realisations of adiabatic quantum computers are built using superconducting qubits and the noise observed in these types of devices has a coloured (non-flat) frequency spectral density [34]. Therefore, we will assume that the elements of the noise matrix evolve in time according to a simple stationary stochastic process which

has a coloured spectral density, the Ornstein-Uhlenbeck process [47];

$$\dot{\delta h}_{ij}(\lambda) = -\tau \delta h_{ij}(\lambda) + \epsilon \eta_{ij}(\lambda) \tag{2.2.1}$$

where τ is the correlation time, ϵ is the noise amplitude and $\eta(\lambda)$ is a random matrix valued function with $\langle \eta(\lambda) \rangle = 0$ and $\langle \eta(\lambda)\eta(\lambda') \rangle = \delta(\lambda - \lambda')$, *i.e.* a white noise process.

2.3 Numerical methods and testing

As an initial test of the generalised Pechukas-Yukawa model, a simple simulation that numerically solved the equations (2.1.34) with the random matrix noise model was developed in MATLAB. We assume that the perturbation takes the form of a large bias, *i.e.* $V = ZH_b$ where $Z \gg 1$. The problem ($H_f = H_0$) and bias (H_b) Hamiltonians are taken to be random matrices drawn from the Gaussian unitary ensemble. The noise term ($\delta h(\lambda)$) is taken as a random matrix drawn from the Gaussian orthogonal ensemble and is assumed to evolve in time according to equation (2.2.1).

The system of equations (2.1.34) is complex and the noise term will fluctuate on a relatively fast time scale compared to the trajectories of the eigenvalues, because of this the stability of the numerical methods that are used is an important consideration. Multistep methods, such as the Adams-Moulton predictor corrector, are particularly stable as they use data from a number of the preceding points to compute the next point [48]. This is in comparison to single-step methods, like the Runge-Kutta method, which only use data from the previous point in the calculation. The Adams-Moulton method essentially works by fitting a cubic polynomial through the last n (which defines the order of the method) data points and then calculating a rough approximation of the integral from the current point to the next; this is the predictor step. The results from the predictor step are then used in the corrector formula to calculate a more accurate value of the integral at the next data point. The Adams-Moulton method requires the first n data points to be calculated using a single-step method. In the simulation a variable order Adams-Moulton method is used to solve (2.1.34) and a simple 2^{nd} order Runge-Kutta method is used to solve (2.2.1). We also attempt to improve numerical accuracy by using a finer time step towards the end of the computation, because the Pechukas gas will contract as the large bias Hamiltonian is turned off and we therefore expect the majority of level and avoided crossings to occur when $\lambda(t) \gtrsim 0$.

Figure 2.3.2 shows an example of the energy spectrum of a 4-qubit system calcu-

lated using the generalised Pechukas-Yukawa model derived in section 2.1. A noise amplitude of $\epsilon = 0.1$, a large bias strength of $Z = 10$ and a short correlation time of $\tau = 0.1$ were used; the magnitude of these values will be typical of those used throughout the rest of this work. The results are compared to those found by direct diagonalization of $\mathcal{H}(t)$ at a number of points in time and it is found that they agree to approximately 3 decimal places which corresponds to a relative error of less than 0.5%, indicating the accuracy of the numerical methods used.

Knowledge of how the energy spectrum of an adiabatic quantum computer evolves over time allows the identification of the critical points in the computation process. Namely, any avoided or level crossings, as at these points there will be a finite probability of the system tunneling out of its current state. The main tunneling mechanism at these critical points will be Landau-Zener-Stückelberg tunneling ([42, 43, 44]) and the probability of excitation from $|m\rangle$ to $|m+1\rangle$ via this mechanism is given by;

$$P_{LZS} = \exp\left(-\frac{\Delta_{m,m+1}^2}{|\langle m| \, Z H_b \, |m+1\rangle| \left|\dot{\lambda}\right|}\right), \tag{2.3.1}$$

where $\Delta_{m,m+1}$ is the minimum separation between levels x_m and x_{m+1}, as shown in Fig. 2.3.1, and $|\dot{\lambda}|$ is the computation speed. Unless stated otherwise, we will always assume that system undergoes uniform evolution, therefore $|\dot{\lambda}| = \frac{1}{T}$, where T is the computation time. These critical points can be readily found by searching for the minima of $|x_m(\lambda) - x_{m+1}(\lambda)|$. Then the sequence of critical points in the spectrum that can lead to excitation out of the ground state can be identified. By applying equation (2.3.1) at these points it is possible to calculate how the level occupation changes over time and hence find the success probability of the computation. This method yields a tree-like structure with branches between adjacent levels at avoided crossings; the probability of occupation can then be visualised as diffusing across this tree structure. The algorithm used to perform this analysis is shown in Fig. 2.3.3 and copy of the MATLAB code is listed in appendix A. A two-state approximation is often used when looking at an AQC operation, e.g. as in [12], this assumes that the minimum gap between the ground and first excited states is the limiting factor for transitions out of the ground state. The algorithm for estimating occupation described here can be viewed as a natural extension of the two-state approximation.

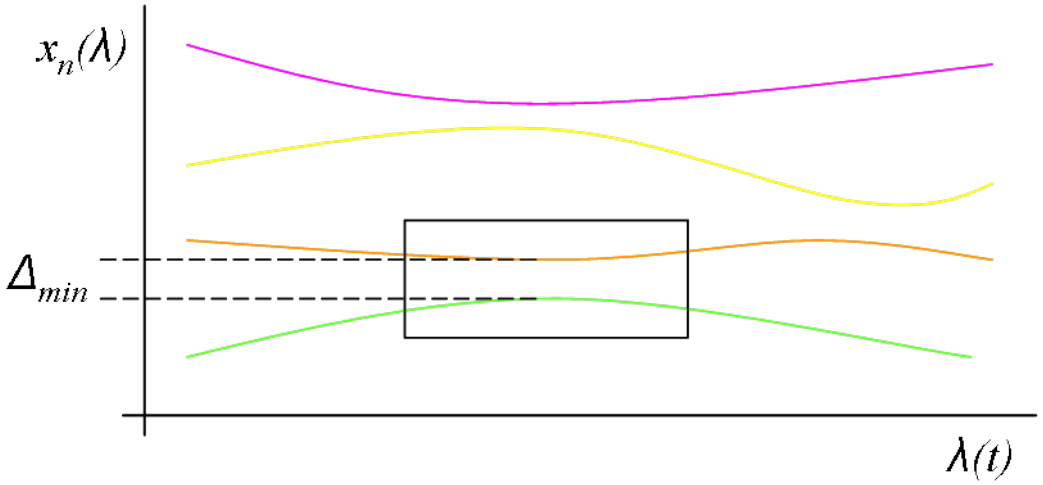

Figure 2.3.1: Example showing a critical point in the energy spectrum of an adiabatic quantum computer, namely an avoided crossing between the ground and first excited state. The minimum gap at this point is denoted Δ_{min}.

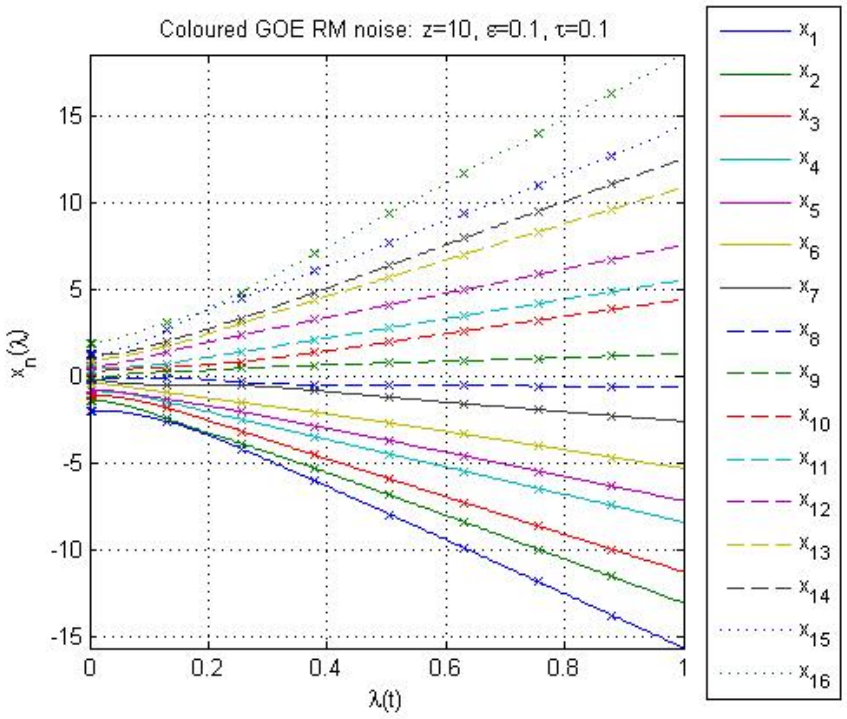

(a) Energy spectrum over time

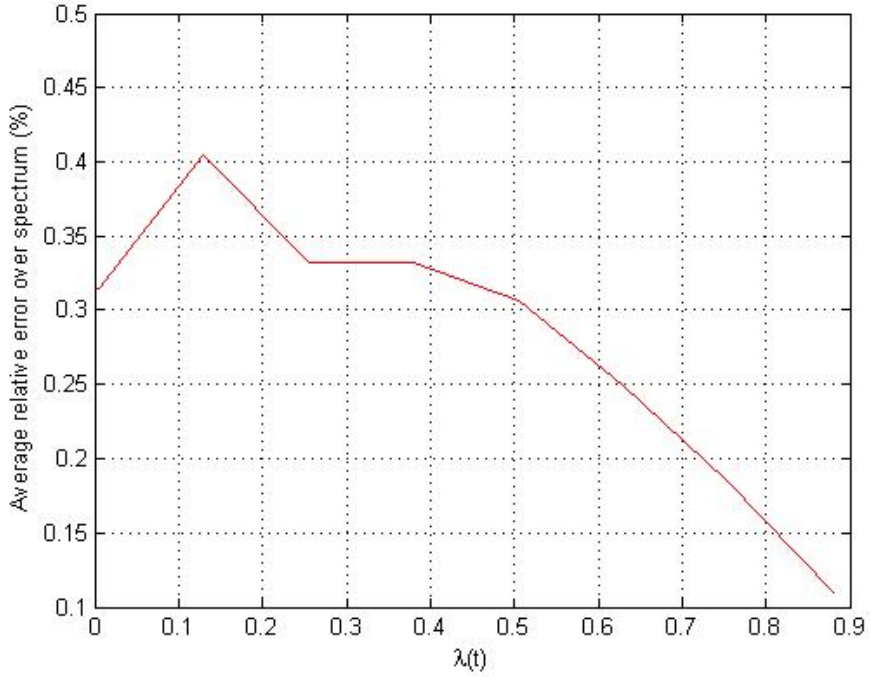

(b) Relative error

Figure 2.3.2: Plots showing a comparison of the energy spectrum calculated using the generalised Pechukas-Yukawa model and the results of direct diagonalisation (crosses) for a 4-qubit system with GUE Hamiltonians and GOE random matrix noise where $Z = 10$, $\epsilon = 0.1$ and $\tau = 0.1$.

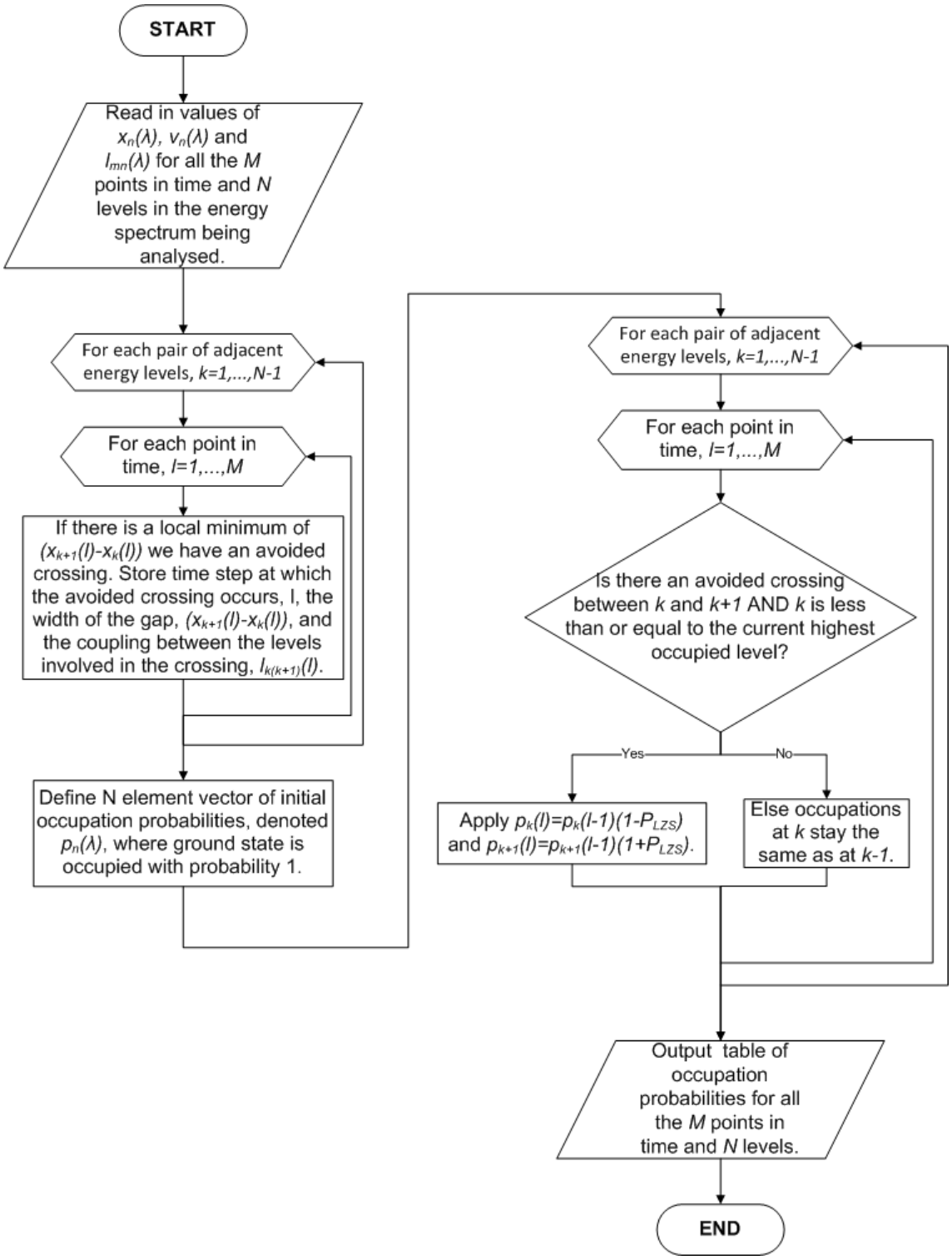

Figure 2.3.3: Flowchart describing algorithm used to estimate the occupation probabilities as a function of time for a given energy spectrum based on analysis of the critical points.

Chapter 3

The CNOT gate

3.1 The CNOT problem Hamiltonian

As an example of a prototypical quantum algorithm, we will study the adiabatic equivalent of the CNOT gate. This can be constructed using the GSQC method described in 1.2.3.3. The CNOT gate is a two qubit gate which in conjuction with single qubit roatations forms one of the simplest sets of universal quantum gates. In this family of universal gates the inter-qubit action of the CNOT gate is necessary to generate the entanglement that is required for quantum computation, because of this it is a fundamental building block in quantum circuits.

As described in section 1.2.3.3, we can construct a problem Hamiltonian using the GSQC method by visualising each qubit as an array of quantum dots that share a single spin polarised electron. A single CNOT gate is a 1 step, 2 qubit algorithm so we require an array of 8 quantum dots (effectively 4 physical qubits) for the GSQC version, this system is shown schematically in Fig. 3.1.1. The CNOT gate will flip the state of the target qubit ($m = 1$) if the state of the control qubit ($m = 0$) is in state 1, therefore we require an identity operator to be applied to $m = 1$ if $m = 0$ is in the state 0 and if $m = 0$ is in 1 we need a NOT gate to be applied to $m = 1$. The single qubit NOT operation is simply described by the well known Pauli matrix σ_x. The multi-qubit recursion relation for the solution state, (1.2.23), for this operation can be written as

$$\left|\psi^1\right\rangle = \left(I + c^\dagger_{010}c_{000}C^\dagger_{11}IC_{10} + c^\dagger_{011}c_{001}C^\dagger_{11}\sigma_x C_{10}\right)\left|\psi^0\right\rangle, \tag{3.1.1}$$

where the 2^{nd} and 3^{rd} terms in the brackets apply the identity and NOT operations respectively in the relevant situations. The Hamiltonian for this operation takes the

form;

$$H_{CNOT} = \left(c^{\dagger}_{010}C^{\dagger}_{11} - c^{\dagger}_{000}C^{\dagger}_{10}\right)(C_{11}c_{010} - C_{10}c_{000}) + \left(c^{\dagger}_{011}C^{\dagger}_{11} - c^{\dagger}_{001}C^{\dagger}_{10}\sigma_x\right)(C_{11}c_{011} - \sigma_x C_{10}c_{001}) + C^{\dagger}_{00}C_{00}C^{\dagger}_{11}C_{11} + C^{\dagger}_{01}C_{01}C^{\dagger}_{10}C_{10}, \quad (3.1.2)$$

where the first and second terms are modifications of the single qubit, single step terms in (1.2.24) that apply identity and NOT operations respectively in the relevant situations. The third term in (3.1.2) is required to penalise states in which one qubit has gone through the CNOT gate without the other.

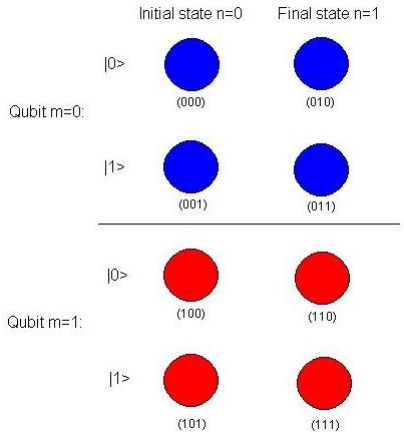

Figure 3.1.1: Schematic of the quantum dot array used to encode a CNOT gate into Hamiltonian form using the GSQC method.

In order to write the Hamiltonian (3.1.2) explicitly we need to define the fermionic creation and annihilation operators explicitly. The theoretical arrays of quantum dots used to represent a single qubit have a basis of 5 possible states, the vacuum state plus the electron occupying each dot in turn, which we describe with the following basis vectors in a $5D$ Hilbert space;

$$|vac\rangle = \begin{pmatrix}1\\0\\0\\0\\0\end{pmatrix}, \; |m00\rangle = \begin{pmatrix}0\\1\\0\\0\\0\end{pmatrix} \; \ldots \; |m11\rangle = \begin{pmatrix}0\\0\\0\\0\\1\end{pmatrix} \quad (3.1.3)$$

We know that the fermionic creation operators must satisfy the following relations;

$$C^{\dagger}_{m00}\left|vac\right\rangle = \left|m00\right\rangle,\ C^{\dagger}_{m01}\left|vac\right\rangle = \left|m01\right\rangle,\ C^{\dagger}_{m10}\left|vac\right\rangle = \left|m10\right\rangle,\ C^{\dagger}_{m11}\left|vac\right\rangle = \left|m11\right\rangle$$
$$\text{and } \left\{C_i, C^{\dagger}_j\right\} = \delta_{ij}, \quad (3.1.4)$$

and from these relations it is straightforward to write 5×5 matrices that perform the desired operation, e.g.

$$c^{\dagger}_{m00} = \begin{pmatrix} 0 & 0 & 0 & 0 & 0 \\ 1 & 0 & 0 & 0 & 0 \\ 0 & 0 & 0 & 0 & 0 \\ 0 & 0 & 0 & 0 & 0 \\ 0 & 0 & 0 & 0 & 0 \\ 0 & 0 & 0 & 0 & 0 \end{pmatrix}. \quad (3.1.5)$$

The creation operators for the $M = 2$ qubit system of the CNOT gate are then constructed by taking the tensor product with the identity operator, e.g.

$$C^{\dagger}_{000} = C^{\dagger}_{00} \otimes I \text{ and } C^{\dagger}_{100} = I \otimes C^{\dagger}_{00}. \quad (3.1.6)$$

Using equation (3.1.2) we can then construct the CNOT Hamiltonian in the $25D$ composite Hilbert space, this can then be truncated to the required $16D$ $\left(\left(2\left(N+1\right)\right)^M\right.$ where $M = 2$ qubits and $N = 1$ steps) Hilbert space by tracing out the vacuum state.

3.2 Initial conditions

The ground state energy of a GSQC Hamiltonian, such as H_{CNOT} (3.1.2), is identically 0 by design [11]. To ensure that we arrive at the desired solution state, as opposed to a state that appears correct but corresponds to starting in a different initial state, it is necessary to add a perturbation to the Hamiltonian defining the initial state, H_{input}. This perturbation ensures that states corresponding to undesired inputs are pushed well above the low-lying states that play a role in the computation. If we assume that the our system begins in one of the computational basis states, the CNOT gate has four possible operations. These four operations and the appropriate perturbations that define their initial states are shown in Table 3.1, where the constant μ simply sets the energy scale.

As mentioned in section 1.3 all the information about the form of the problem Hamiltonian ($H_f = H_0 = H_{CNOT} + H_{input}$) is encoded in the initial conditions of

IN	OUT	H_{input}
$\|00\rangle$	$\|00\rangle$	$-\mu\left(c^{\dagger}_{000}c_{000}+c^{\dagger}_{100}c_{100}\right)$
$\|01\rangle$	$\|01\rangle$	$-\mu\left(c^{\dagger}_{000}c_{000}+c^{\dagger}_{101}c_{101}\right)$
$\|10\rangle$	$\|11\rangle$	$-\mu\left(c^{\dagger}_{001}c_{001}+c^{\dagger}_{100}c_{100}\right)$
$\|11\rangle$	$\|10\rangle$	$-\mu\left(c^{\dagger}_{001}c_{001}+c^{\dagger}_{101}c_{101}\right)$

Table 3.1: The operations of the CNOT gate for the four computational basis states and their corresponding H_{input}. In H_{input}, μ sets the energy scale.

the eigenvalue gas (*i.e.* $x_n(\lambda=1)$, $v_n(\lambda=1)$ and $l_{mn}(\lambda=1)$). For the sake of generality, the initial conditions for the Pechukas gas are calculated using a first order perturbation theory expansion in terms of Z^{-1} at $\lambda(t)=1$, where

$$H_i=\mathcal{H}(1)=H_0+ZH_b+\delta h(1)\equiv Z\left(H_b+Z^{-1}H_0+Z^{-1}\delta h(1)\right). \tag{3.2.1}$$

For the initial eigenvalue positions, we have

$$x_n(1)=ZH_b\left|n^{(0)}\right\rangle+\left\langle n^{(0)}\right|\left(H_{CNOT}+H_{input}\right)\left|n^{(0)}\right\rangle+\left\langle n^{(0)}\right|\delta h(1)\left|n^{(0)}\right\rangle, \tag{3.2.2}$$

where we assume that H_b has a nondegenerate, well spaced energy spectrum with eigenvalues E_n. Using the definitions (2.1.22) and (2.1.23), this gives

$$x_n(1)=zE_n+\left(H_{CNOT}+H_{input}\right)_{nn}+\left(\delta h(1)\right)_{nn}, \tag{3.2.3}$$

$$v_n(1)=zE_n, \tag{3.2.4}$$

$$l_{nm}(1)=\left(E_n-E_m\right)z\left(\left(H_{CNOT}+H_{input}\right)_{nm}+\left(\delta h(1)\right)_{nm}\right). \tag{3.2.5}$$

This approach should be more representative of a generic implementation of an AQC system than direct calculation from a specific H_b.

Throughout this work, the initial noise term $\delta h(1)$ will be a random matrix drawn from the GOE with amplitude ϵ. We will take the numerical constants $\mu=0.1$, $Z^{-1}=0.1$ and $\tau=0.1$. We always assume that at $\lambda(t)=1$ the ground state is occupied with probability 1.

Chapter 4

The energy spectra of the CNOT gate

The numerical methods discussed in section 2.3 were used to solve the generalised Pechukas-Yukawa system, (2.1.34), for the example of the CNOT gate, (3.1.2), with generic initial conditions calculated perturbatively, (3.2.5).

We start by examining the case of an idealised system where there is an absence of noise, $\epsilon = 0$.The energy spectra as a function of the perturbation strength or 'time' $\lambda(t)$ for the 4 operations of the CNOT gate are shown in Fig. 4.0.1. Initially, at $\lambda = 1$ we have a well spaced spectrum due to the large bias z, as required in the AQC scheme. As $\lambda(t)$ decreases and the perturbation is switched off we see a contraction of the eigenvalue gas to a densely packed region near $\lambda \gtrsim 0$. At $\lambda = 0$, the system reaches the final state that encodes the results of the computation and we can see that the $x_n(0)$ are in good agreement with the values found by direct diagonalisation of $\mathcal{H}(0) = H_{CNOT} + H_{input} = H_0$; This confirms the accuracy of the numerical methods set out in section 2.3.

The final region, where $\lambda \gtrsim 0$, will be of crucial importance to the success of computation process, as it is in this region of closely packed levels where avoided and level crossings between adjacent levels will be found and therefore where tunneling out of the ground state is most likely to occur. In the idealised noiseless situation shown in Fig. 4.0.1 there are number of level crossings between adjacent energy levels in this region in all four spectra. Crucially, in the $|01\rangle \rightarrow |01\rangle$, $|10\rangle \rightarrow |11\rangle$ and $|11\rangle \rightarrow |10\rangle$ operations there are crossings between the ground and first excited states, which therefore means there is 0 probability of the system being successfully found in the ground state at $\lambda = 0$. These degeneracies correspond to different solutions of the characteristic equation having the same eigenvalue because of symmetries in the Hamiltonian $\mathcal{H}(\lambda)$. These degeneracies are clearly not desirable

in an AQC system as they obstruct the computation process.

The $|01\rangle \rightarrow |01\rangle$, $|10\rangle \rightarrow |11\rangle$ and $|11\rangle \rightarrow |10\rangle$ operations represent examples of when the usual stipulation that $[H_i, H_f] \neq 0$ has not been met. This situation could be avoided by an alternative choice of initial conditions (H_b) but a suitable choice may not be so clear if you have a particularly complex problem Hamiltonian or if there are limitations on the controllability of the system. However, the effects of noise have not been taken into account yet. The addition of a generic perturbation to the system should break the symmetries and split the degeneracies; in reality, all physical systems will be subject to some form of perturbation from noise.

The 'time' dependence of the velocities ($v_n(\lambda)$) and coupling strengths ($l_{mn}(\lambda)$) of the eigenvalue gas particles were also investigated. Figure 4.0.2 shows the 'time' dependence of $v_n(\lambda)$ for the $|00\rangle \rightarrow |00\rangle$ operation in an ideal noise-free system. We can see that level velocities are constant at the start of the computation process when the levels are well spaced. As $\lambda(t) \rightarrow 0$ and the eigenvalue gas contracts the $1/\left(x_n - x_k\right)^3$) term in the equation of motion for $v_n(\lambda)$ in (2.1.34) becomes the dominant term and we see some variation in the velocities of the close packed levels, although some do remain constant. The inter-particle coupling strengths ($l_{mn}(\lambda)$) are all shown to be constant in 'time' in Fig. 4.0.3. This arises from the initial values calculated using (3.2.5), a number of them are equal to 0. We can see that for the coupling strengths that are initially non-zero there will be no other non-zero couplings that can contribute to the sum in the equation of motion (2.1.34) and therefore all $\dot{l}_{mn}(\lambda) = 0$.

We now investigate the effects of the noise model described in section 2.2 on the dynamics of the eigenvalue gas. Throughout this work, we will consider noise at a range of different amplitudes (ϵ); usually $\epsilon = 0.025,\ 0.05,\ 0.075$ and 0.1. We can see from the equations (2.1.34) that the noise should have a significant effect on the dynamics as all three equations of motion are strongly dependent on $\dot{\delta h}(\lambda)$. The effects of the noise should be particularly noticeable as $\lambda(t)$ is near zero and the levels become more densely packed, because a number of the noise terms depend on the inverse of the gaps between levels.

In Fig. 4.0.4 we can see that the main effect of the noise on the energy spectra is to split all the degeneracies into avoided crossings, as expected. This means there will always be a finite success probability for all 4 operations of the CNOT gate when $\epsilon > 0$. The majority of these avoided crossings are in the densely packed region where $\lambda \gtrsim 0$ and this is therefore where we expect excitation out of the ground state to occur. The algorithm described in section 2.3 will be used to analyse the sequences of crossings in these spectra and estimate the level occupations. It is important to note that the noise perturbations will drive the $x_n(0)$ and therefore $|0(\lambda = 0)\rangle$

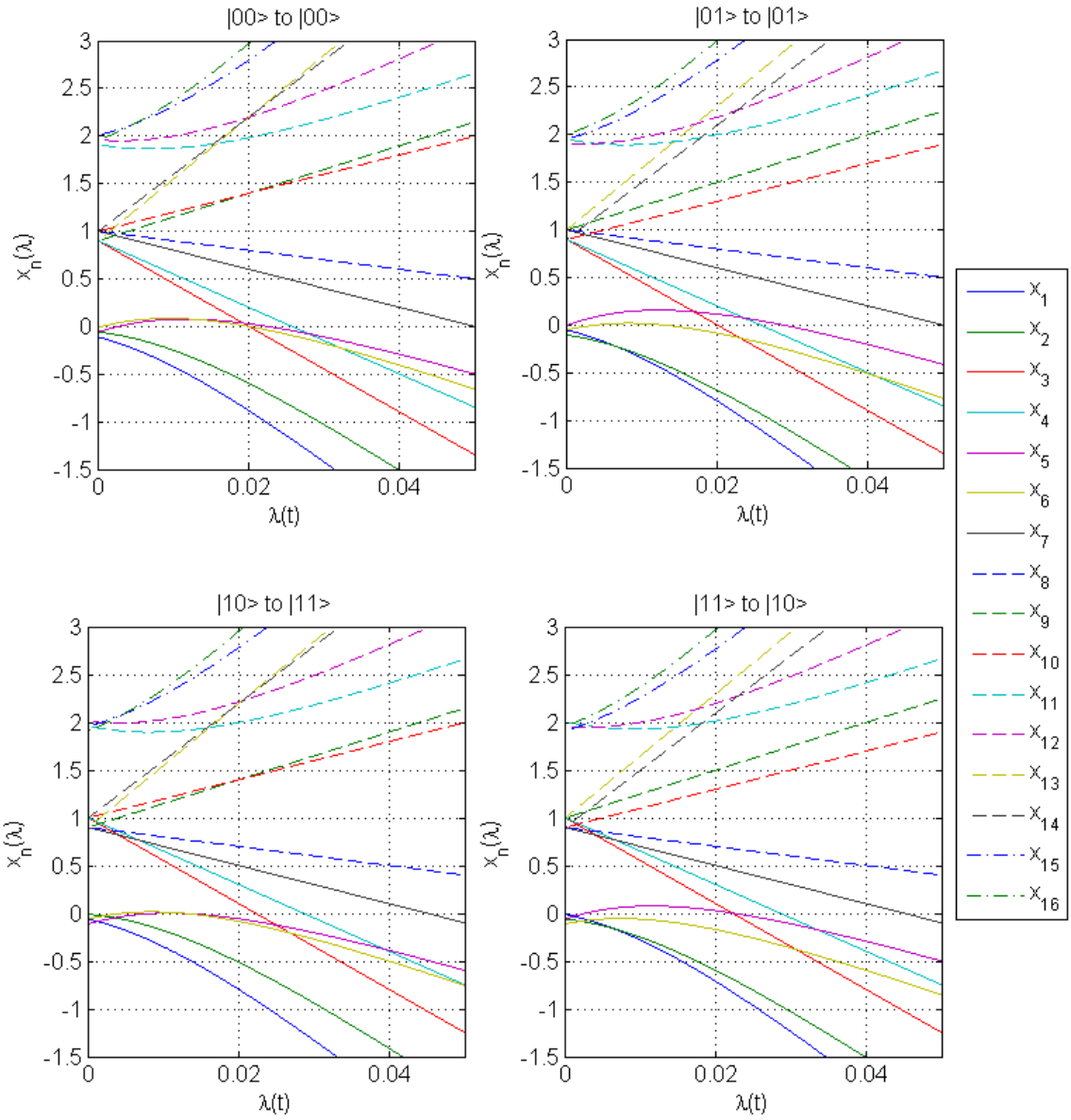

Figure 4.0.1: The energy spectra of the 4 possible operations of the adiabatic CNOT gate in the absence of noise. The blue crosses show the results of direct diagonalisation of the relevant H_0 and agree with the evolution of the Pechukas-Yukawa gas to 4 significant figures.

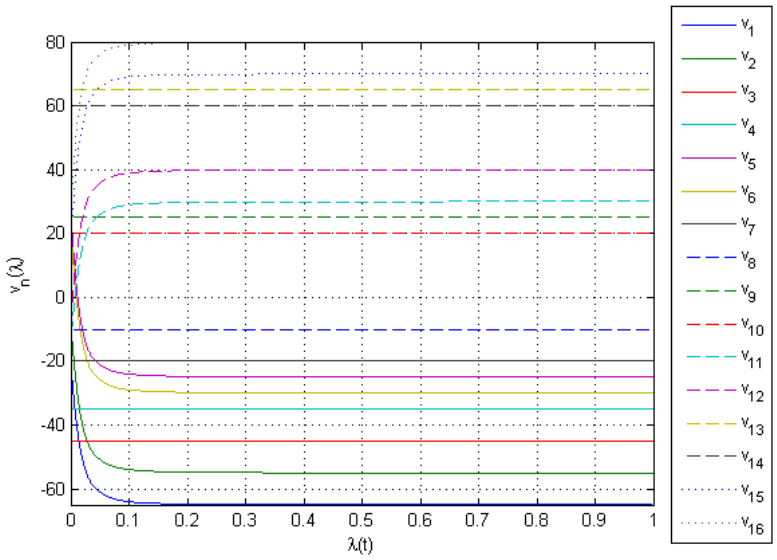

Figure 4.0.2: Plot showing the particle velocities ($v_n(\lambda)$) for the $|00\rangle \rightarrow |00\rangle$ operation of the CNOT gate in the absence of noise.

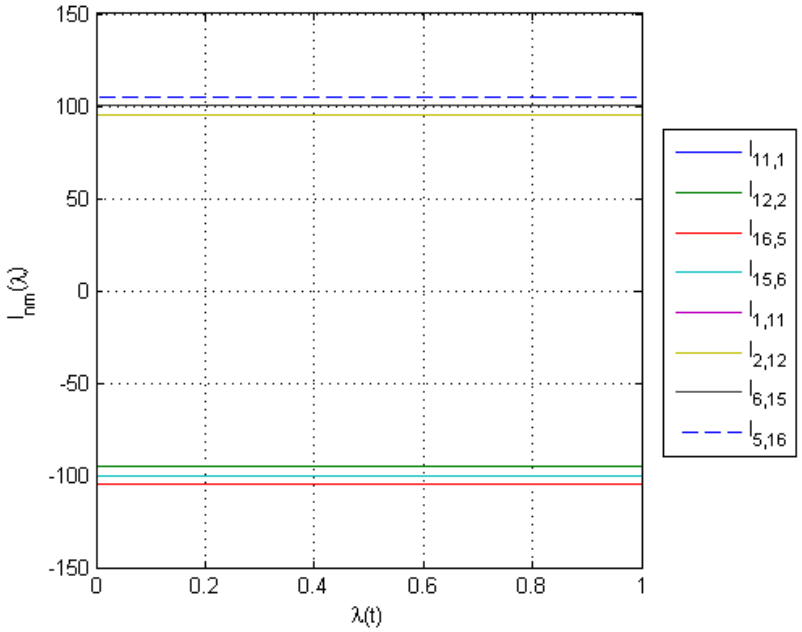

Figure 4.0.3: Plot showing the non-zero particle-particle coupling strengths ($l_{mn}(\lambda)$) for the $|00\rangle \rightarrow |00\rangle$ operation of the CNOT gate in the absence of noise. All the other coupling strengths for this operation are equal to zero at all times.

away from the ideal solution state. This is clearly an undesirable effect on an AQC process and it will be considered in greater detail in the following chapter 5.

The effects of a coloured noise source on the 'time' dependence of the level velocities ($v_n(\lambda)$) and coupling strengths ($l_{mn}(\lambda)$) are shown in Fig. 4.0.5 and Fig. 4.0.6 respectively. In both cases, we see rapid fluctuations when $\lambda(t)$ is close to zero. This is because the noise terms in the equations of motion become the dominant terms in the dynamics, as they depend on the rapidly fluctuating $\delta\dot{h}(\lambda)$ and the inverse of the gaps. The $l_{mn}(\lambda) = 0$ in the ideal case now also show some fluctuation because of the noise term outside the sum in the equation of motion. These results serve to confirm the fact that noise has a considerable effect on the eigenvalue dynamics in the last crucially important moments of the computation process.

As mentioned in section 1.4, the applicability of random matrix theory to closed AQC systems has been studied previously in [17] and [18] by looking at the distributions of gaps in the spectra. We now go on to investigate the effects of noise on the nearest neighbour spacing statistics. The distribution of the average energy gap, $\Delta_{m,m+1}$, at avoided crossings for each noise realisation of the $|00\rangle \rightarrow |00\rangle$ operation at a range of noise amplitudes is shown in Fig. 4.0.7. The distributions are Gaussian in shape and shifted away from zero, which shows that we have level repulsion at avoided crossings, as expected. The mean values of the distributions, $\overline{\Delta_{m,m+1}}$, appear to generally increase with ϵ which can be explained by the fact that noise fluctuations in the trajectories of the energy levels will drive them apart, widening the gaps.

The minimum gap between the ground and first excited states, Δ_{01}, is often seen as the limiting factor in AQC and the results of [17] and [18] suggest that it sometimes shows different behaviour to spacings in the bulk of the spectrum. The spacing distribution for the gaps at avoided crossings between $x_0(\lambda)$ and $x_1(\lambda)$ for the $|00\rangle \rightarrow |00\rangle$ operation are shown in Fig. 4.0.8(a). The distribution is unimodal and has an elongated tail reminiscent of the Wigner distributions of random matrix theory [46]. The mean of the distribution is approximately constant, although we do see some variation as a result of the noise. We also see a degree of level repulsion as the distribution has a lack of small spacings and is shifted away from zero gap. This will be due to the fact that we have intrinsic level repulsion, *i.e.* we have $\Delta_{01} \neq 0$ when $\epsilon = 0$.

In the ground state gap distribution for the $|01\rangle \rightarrow |01\rangle$ operation, shown in Fig. 4.0.8(b), we have a more Poissonian-like distribution with an abundance of smaller gaps, which shows a lack of level repulsion. This is because it has a degeneracy at $\epsilon = 0$ and it therefore has no intrinsic level repulsion and the non-zero gap is created by the noise. The mean gap width, $\overline{\Delta_{01}}$, can be seen to clearly increase

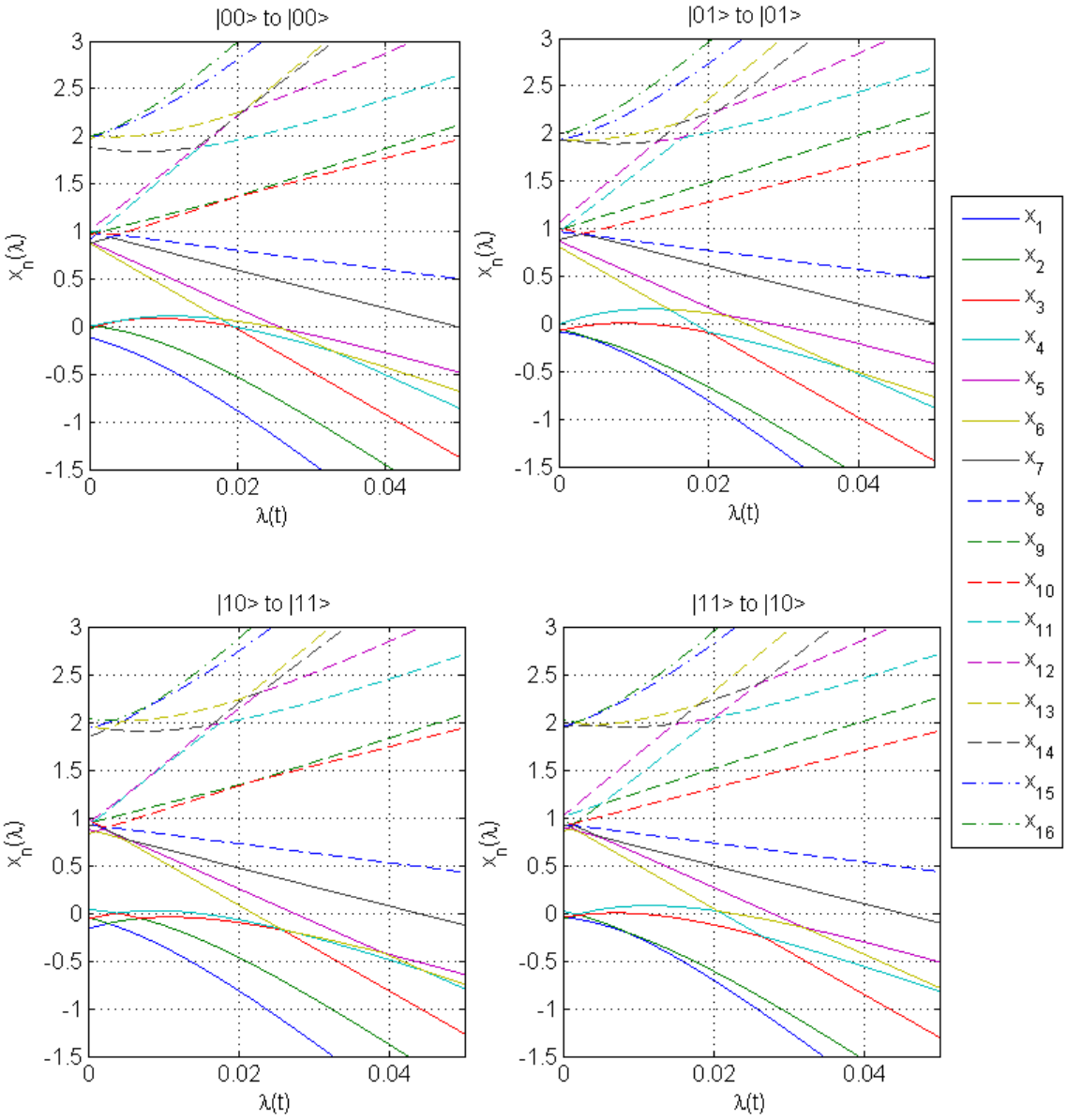

Figure 4.0.4: The energy spectra of the 4 possible operations of the adiabatic CNOT gate in the presence of coloured noise of amplitude $\epsilon = 0.1$.

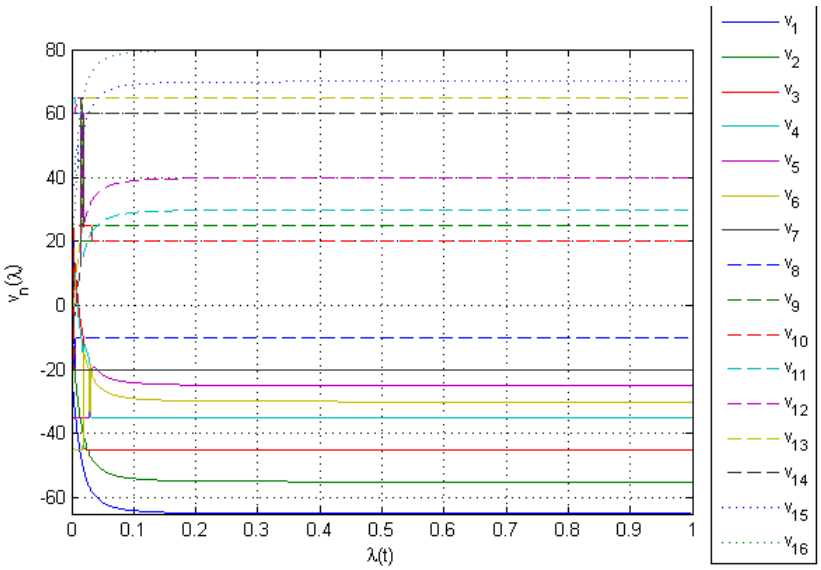

Figure 4.0.5: Plot showing the particle velocities ($v_n(\lambda)$) for the $|00\rangle \rightarrow |00\rangle$ operation of the CNOT gate in the presence of coloured noise of amplitude $\epsilon = 0.1$.

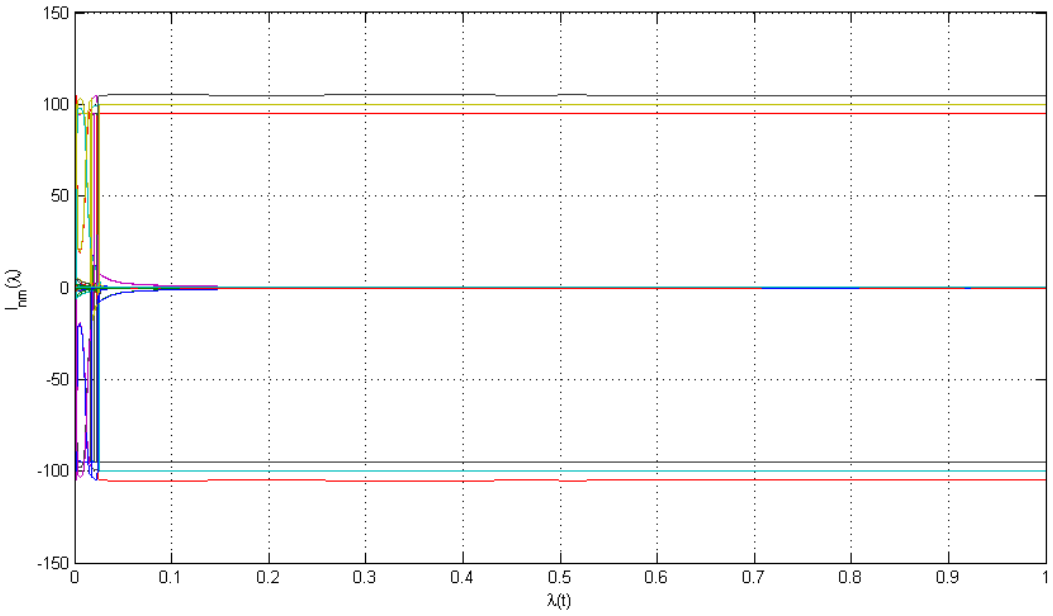

Figure 4.0.6: Plot showing the non-zero particle-particle coupling strengths ($l_{mn}(\lambda)$) for the $|00\rangle \rightarrow |00\rangle$ operation of the CNOT gate in the presence of coloured noise of amplitude $\epsilon = 0.1$.

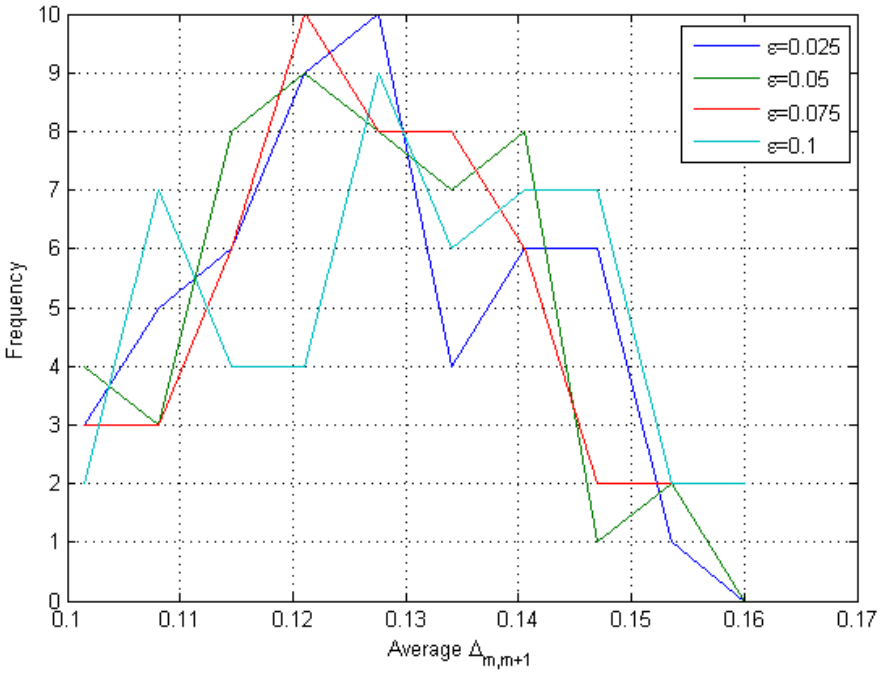

Figure 4.0.7: Plot showing the distributions of average energy gap width ($\Delta_{m,m+1}$) at avoided crossings in the energy spectra of each noise realisation for the $|00\rangle \rightarrow |00\rangle$ operation of the CNOT gate at a range of noise amplitudes. The mean values of the distributions are $\overline{\Delta_{m,m+1}} = 0.1262,\ 0.1250,\ 0.1275$ and 0.1296 for $\epsilon = 0.025,\ 0.05,\ 0.075$ and 0.1 respectively.

proportionally with the noise amplitude. The ground state spacing distributions for the $|10\rangle \rightarrow |11\rangle$ and $|11\rangle \rightarrow |10\rangle$ operations are similar to that of the $|01\rangle \rightarrow |01\rangle$ operation, as they also have no intrinsic level repulsion.

For spacings between states in the bulk of the spectrum we will have some multimodal distributions as they tend to be involved in a greater number of avoided crossings. An example of this is shown in Fig. 4.0.9 for Δ_{45} for the $|01\rangle \rightarrow |01\rangle$ operation, where we have a Poissonian peak at small spacings and then a Gaussian peak at larger spacings.

The Brody parameter offers a convenient method of determining whether an energy spectrum is regular or irregular. If the system's spectrum is regular we know that its dynamics are controlled by symmetries and conservation laws; whereas if they are irregular, the dynamics will be complex and chaotic resulting from a lack of symmetries. The Brody distribution interpolates from a regular Poissonian nearest neighbour spacing distribution at $q = 0$ to an irregular Wigner nearest neighbour spacing distribution for the GOE at $q = 1$,

$$p(s) = (q+1)a_q s^q e^{-a_q s^{q+1}} \tag{4.0.1}$$

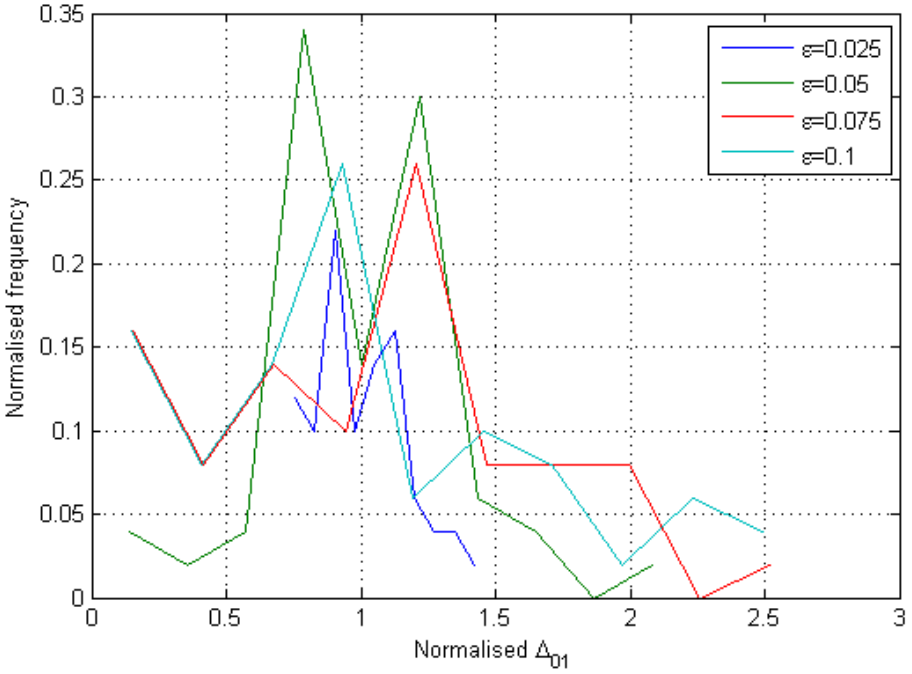

(a) $|00\rangle \rightarrow |00\rangle$

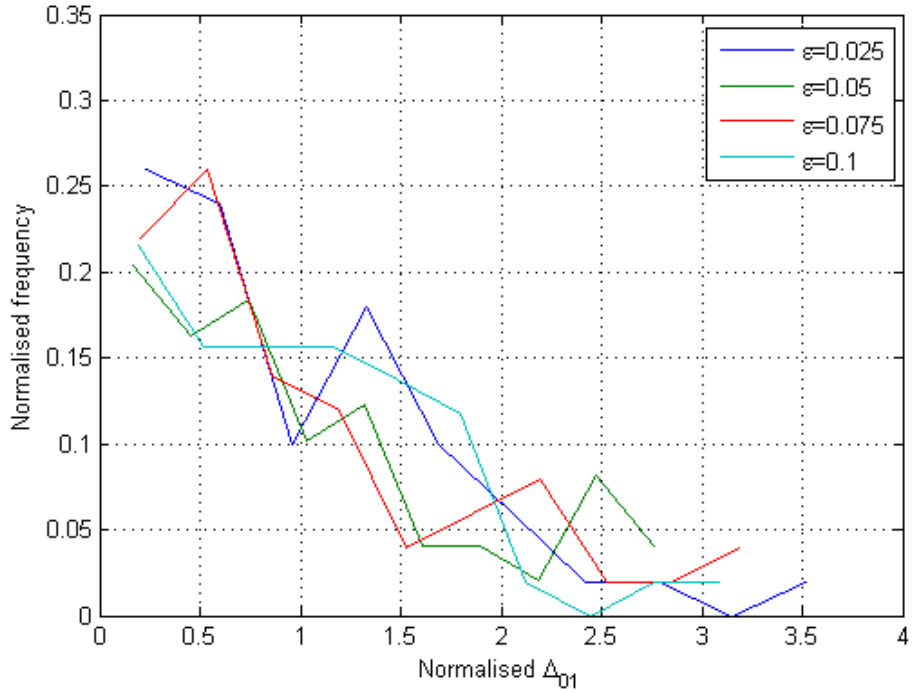

(b) $|01\rangle \rightarrow |01\rangle$

Figure 4.0.8: Distribution of minimum ground state energy gaps for the $|00\rangle \rightarrow |00\rangle$ and $|01\rangle \rightarrow |01\rangle$ operations of the CNOT gate at a range of noise amplitudes. The gap width is renormalised by $\Delta_{01}/\overline{\Delta_{01}}$. The mean values of the distributions for $\epsilon = 0.025,\ 0.05,\ 0.075$ and 0.1 respectively are: $\overline{\Delta_{01}} = 0.0480,\ 0.0461,\ 0.0399$ and 0.0423 for the $|00\rangle \rightarrow |00\rangle$ operation and $\overline{\Delta_{01}} = 0.0007,\ 0.0013,\ 0.0017$ and 0.0029 for the $|01\rangle \rightarrow |01\rangle$ operation.

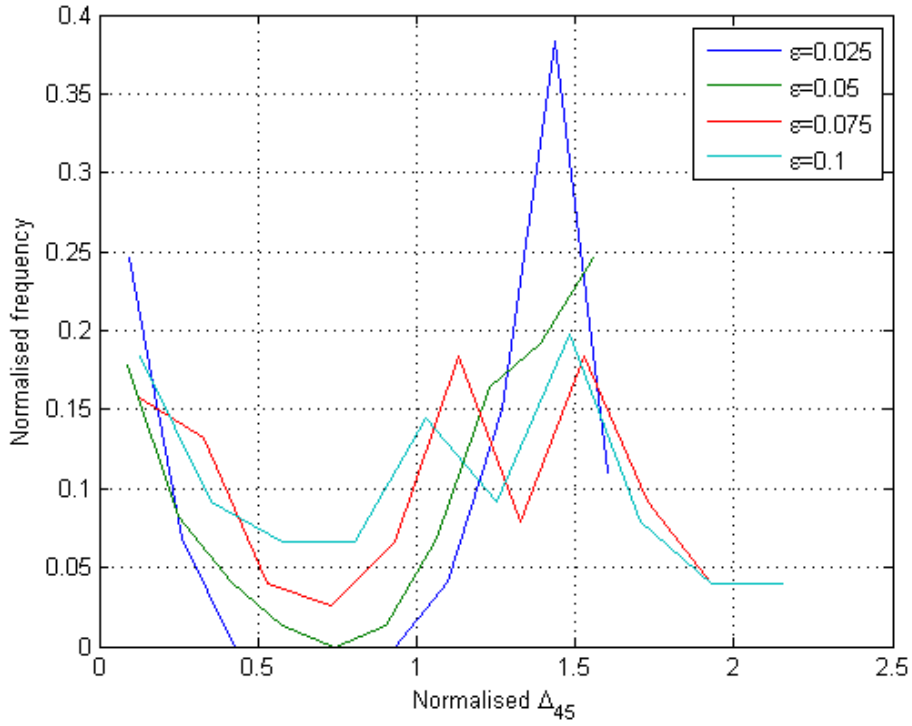

Figure 4.0.9: Distribution of minimum gaps between $x_4(\lambda)$ and $x_5(\lambda)$ in the bulk of the spectrum for the $|01\rangle \rightarrow |01\rangle$ operation of the CNOT gate at a range of noise amplitudes. The gap width is renormalised by $\Delta_{45}/\overline{\Delta_{45}}$. The mean values of the distributions are $\overline{\Delta_{45}} = 0.1190,\ 0.1236,\ 0.1171$ and 0.1249 for $\epsilon = 0.025,\ 0.05,\ 0.075$ and 0.1 respectively.

where q is the Brody parameter,

$$a_q = \left[\Gamma\left(\frac{q+2}{q+1}\right)\right]^{q+1}, \tag{4.0.2}$$

s are the dimensionless nearest neighbour energy gaps and $\Gamma(q)$ is Euler's gamma function [46]. The Brody parameter therefore acts as a measure of the regularity of an energy spectrum. In order to calculate the Brody parameter we must first renormalise the density of states to unit average local level density, so that spacings across the spectrum are comparable. This procedure is known as unfolding and was done by smoothing the integrated density of states by fitting a cubic spline to it; the unfolded energy eigenvalues were then taken from the equation for the spline. The Brody distribution function can then be fitted to the nearest neighbour spacing distribution of the unfolded energy levels so that the Brody parameter for the spectrum can be extracted. This procedure was carried out for the energy levels, x_n, at each point in $\lambda(t)$ and the average value of the Brody parameter as a function of 'time' was calculated for each of the four CNOT gate operations.

The results for $\epsilon = 0$ and 0.1 are shown in Fig. 4.0.10 and we can see that the increase in irregularity is negligibly small, which is surprising considering we have a reasonably large random matrix term, $\delta h(\lambda)$, in the system's Hamiltonian. This suggests that the overall dynamics of the system are dominated by the problem (H_0) and the bias (H_b) Hamiltonians as opposed to the irregularities caused by the noise. These results could suffer from small sample size effects as we have a relatively small spectrum of 16 levels, but as shown in [49] averaging over an ensemble of noise instances should alleviate these.

We have studied the effects of noise on the operations of the adiabatic CNOT gate by looking at their eigenvalue dynamics and spectral statistics. We have shown that there exists a number of level crossings in the spectra for the case of an ideal noise-free system ($\epsilon = 0$). Crucially, in some cases there are level crossings between the ground and first excited state, which means there will be a zero probability of successfully remaining in the ground state. The introduction of noise into the system breaks all the degeneracies, allowing a finite success probability. As the amplitude of the noise is increased we see a widening in the gaps at avoided crossings. The irregular noise term does introduce some fluctuations into the eigenvalue dynamics, but we have shown that the overall dynamics of the system remain regular even at relatively large noise amplitudes. This suggest that the system has a degree of inherent stability and robustness against the effects of noise.

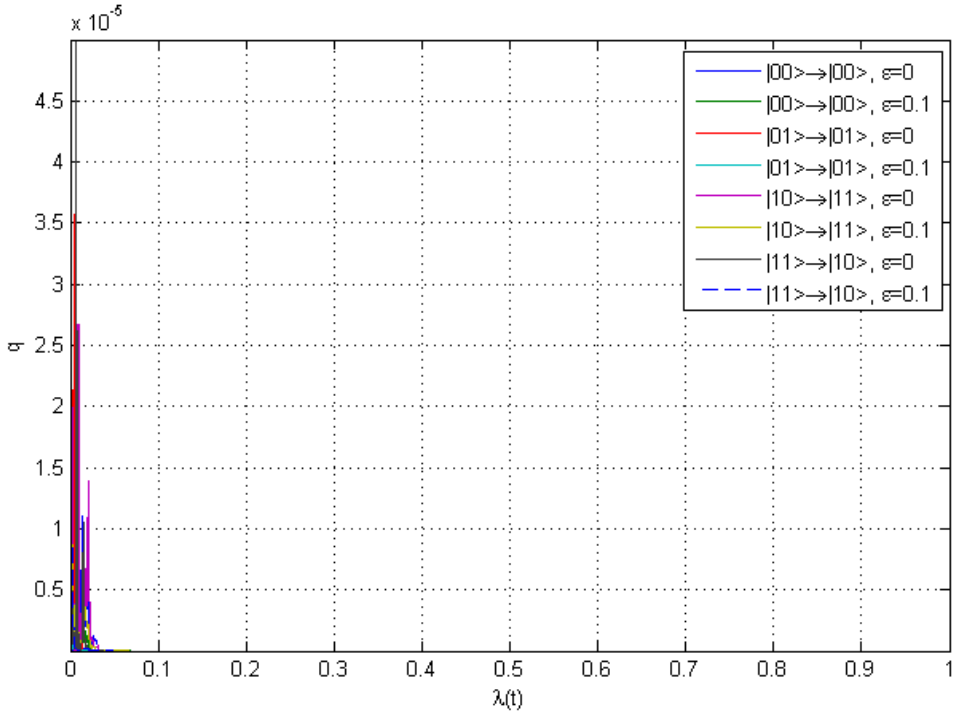

Figure 4.0.10: The Brody parameter, q, as a function of 'time' for all four operations of the CNOT gate with $\epsilon = 0$ and 0.1. These values of q are found by fitting the Brody distribution to the unfolded nearest neighbour spacing distribution and the average value of the coefficient of determination was $R^2 = 0.7488$.

Chapter 5

The statistics of level occupation for the CNOT gate

It is desirable to be able to run an adiabatic quantum computation process relatively quickly, but at the same time we must try to ensure that the system remains in the ground state so that solution can be accurately read out. Therefore, a compromise between speed and adiabaticity must be reached. Knowledge of the relationship between the computation rate or speed, $\dot{\lambda} = 1/T$, and the success probability, *i.e.* the probability of the system being found in the ground state at $\lambda(t) = 0$ given that it was initially in the ground state with certainty, $P(0(\lambda = 0)|0(\lambda = 1))$, will be very informative when trying to find this balance. The effects of noise on this relationship are also an important consideration that should be taken into account. In order to investigate this relationship, the energy spectra for an ensemble of 50 random noise realisations for each of the 4 CNOT gate operations were generated using the numerical techniques discussed in section 2.3 for solving the generalised Pechukas-Yukawa system ((2.1.34)). These spectra were then analysed using the level occupation algorithm described in section 2.3 to find the average success probabilities at a range of different computation speeds. It is important to note that this algorithm allows us to calculate the probability of the system being found in the final ground state of the system's total Hamiltonian (*i.e.* $\mathcal{H}(\lambda = 0) = H_f + \delta h(\lambda = 0) = (H_{CNOT} + H_{input}) + \delta h(\lambda = 0))$ as opposed to the solution state (*i.e.* the ground state of $H_f = H_{CNOT} + H_{input}$). The distinction between these two variables when noise comes into effect will be discussed later on in this section.

The success probability as a function of computation speed for the $|00\rangle \rightarrow |00\rangle$ operation at a range of noise amplitudes is shown in Fig. 5.0.1, including the case of an ideal closed system ($\epsilon = 0$). In general, we see a polynomial increase in

success probability as the speed decreases, *i.e.* $P \propto T^{-\gamma}$. As the speed decreases further we find that the success probability tends to unity, as expected from the adiabatic theorem (1.2.14). These general trends and the polynomial dependence are in agreement with the findings of [40] for random problem Hamiltonians drawn from the GUE. A fit to the polynomial region of the $\epsilon = 0$ curve yields a scaling exponent of $\gamma \approx 4/3$, whereas for $\epsilon > 0$ we find the scaling exponents to all be $\gamma \approx 1$. The fact that this scaling remains constant as ϵ increases is heartening in terms of the performance of AQC. When the noise source is switched on we see a significant prefactor shift of the curves towards slower speeds as well as a decrease in γ. This means that in some situations a speed 10^2 slower is required to achieve the same chance of success. This is because the introduction of noise will split any degeneracies into avoided crossings and it will also lead to fluctuations in the level trajectories creating more avoided crossings. This increase in the number of avoided crossings results in more opportunities for the system to be excited out of the ground state and into higher levels, therefore a significantly slower speed is required to achieve the same success probability as in the ideal case. This effect is clearly not favourable, but some degree of noise is an inevitability in any physical system and its effects must be considered.

An interesting feature to note in Fig. 5.0.1 is that, as ϵ increases we see a prefactor shift in the curves back towards faster computation speeds. This can be seen as being beneficial in the context of AQC as it means that the success probability at a given computation speed increases linearly with noise amplitude.This occurs because stronger noise fluctuations will widen the energy gaps at avoided crossings, as predicted by Fig. 4.0.7 where the average energy gaps generally increase with noise amplitude, and therefore decrease the chance of excitation at that particular avoided crossing. However, at $|\dot{\lambda}| \approx 10^{-5}$ we see a change in the scaling and the curves of increasing amplitude reverse in order. This can be explained by looking at whether higher levels come into play in terms of the occupation, as shown in Fig. 5.0.2. For small ϵ, we see a very sudden switch from $P_1 \gg P_0$ to $P_0 \gg P_1$ at $|\dot{\lambda}| \approx 10^{-5}$ and no occupation of the higher levels. This shows that the avoided crossing between $x_0(\lambda)$ and $x_1(\lambda)$ is the limiting factor, meaning the success probability saturates quickly and the gradient of the logarithmic plot stays constant. For larger ϵ, we have a more complicated evolution of the level occupation as higher levels come into effect and therefore the switch from $P_1 \gg P_0$ to $P_0 \gg P_1$ is not as sudden meaning the success probability saturates more slowly and the gradient decreases. This slow down in scaling is proportional to ϵ which leads to the reversal of the ordering of curves of constant ϵ seen in Fig. 5.0.1.

The dependence of the success probability on the computation speed for the

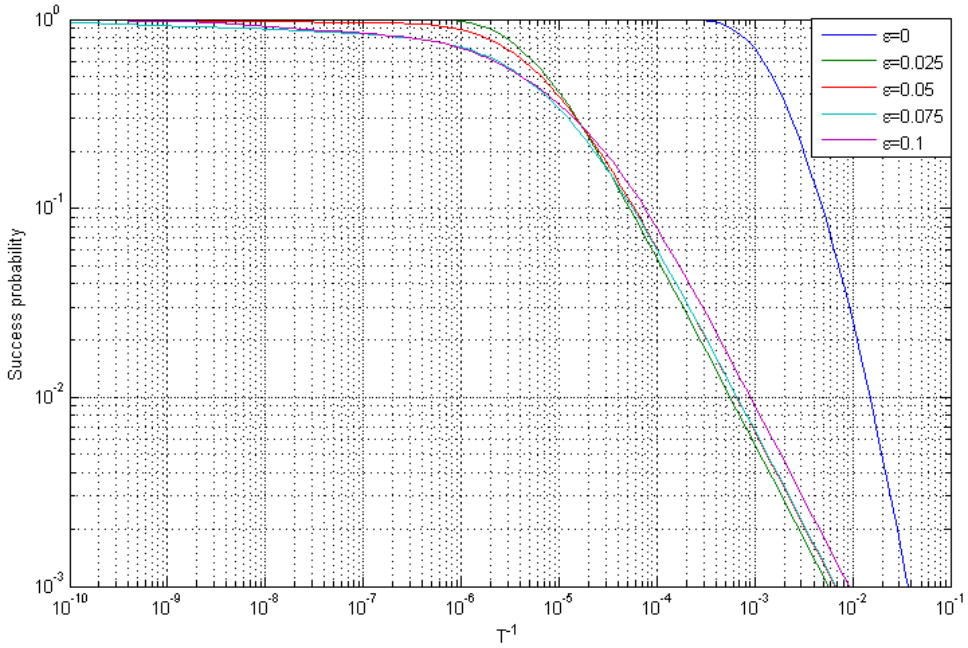

Figure 5.0.1: Plot of average success probability against computation speed for the $|00\rangle \rightarrow |00\rangle$ operation of the CNOT gate at various noise amplitudes.

$|01\rangle \rightarrow |01\rangle$ operation of the CNOT gate is shown in Fig. 5.0.5. For this operation, we do not have a curve for an ideal system ($\epsilon = 0$) to compare the effects of noise against, as the success probability will be zero at all speeds when $\epsilon = 0$, because of degeneracy between the ground and first excited states. The same general trends seen in Fig. 5.0.1 hold true in Fig. 5.0.3, in that the success probability increases polynomially with computation time before saturating at one. In this case, we also have constant scaling exponents of $\gamma \approx 1$ and therefore an approximately inverse linear relationship between success probability and computation speed. We can also see that the prefactor shift of the curves is much greater than in Fig. 5.0.1. This will be due to the fact that noise will have a much greater influence on the gap widths at avoided crossings, as they are the result of noise-induced level splitting in this case. The increase in success probability with noise amplitude remains for all speeds and we do not see the reversal seen in Fig. 5.0.1. This is because the noise-induced ground state gaps in the spectrum of the $|01\rangle \rightarrow |01\rangle$ operation are generally narrower than those seen in the spectrum of the $|00\rangle \rightarrow |00\rangle$ operation and therefore the occupation will still be able to spread into higher excited states at relatively slow speeds. This means we do not see the sudden switch in behaviour as ϵ increases that we have for the $|00\rangle \rightarrow |00\rangle$ operation.

Another feature in Fig. 5.0.3 is the fluctuation in the $\epsilon = 0.1$ curve at $|\dot{\lambda}| \approx 10^{-3}$. This can again be explained by looking at the role that higher levels play in the level

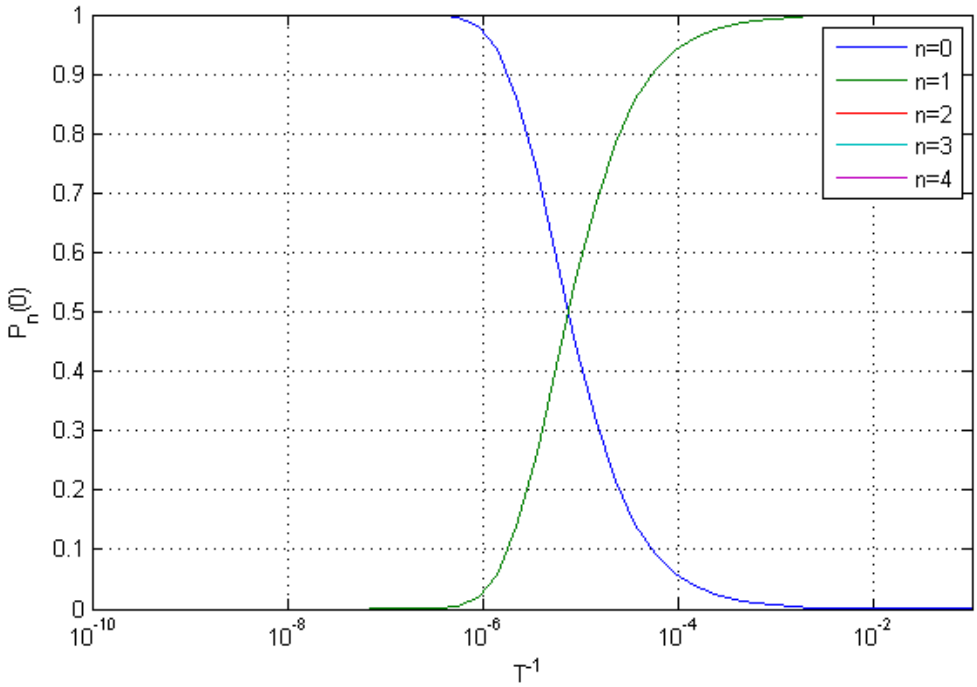

(a) $\epsilon = 0.025$

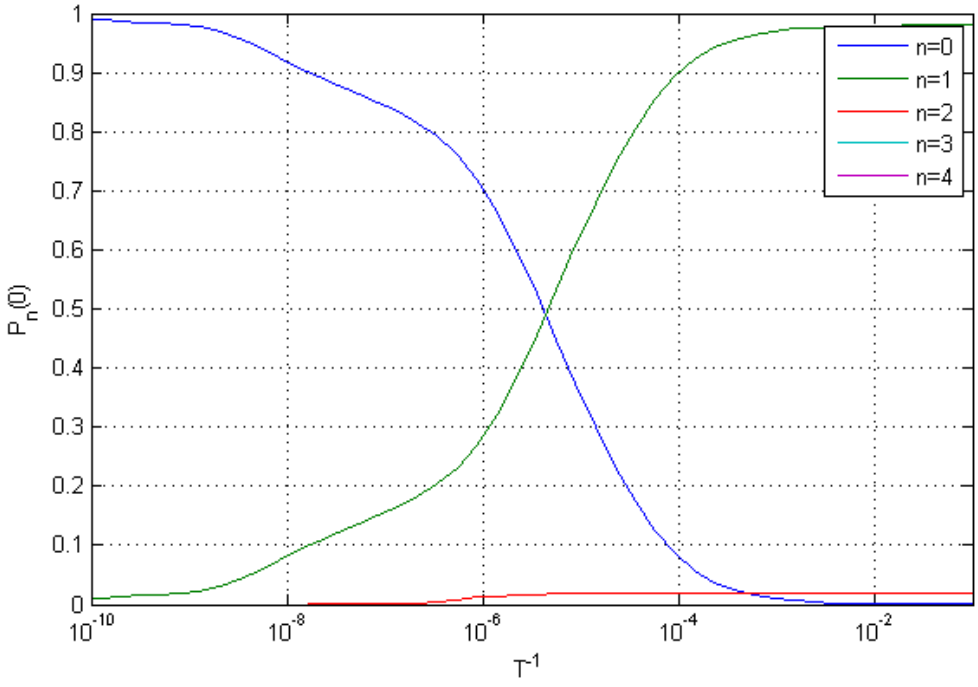

(b) $\epsilon = 0.1$

Figure 5.0.2: Plot of average occupation of the lowest 5 levels at $\lambda(t) = 0$ for the $|00\rangle \rightarrow |00\rangle$ operation at $\epsilon = 0.025$ and 0.1. The occupation of all levels above $n = 4$ is zero.

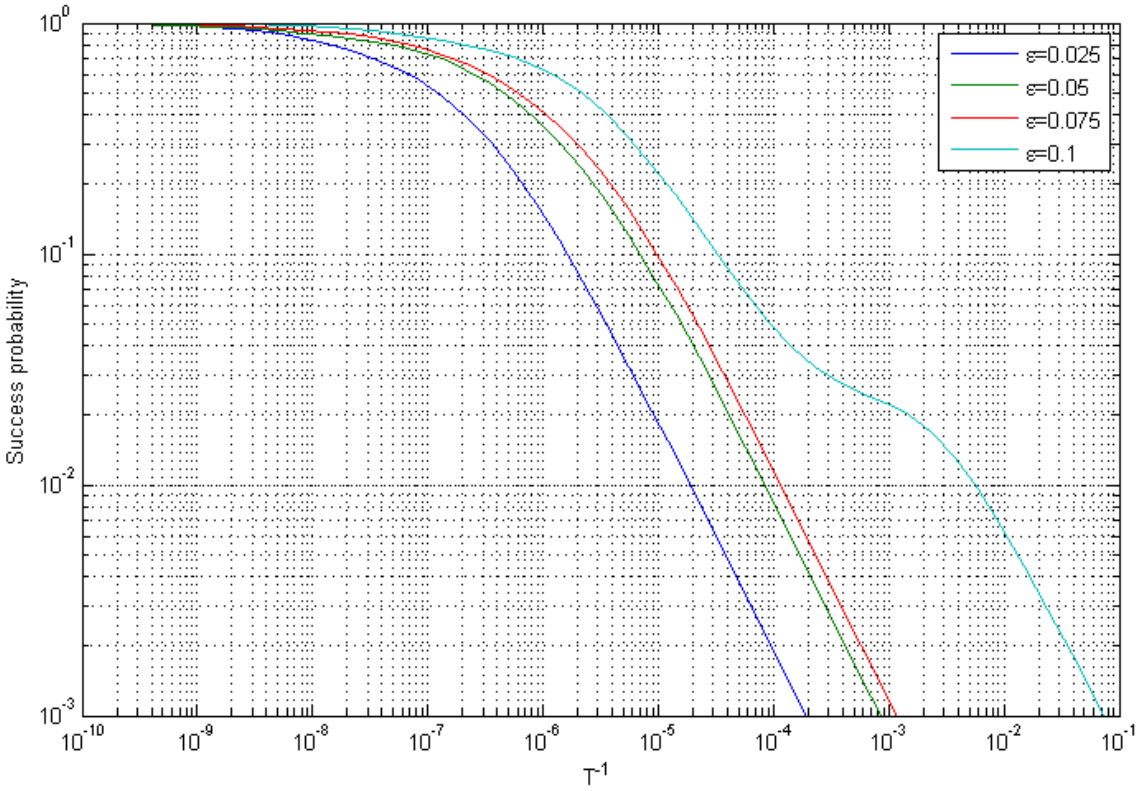

Figure 5.0.3: Plot of average success probability against computation speed for the $|01\rangle \rightarrow |01\rangle$ operation of the CNOT gate at various noise amplitudes.

occupation statistics. Figure 5.0.4 shows that at $|\dot{\lambda}| \approx 10^{-3}$ the occupation of the first and second excited states both fall away quickly as the success probability increases. This switch in occupations will lead to the fluctuation we see in Fig. 5.0.3.

The dependence of the success probability on the computation speed and noise amplitude for the $|10\rangle \rightarrow |11\rangle$ and $|11\rangle \rightarrow |10\rangle$ operations of the CNOT gate are shown in Fig. 5.0.5 and Fig. 5.0.6 respectively. They both show very similar trends to the $|01\rangle \rightarrow |01\rangle$ case in Fig. 5.0.3 and in all three cases we find a constant scaling exponent of $\gamma \approx 1$. This is to be expected as they all have similar spectra, where noise fluctuations and symmetry breaking create the sequences of avoided crossings across which the occupation diffuses. There is a kink in the $\epsilon = 0.025$ curve of Fig. 5.0.5; this can be explained by the same mechanism that causes the one seen in the $\epsilon = 0.1$ curve of Fig. 5.0.3. We can also see that the $\epsilon = 0.05$ and $\epsilon = 0.075$ curves in Fig. 5.0.6 cross; this is readily explained by the mechanism that leads to the crossing of curves of constant ϵ in the $|00\rangle \rightarrow |00\rangle$ case.

As we have seen, there are situations where an increase in noise amplitude will increase the success probability of an AQC process, but it may not be wholly beneficial, as it will also drive the final state of the system away from the desired solution

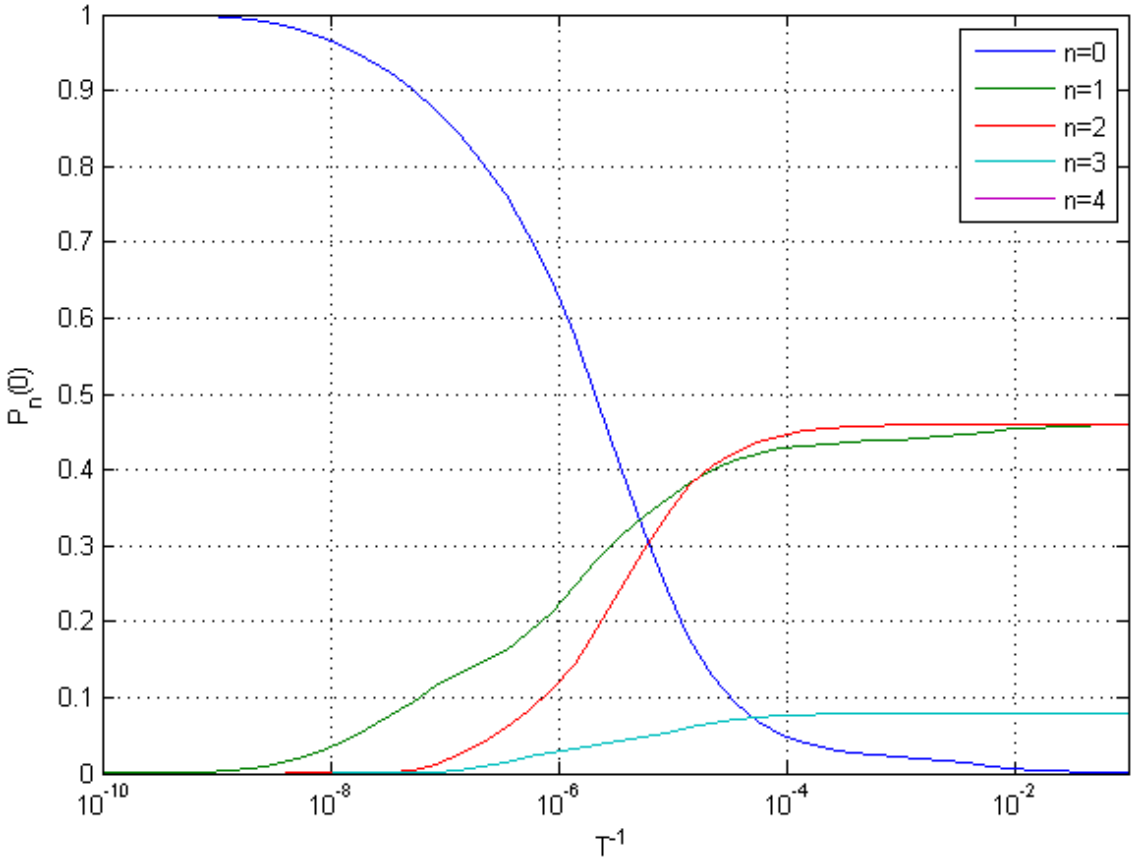

Figure 5.0.4: Plot of average occupation of the lowest 5 levels at $\lambda(t) = 0$ for the $|01\rangle \rightarrow |01\rangle$ operation at $\epsilon = 0.1$. The occupation of all levels above $n = 4$ is zero.

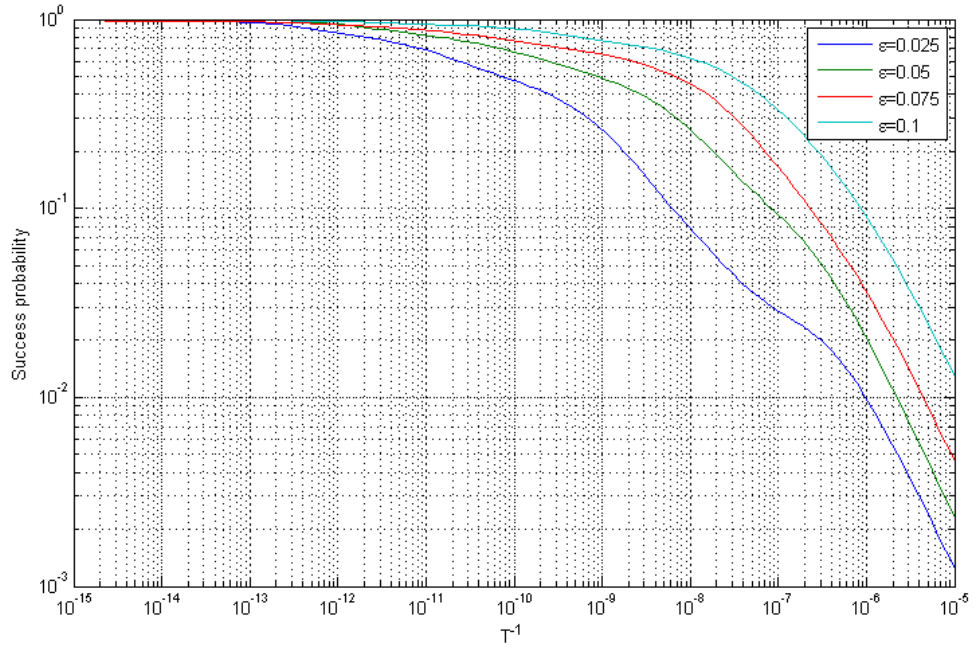

Figure 5.0.5: Plot of average success probability against computation speed for the $|10\rangle \rightarrow |11\rangle$ operation of the CNOT gate at various noise amplitudes.

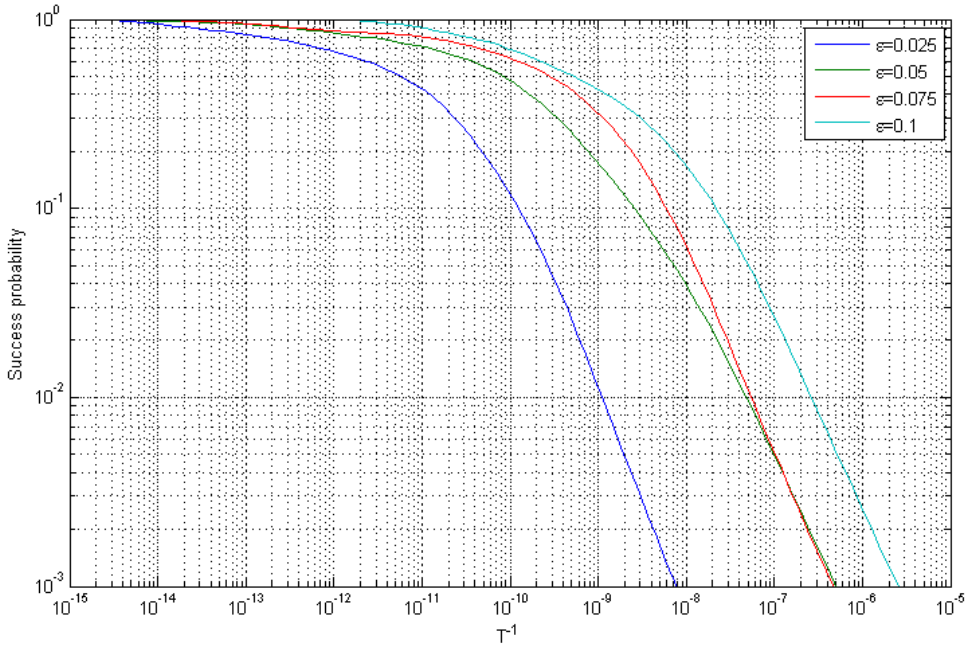

Figure 5.0.6: Plot of average success probability against computation speed for the $|11\rangle \rightarrow |10\rangle$ operation of the CNOT gate at various noise amplitudes.

state. This will affect the probability of the measurement of the final state yielding the correct result. This is a different issue to the aforementioned success probability in that, even if the system evolves at an infinitely slow rate, so that it will be in the ground state at $\lambda = 0$ with certainty, if noise perturbations have driven $|\psi(\lambda = 0)\rangle$ away from the ideal solution state the correct answer will not always be found upon measurement. This is an important effect that must be accounted for when we are studying the effect of noise in an AQC system.

To investigate this we introduce a measure of closeness between the ideal ground state (*i.e.* when $\epsilon = 0$) and the noise perturbed ground state (*i.e.* where $\epsilon > 0$), namely the fidelity of the final state;

$$F = |\langle 0_{ideal}(\lambda = 0)|0_{noise}(\lambda = 0)\rangle|^2 . \tag{5.0.1}$$

We calculate the fidelity by direct diagonalisation of; $H_0 = H_{CNOT} + H_{input}$ to find $|0_{ideal}(\lambda = 0)\rangle$ and, $H_0 + \delta h(0)$ to give $|0_{noise}(\lambda = 0)\rangle$. This is then averaged over an ensemble of noise realisations. Another way of taking this issue into account would be to define success probability of an AQC in the presence of noise as $P = |\langle 0_{ideal}|\psi(0)\rangle|^2$ instead of simply the ground state occupation at $\lambda = 0$, as in [7]. This is not possible with our current approach as we do not have specific knowledge of the state vector, but we can look at the relationship between these two important factors.

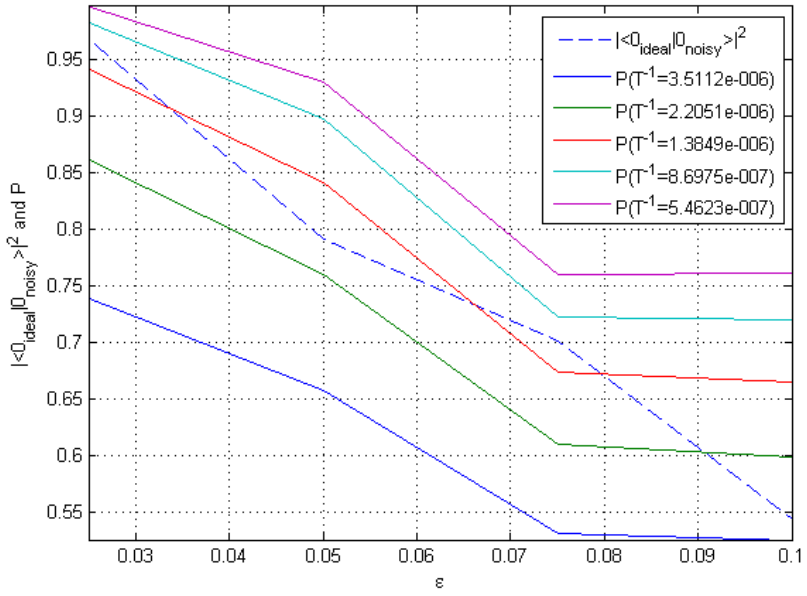

Figure 5.0.7: Plot showing the average fidelity of the final state and average success probability as functions of noise amplitude for the $|00\rangle \rightarrow |00\rangle$ operation.

In other recent work [50] (manuscript included in appendix C), we investigated the time average of this quantity for a large set of random problem instances and found that it generally increased smoothly with the final ground state occupation, although these results did not take into account the effects of noise.

The fidelity of the final state and the success probability of the $|00\rangle \rightarrow |00\rangle$ operation are shown as functions of noise amplitude in Fig. 5.0.7. As ϵ increases, $|0_{noise}(\lambda = 0)\rangle$ is driven further away from $|0_{ideal}(\lambda = 0)\rangle$ and the fidelity decreases linearly. We can also clearly see that success probabilities that are comparable to the fidelity lie at speeds above the reversal in Fig. 5.0.1, as they too decrease linearly with ϵ.

Figure 5.0.8 shows the relationship between the fidelity, success probability and noise amplitude for the $|01\rangle \rightarrow |01\rangle$ operation of the CNOT gate. In this case, we can see that the success probability at a given speed increases linearly with ϵ, whereas the fidelity of the final state decreases linearly, so we have a trade-off between these two effects. Therefore, at the intersection of the lines we have an optimal noise amplitude that maximises both the fidelity and the success probability.

The fidelity and the success probability of the $|10\rangle \rightarrow |11\rangle$ and $|11\rangle \rightarrow |10\rangle$ operations behave in a similar fashion to the $|01\rangle \rightarrow |01\rangle$ operation, as seen in Fig. 5.0.9 and Fig. 5.0.10 respectively. This is because their spectra show similar trends and properties and therefore they show similar behaviour with respect to level occupation.

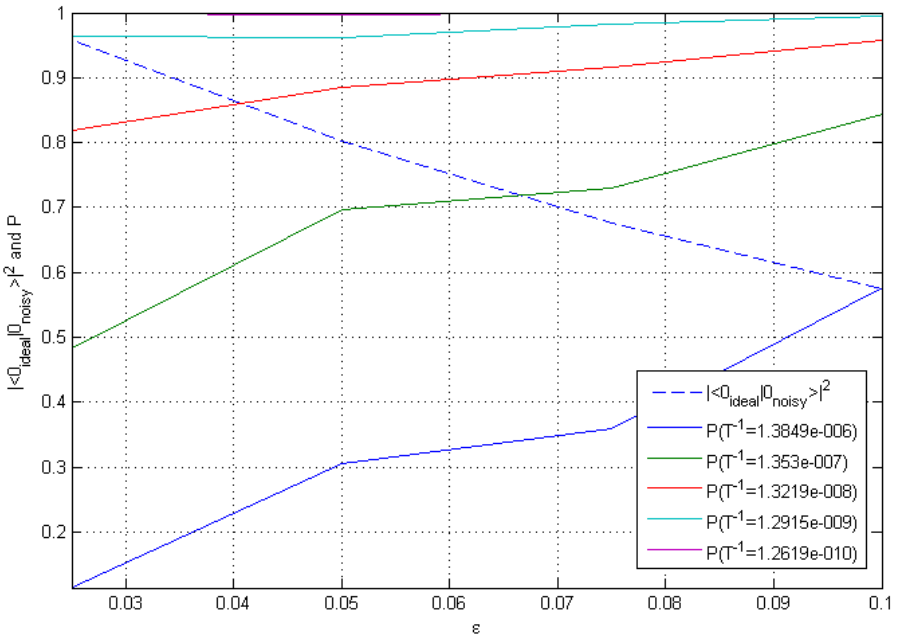

Figure 5.0.8: Plot showing the average fidelity of the final state and average success probability as functions of noise amplitude for the $|01\rangle \rightarrow |01\rangle$ operation.

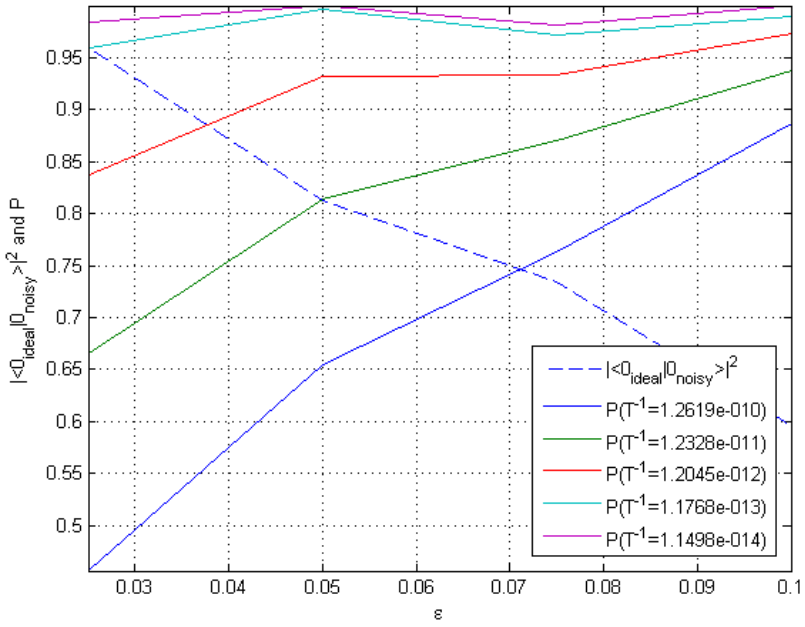

Figure 5.0.9: Plot showing the average fidelity of the final state and average success probability as functions of noise amplitude for the $|10\rangle \rightarrow |11\rangle$ operation.

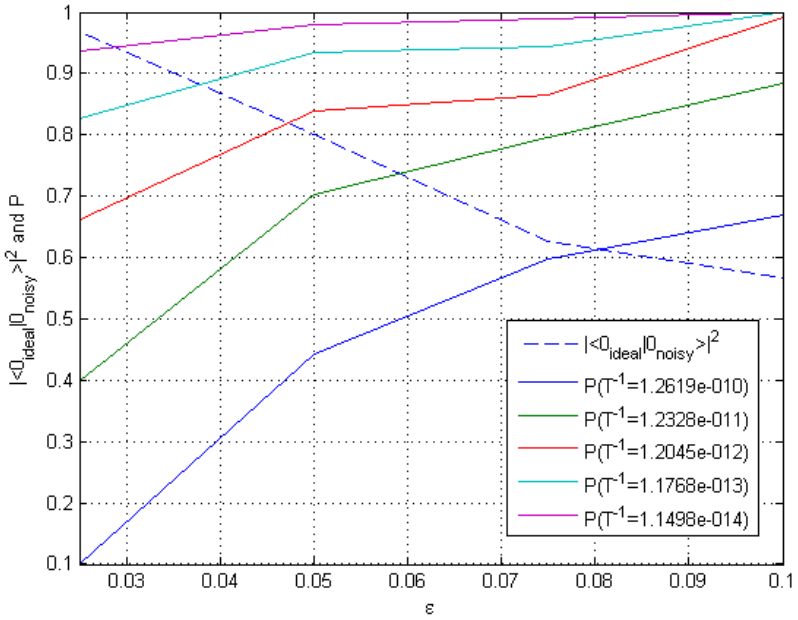

Figure 5.0.10: Plot showing the average fidelity of the final state and average success probability as functions of noise amplitude for the $|11\rangle \rightarrow |10\rangle$ operation.

Certain types of algorithms, particularly optimisation problems like the traveling salesman (TSP), are suited to a less stringent version of AQC known as approximate adiabatic quantum computation (AAQC). In AAQC we require only that the system remains close to, but not necessarily in, its ground state, as for optimisation problems like the TSP this will still yield a near-optimal result. This relaxation of requirements will allow the computation process to be run at significantly faster speeds [51]. The fact that we do not see a significant deviation away from the ground state in Fig. 5.0.2 and Fig. 5.0.4, even when the success probability ~ 0, for a generic adiabatic algorithm is a promising result for AAQC.

To summarise, we have found that the success probability of the CNOT gate algorithm scaled polynomially as a function of computation speed. This scaling was shown to be independent of the amplitude of the noise, which is a promising point to note in terms of the performance of a realistic AQC process. Somewhat counterintuitively, we have also seen that in some situations, noise increases the success probability at a given speed, particularly when there are degeneracies in the energy spectra. However, it was noted that this increase comes at the expense of the fidelity of the final state, but an optimal compromise between the two factors exists. We have shown that an insight into spectral properties and statistics can be useful when trying to explain level occupation phenomena.

Chapter 6

The CNOT gate with an artificial noise source

In the previous chapter, 5, we saw that the intrinsic noise in a physical system can improve the performance of an AQC in some situations. We now look at this from a different viewpoint and envisage a system with a negligibly low level of intrinsic noise and try to enhance its performance by adding a specifically tailored artificial noise source. This can be seen as a stochastic search for an alternative, and possibly more efficient, path between the initial and final Hamiltonians than simple linear interpolation.

To achieve this we require a perturbation term with a time-dependent amplitude, which is large enough to widen the energy gaps at avoided crossings throughout the majority of the computation process but then tends to zeros as $\lambda(t) \to 0$. We need to be particularly careful in the region where $\lambda(t) \gtrsim 0$ where the energy levels are densely packed and the majority of excitation occurs, as we would like to retain positive effects of noise, while at the same time minimising the negative effect on the fidelity of the final state. As an example of this scheme, we retain the same noise model used throughout this work except that we introduce a time-dependent amplitude of the form

$$\epsilon(\lambda) = \epsilon_0 \tanh(\alpha\lambda), \tag{6.0.1}$$

where α is a constant determining the rate of decay as $\lambda(t) \gtrsim 0$.

The dependence of the success probability on the computation speed for the $|00\rangle \to |00\rangle$ operation with an artificial noise source is shown Fig. 6.0.1. The constant α was varied in order to find the type of behaviour we were looking for. It was found that a value of $\alpha = 10$ yielded a significant prefactor improvement, up to 10^2 in some cases, over the results for a noise source with a constant amplitude. This improvement occurs because we have strong noise fluctuations that drive the levels

and their trajectories away from each other in the early part of the computation process where there is little chance of excitation. Then as the system moves into the critical final part of the evolution where the levels are densely packed, the strength of the artificial perturbations are reduced to zero to avoid creating any more avoided crossings and therefore reducing the chance of excitation.

The effects of an artificial noise source on the success probabilities of the other operations of the CNOT gate are shown in Fig. 6.0.2, Fig. 6.0.3 and Fig. 6.0.4. A value of $\alpha = 10$ was again used and the results are compared to those for a noise source with a constant amplitude. We again see a significant prefactor improvement. Particularly for the $|11\rangle \rightarrow |10\rangle$ operation, where there is a remarkable improvement of over 5 orders of magnitude. These improvements will occur for the same reasons described for the $|00\rangle \rightarrow |00\rangle$ operation.

Another advantage of this scheme is the fact that the artificial noise will not affect the fidelity of the final state. As we can see from (6.0.1), $\epsilon(0) = 0$ and therefore the final ground state will coincide with the desired solution state yielding $F = 1$.

In this chapter we have shown that it is possible to drastically improve the performance of an AQC by the addition of a specifically engineered artificial noise source. This would allow the same computation to be run at speeds of up to 10^5 times faster while still maintaining the same success probability. This scheme can also be realised in such a way that it will have no adverse effect on the fidelity of the final ground state. Although these results are heartening, it is important to note that they are based on the assumption that we have a physical system with a negligibly small amount of intrinsic noise, which in terms of current technologies is fairly unrealistic. Despite this, these results do lend support to the idea that simple linear interpolation between initial and final Hamiltonians is not always the most efficient evolution path. This idea is an important consideration which should be taken account of when discussing the performance of AQC, e.g. as in [20].

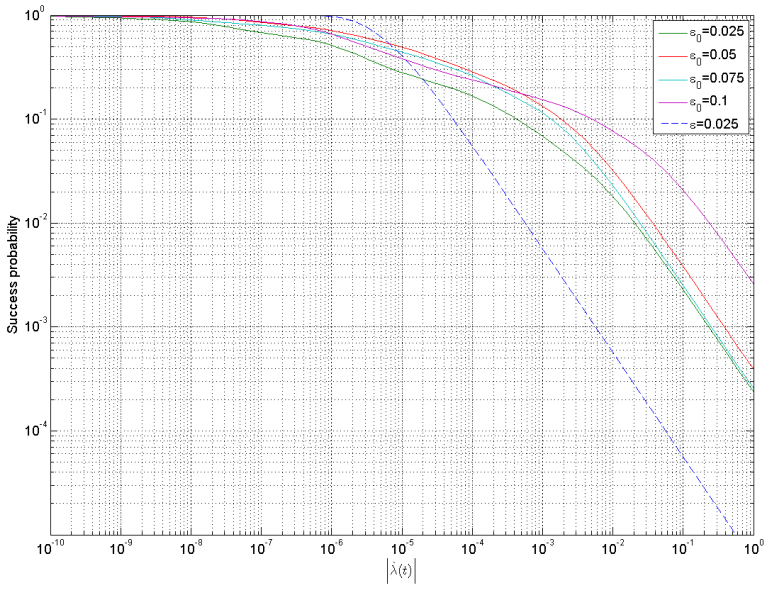

Figure 6.0.1: Plot of average success probability against computation speed for the $|00\rangle \rightarrow |00\rangle$ operation of the CNOT gate with an artificial noise source at a range of values for ϵ_0 and $\alpha = 10$. For comparative purposes, the results for a noise source with a constant amplitude of $\epsilon = 0.025$ are also shown.

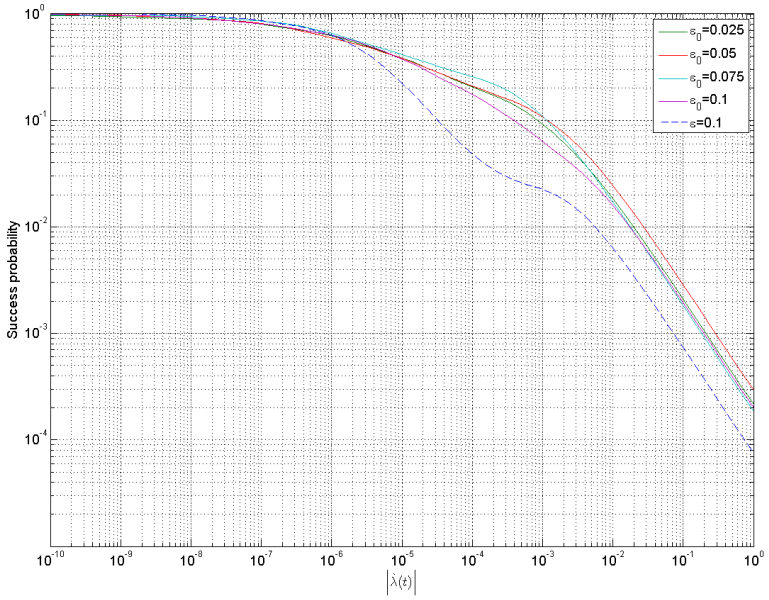

Figure 6.0.2: Plot of average success probability against computation speed for the $|01\rangle \rightarrow |01\rangle$ operation of the CNOT gate with an artificial noise source at a range of values for ϵ_0 and $\alpha = 10$. For comparative purposes, the results for a noise source with a constant amplitude of $\epsilon = 0.1$ are also shown.

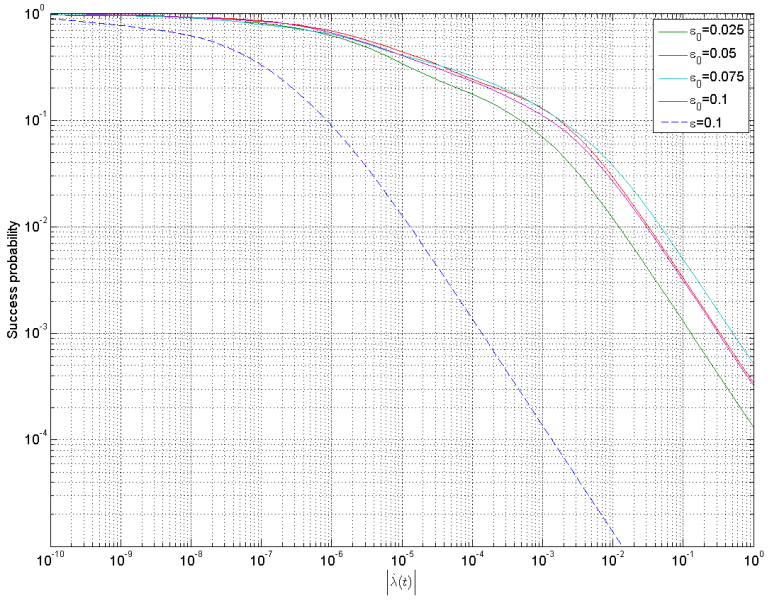

Figure 6.0.3: Plot of average success probability against computation speed for the $|10\rangle \rightarrow |11\rangle$ operation of the CNOT gate with an artificial noise source at a range of values for ϵ_0 and $\alpha = 10$. For comparative purposes, the results for a noise source with a constant amplitude of $\epsilon = 0.1$ are also shown.

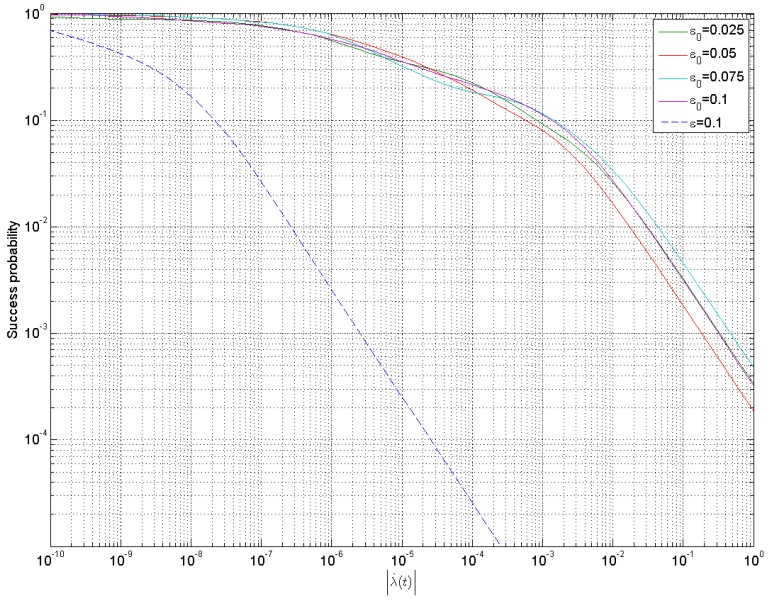

Figure 6.0.4: Plot of average success probability against computation speed for the $|11\rangle \rightarrow |10\rangle$ operation of the CNOT gate with an artificial noise source at a range of values for ϵ_0 and $\alpha = 10$. For comparative purposes, the results for a noise source with a constant amplitude of $\epsilon = 0.1$ are also shown.

Chapter 7

The extended Pechukas-Yukawa system

In the results presented in chapters 5 and 6, the level occupation probabilities are estimated by analysis of the structure of the energy spectrum. However, as noted in chapter 5 it would be beneficial to have a complete description of the state of a quantum system, as opposed to just the occupations. In light of this we now derive a novel extended version of the Pechukas-Yukawa framework that allows a complete description of the quantum state.

If we start with the operator equation of motion derived during the derivation of the generalised Pechukas-Yukawa model (2.1.9),

$$\frac{d}{d\lambda}A_{nm} = i\sum_k \left(H_{nk}A_{km} - A_{nk}H_{km}\right) + \langle n| \frac{\partial A}{\partial \lambda} |m\rangle \,, \tag{7.0.1}$$

and insert the density operator, $\rho = |\psi\rangle \langle\psi|$, for A we have

$$\frac{d}{d\lambda}\rho_{nm} = i\sum_k \left(H_{nk}\rho_{km} - \rho_{nk}H_{km}\right) + \langle n| \frac{\partial \rho}{\partial \lambda} |m\rangle \,. \tag{7.0.2}$$

The term outside the sum, the partial time derivative of ρ is described by the Von Neumann equation, $\partial\rho/\partial\lambda = -i\left[\mathcal{H}, \rho\right]$ and we also know that

$$\frac{\partial \rho}{\partial \lambda} = \frac{\partial \rho}{\partial t}\frac{\partial t}{\partial \lambda}, \tag{7.0.3}$$

therefore we have

$$\langle n| \frac{\partial \rho}{\partial \lambda} |m\rangle = \frac{\partial t}{\partial \lambda} \langle n| - i\left[\mathcal{H}, \rho\right] |m\rangle = -i\frac{\partial t}{\partial \lambda}\left(\langle n| \mathcal{H}\rho |m\rangle - \langle n| \rho\mathcal{H} |m\rangle\right), \tag{7.0.4}$$

where $\mathcal{H}$ is the Hamiltonian not the operator H. We can define the density operator

as an element by element sum

$$\rho = \sum_{a,b} \rho_{ab} \left|a\right\rangle \left\langle b\right|, \tag{7.0.5}$$

and insert it into (7.0.4) to give

$$\left\langle n\right| \frac{\partial \rho}{\partial \lambda} \left|m\right\rangle = -i \frac{\partial t}{\partial \lambda} \sum_{a,b} \rho_{ab} \left(\left\langle n\right| \mathcal{H} \left|a\right\rangle \left\langle b|m\right\rangle - \left\langle n|a\right\rangle \left\langle b\right| \mathcal{H} \left|m\right\rangle \right). \tag{7.0.6}$$

Using the eigenvalue equation $\mathcal{H} \left|n\right\rangle = x_n \left|n\right\rangle$ we have

$$\left\langle n\right| \frac{\partial \rho}{\partial \lambda} \left|m\right\rangle = -i \frac{\partial t}{\partial \lambda} \sum_{a,b} \rho_{ab} \left(x_a \left\langle n|a\right\rangle \left\langle b|m\right\rangle - x_m \left\langle n|a\right\rangle \left\langle b|m\right\rangle \right), \tag{7.0.7}$$

due to orthgonality, $\langle n|m\rangle = \delta_{nm}$, the only non-zero contribution to this sum will come when $n = a$ and $m = b$, which gives

$$\left\langle n\right| \frac{\partial \rho}{\partial \lambda} \left|m\right\rangle = -i \frac{\partial t}{\partial \lambda} \rho_{nm} \left(x_n - x_m \right). \tag{7.0.8}$$

Therefore we have

$$\frac{d}{d\lambda} \rho_{nm} = i \sum_k \left(H_{nk} \rho_{km} - \rho_{nk} H_{km} \right) - i \rho_{nm} \left(x_n - x_m \right), \tag{7.0.9}$$

where H_{ab} is defined by the following identity found during the derivation of the standard Pechukas-Yukawa model [46]

$$H_{ab} = \frac{V_{ab}}{i \left(x_a - x_b \right)}, \tag{7.0.10}$$

which is analogous to equation (2.1.13) for the generalised Pechukas-Yukawa system.

If we first consider the diagonal elements of the density matrix, *i.e.* where $n = m$ in (7.0.9), we have

$$\frac{d}{d\lambda} \rho_{nn} = i \sum_{k \neq n} \left(H_{nk} \rho_{kn} - \rho_{nk} H_{kn} \right) - 0. \tag{7.0.11}$$

Then, using (7.0.10) and the Yukawa dynamical variable, $l_{nm} = (x_n - x_m) V_{nm}$, we

have

$$\frac{d}{d\lambda}\rho_{nn} = \sum_{k\neq n}\left(\frac{V_{nk}\rho_{kn}}{(x_n - x_k)} - \frac{\rho_{nk}V_{kn}}{(x_k - x_n)}\right), \tag{7.0.12}$$

$$= \sum_{k\neq n}\left(\frac{V_{nk}\rho_{kn} + \rho_{nk}V_{kn}}{(x_n - x_k)}\right), \tag{7.0.13}$$

$$= \sum_{k\neq n}\left(\frac{l_{nk}\rho_{kn} + \rho_{nk}l_{kn}}{(x_n - x_k)^3}\right). \tag{7.0.14}$$

As both l and ρ are Hermitian we can say that

$$\frac{d}{d\lambda}\rho_{nn} = \sum_{k\neq n}\left(\frac{2\left|l_{nk}\rho_{kn}\right|}{(x_n - x_k)^3}\right) = \dot{p}_n, \tag{7.0.15}$$

where p_n are the occupations or populations of a given eigenlevel n.

If we now consider the case of the off-diagonal elements of ρ, *i.e.* where $n \neq m$ in (7.0.9), we have

$$\frac{d}{d\lambda}\rho_{nm} = i\sum_{k\neq n,m}\left(H_{nk}\rho_{km} - \rho_{nk}H_{km}\right) - i\frac{\partial t}{\partial\lambda}\rho_{nm}\left(x_n - x_m\right). \tag{7.0.16}$$

Using (7.0.10) and $l_{nm} = (x_n - x_m)V_{nm}$ we have

$$\frac{d}{d\lambda}\rho_{nm} = \sum_{k\neq n,m}\left(\frac{V_{nk}\rho_{km}}{(x_n - x_k)} - \frac{\rho_{nk}V_{km}}{(x_k - x_m)}\right) - i\frac{\partial t}{\partial\lambda}\rho_{nm}\left(x_n - x_m\right), \tag{7.0.17}$$

$$= \sum_{k\neq n,m}\left(\frac{l_{nk}\rho_{km}}{(x_n - x_k)^2} + \frac{\rho_{nk}l_{km}}{(x_m - x_k)^2}\right) - i\frac{\partial\lambda}{\partial t}\rho_{nm}\left(x_n - x_m\right). \tag{7.0.18}$$

These terms, ρ_{nm}, describe the inter-level coherences, *i.e.* the matrix element between eigenstates $|n\rangle$ and $|m\rangle$.

We now have a pair of equations,

$$\dot{p}_n = \sum_{k\neq n}\left(\frac{2\left|l_{nk}\rho_{kn}\right|}{(x_n - x_k)^3}\right)$$

$$\dot{\rho}_{nm} = \sum_{k\neq n,m}\left(\frac{l_{nk}\rho_{km}}{(x_n - x_k)^2} + \frac{\rho_{nk}l_{km}}{(x_m - x_k)^2}\right) - i\frac{\partial\lambda}{\partial t}\rho_{nm}\left(x_n - x_m\right), \tag{7.0.19}$$

that when used in conjunction with the standard Pechukas-Yukawa equations, (1.3.2), form a closed system of classical equations of motion that fully capture both the dynamics of the eigenvalues and the state of the system. They therefore completely describe the dynamics of the quantum system and this is done without making

any simplifications or assumptions. It may also be possible to generalise (7.0.19) to the dissipative case by starting with a master equation instead of the Von Neumann equation. These equations could be a useful result as they allow the use of techniques and approaches from classical physics, that do not neccesarily have a quantum analogue, to be readily applied to quantum mechanical systems.

Chapter 8

Conclusions

In this work we have derived a generalised stochastic form of the Pechukas-Yukawa model of eigenvalue dynamics. This allowed us to take into account the effects of a simple, yet generic, coloured noise source on the system's evolution. We used this approach to study an example of a prototypical adiabatic quantum algorithm which involves 4 qubits; the GSQC form of the CNOT gate.

We have studied the energy spectra and their spectral properties and seen how noise affects these. In particular, we showed that the presence of noise will break any degeneracies in the spectrum that might obstruct the computation process without significantly disturbing the regularity of the eigenvalue dynamics. We then studied the effects of noise on the statistics of level occupation by analysing the sequences of avoided crossings in the spectra that can lead to excitation out of the ground state. In general, we found that the success probability scales polynomially with the computation speed and noise introduces a shift of prefactor into this relationship. We then investigated a theoretical situation where we have the opportunity to greatly improve the success rate of the computation by the addition of a specifically tailored artificial noise source. Finally, we formulated an extended version of the Pechukas-Yukawa model that provides a complete description of the dynamics of the quantum state, as well as the eigenvalues. This maintains the key benefit of being an exact map to a classical system of equations of motion. We have demonstrated that an eigenvalue dynamics approach can offer an insightful alternative to the Schrödinger picture, as we have shown that detailed knowledge of a quantum system's energy spectrum and its properties can help explain the system's behaviour. From these results there are two main conclusions we can draw.

The first is on the relative robustness of an AQC process against the effects of noise. In chapter 4, we showed that despite the addition of a relatively strong irregularity into our system, *i.e.* noise, the overall eigenvalue dynamics remain regular. This is a promising result, as it means that small random fluctuations in

the Hamiltonian should not lead to radical changes in the dynamics of the system and therefore we can expect the results of the computation to be reasonably close to the desired results. This demonstrates the stability of the AQC process in the presence of noise. We have also shown that the polynomial dependence of the success probability on the computation speed is independent of the noise amplitude. This result demonstrates the robustness of the performance of AQC in the presence of noise. In fact we have shown that in some situations, noise can provide a linear increase in the success probability at a given speed. Although this improvement comes at the cost of the fidelity of the final state, there exists a noise amplitude that offers an optimal compromise. The idea of noise providing an improvement in the performance of a device is counter-intuitive, however there is some precedence for this in the context of AQC, [7, 12].

The second main conclusion we can draw from this work is with regards to the choice of initial conditions in AQC. We have analysed situations where symmetries in the Hamiltonian lead to degeneracies in the spectrum, including some where degeneracies between the ground and first excited state would lead to failure of the computation process. We have shown that in realistic systems, where the perturbative effects of noise are taken into account, all of these symmetries and degeneracies will be broken naturally. This means there will always be a finite success probability in practical AQC systems and therefore we can say that the conventional stipulation that the initial and final Hamiltonians do not commute is unnecessary. In fact, it is when the initial and final Hamiltonians commute that we see the greatest noise-enhancement of the performance. This is an important result as it removes a restriction on the choice of initial Hamiltonian that may prove practically impossible to realise for universal AQC.

These results have been published in [52] and a copy of the manuscript is included in appendix B.

8.1 Suggestions for further work

We believe there are a number of different directions in which this work could be taken that may provide some fruitful and insightful results.

The most straightforward extension of this work would be to look at the effects of noise on different types of adiabatic quantum algorithms. Determining how the computation time of a given algorithm scales with input size (no. of qubits), effectively the algorithmic efficiency, is a crucial step in evaluating its performance and practicality. Therefore, it would be interesting to investigate how noise affects this scaling in an algorithm with a variable input size. As mentioned in section 1.2.3.2,

an example of an **NP-complete** algorithm that is often studied is the boolean satisfiability (**SAT**) problem and that prior attempts to determine whether AQC can be used to efficiently solve this problem have been mixed. It is currently believed that relatively easy **SAT** problem instances, which have a high degree of structure to them, can be solved efficiently using AQC (e.g. as in [6]), but there is some debate as to whether this holds for hard instances of the **SAT** problem (e.g. as reviewed in [17]). So far, to our knowledge, the effects of noise on the efficiency on the different types of **SAT** problem instances have not been directly explored. It could be the case that the addition of noise may affect the structure in the Hamiltonian that determines the efficiency of that particular problem instance.

When discussing the efficiency of any computational algorithm it is necessary to consider its performance in the limit of large system sizes. Unfortunately, the number of dimensions of the Hilbert space required to describe the state of a quantum information processing system in the Schrödinger picture grows exponentially with the number of qubits; this means it is very difficult to try to evaluate the behaviour of quantum algorithms in the limit of large input sizes. The method of numerically solving the Pechukas-Yukawa equations used in the simulations in section 2.3 suffers from the same scalability problems as directly solving the Schrödinger equation (*i.e.* the dimension of the phase space needed to describe the state of the eigenvalue gas grows exponentially with the input size). However, the eigenvalue gas described by the Pechukas-Yukawa equations is a classical system unlike the Schrödinger equation, which means that techniques for dealing with large systems from classical statistical physics are applicable. The use of Klimontovich's kinetic approach (described in [53]) is proposed in [40]; where the Pechukas-Yukawa system of equation are rewritten as a BBGKY (Bogoliubov-Born-Green-Kirkwood-Yvon) type chain of equations for the macroscopic (or average) distribution functions $f_1 = \langle F_1 \rangle$, $f_2 = \langle F_2 \rangle$, $g_2 = \langle G_2 \rangle$,..., where

$$F_1(x, v, t) = \sum_{1 \leq i \leq N} \delta(x - x_i(t))\delta(v - v_i(t)), \tag{8.1.1}$$

$$F_2(x^{(m)}, v^{(m)}, x^{(n)}, v^{(n)}, l^{(mn)}, t) = \sum_{1 \leq i < j \leq N} \delta(x^{(m)} - x_i(t))\delta(v^{(m)} - v_i(t)) \\ \delta(x^{(n)} - x_j(t))\delta(v^{(n)} - v_j(t))\delta(l^{(mn)} - l_{ij}(t)) \text{ and} \tag{8.1.2}$$

$$G_2(l, t) = \sum_{1 \leq i < j \leq N} \delta(l - l_{ij}(t)) \tag{8.1.3}$$

are the microscopic distribution functions. Then using the standard method of

truncating the BBGKY chain an equation of motion for f_1 can be derived. Recent results have suggested that the bulk of the eigenspectrum of an adiabatic quantum computer may have little effect on the overall dynamics of the system (see [18]) and that it is the eigenlevels on the edges of the spectrum that are important. This means that large systems could be investigated by directly simulating a few eigenvalues on the edges of the spectrum using the Pechukas-Yukawa equations and then taking account of the long-range influence of the bulk of the spectrum statistically using the kinetic equations.

In section 6, we explored the idea of making use of a controllable artificial noise source to try to improve the performance of an AQC operation. A more obvious choice of variable to control is the computation speed, $\left|\dot{\lambda}\right|$, as we know that decreasing this will directly increase the success probability. However, at the same time we would clearly like to be able to run practical computations as fast as possible. In light of this, we envision an AQC system whose speed is dynamically controlled. This would allow the computation to be run relatively quickly for the majority of the evolution but then the speed could be reduced at the critical points where excitation out of the ground state may occur (e.g. near avoided crossings), therefore allowing a high rate of success to be achieved at relatively short total computation times. To realise this we would require a type of continuous, weak measurement that could detect when the system is approaching one of these critical points. In [29], non-destructive continuous measurement of the ground state curvature of a flux qubit was demonstrated experimentally using the impedance measurement technique with a high quality tank circuit. The ground state curvature would be a suitable control variable, as we expect it to increase at avoided crossings. This could be readily modeled using the Pechukas-Yukawa formalism as the ground state curvature will be proportional to $|l_{01}(\lambda)|$. To properly analyse the effects of this control system we will need to be able to calculate the probabilities of level occupation in the continuum within the Pechukas-Yukawa formalism as opposed to the discrete algorithm detailed in section 2.3; the derivation of a novel extension of the Pechukas-Yukawa equation that would allow this is detailed in chapter 7. The computation speed within these equations can be defined in a such way that it is dynamically related to $|l_{01}(\lambda)|$. We therefore have all the necessary components to model an AQC system where the computation speed is dynamically controlled via a feedback loop that performs continuous measurement of the ground state curvature and then analyse the effects of this control system on the success probability. Feedback control systems are widely used in many engineering applications and their theory is a well understood branch of control systems theory [54]; we would be able to draw on this knowledge when designing a feedback controller for an AQC system.

In other recent results, [50] and appendix C, we have explicitly investigated the relationship between the success probability and the minimum ground state energy gap in AQC. We show that there exists a rich structure in the distribution of these two figures of merit. The structure of distinct sharp edges and densely populated bands seen in the distribution is reminiscent of the projection of a higher dimensional surface on to a plane. One possible explanation of this could be that the the structure we see is the shadow of the system's surface of adiabatic invariance. An adiabatic invariant is a constant of motion of a dynamical system that is preserved in the adiabatic limit, because of this they can be considered to be an asymptotic statement. They are well known in classical mechanics [55]. Knowledge about the adiabatic invariants of an AQC could prove to be very insightful, as it would improve our understanding of the relationship between the system's control parameters and measures of its performance. This could have a major impact on algorithm and system design in the field of AQC. The Pechukas-Yukawa formalism would be a particularly useful tool in this endeavour. By taking advantage of the fact that it reduces the dynamics of a quantum system to a system of classical equations of motion; approaches and techniques from the study of adiabatic invariants in classical mechanics could then be applied. For instance, the action of a classical system is always an adiabatic invariant. It would be possible to write a Hamiltonian and Lagrangian for the Pechukas gas and therefore formulate the action integral for a generic quantum system.

Appendix A

Program listings

A.1 Simulation programs

The following MATLAB script and dependent functions will generate the energy spectra for a large set of noise realisations applied to a specific operation of the adiabatic CNOT gate;

```
%*************************************************************************
%CNOT gate noise instance generator
%*************************************************************************
%This script generates a set number of random noise instances and applies them
%to the evolution of the adaiabatic CNOT gate using the generalised
%Pechukas-Yukawa model
%
%Dependencies: coloured_noise.m, generalised_perturb_initial.m,
%generalised_pechukas_yukawa_system.m
%*************************************************************************

clc
clear

global levels nu_vec tau lambda_step lambda_length dh_vec;

%Seed random number generator
RandStream.setDefaultStream(RandStream('mt19937ar','seed',100));

%Define constants and parameters
levels=16; %no. of energy levels in the system
momenta=levels^2; %no. of l_mn needed to describe the interactions in the ↩
    Pechukas gas
CNOT_op=1; %CNOT operation |00> -> |00>
epsilon=-0.1; %energy scale
z=10; %bias
Eb=[-8:-1,1:8]; %Eigenspectrum of H_b (initial Hamiltonian)
d=-0.1;
dd=[d,d,d,d,d,0,0,0,d,0,0,0,d,0,0,0];
%apply small random perturbations to eigenspectrum of H_b
for k=1:levels
    Eb(k)=Eb(k)+1.5*(dd(k)/d);
end
```

```
33 tau=0.1; %noise correlation time
34 n_repeats=50; %no. of repeats at each given noise amplitude
35 amp_range=[0.025,0.05,0.075,0.1]; %noise amplitudes
36 lambda_step=0.005; %noise time step
37 lambda_fine_step=0.00001; %fine step to use when integrating for lambda(t) near 0
38 lambda=1:-lambda_step:0; %noise time interval
39 lambda_fine=[1:-lambda_step:0.1,0.1-lambda_fine_step:-lambda_fine_step:0]; %↩
       Pechukas integration time interval
40 lambda_length=length(lambda);
41 save_dir='C:\Documents and Settings\phrdw2\My Documents\CNOT data\00to00'; %root ↩
       directory
42
43 %Set up CNOT Hamiltonian
44 c_00=zeros(5);
45 c_00(1,2)=1;
46 c_00=qo(c_00);
47 c_01=zeros(5);
48 c_01(1,3)=1;
49 c_01=qo(c_01);
50 c_10=zeros(5);
51 c_10(1,4)=1;
52 c_10=qo(c_10);
53 c_11=zeros(5);
54 c_11(1,5)=1;
55 c_11=qo(c_11);
56 I=identity(5);
57 c_000=tensor(c_00,I);
58 c_100=tensor(I,c_00);
59 c_001=tensor(c_01,I);
60 c_101=tensor(I,c_01);
61 c_010=tensor(c_10,I);
62 c_110=tensor(I,c_10);
63 c_011=tensor(c_11,I);
64 c_111=tensor(I,c_11);
65 H_cnot=c_010'*(c_110'*c_110+c_111'*c_111)*c_010 - c_010'*(c_110'*c_100+c_111'* ↩
       c_101)*c_000 - c_000'*(c_100'*c_110+c_101'*c_111)*c_010 + c_000'*(c_100'* ↩
       c_100+c_101'*c_101)*c_000...
66       +c_011'*(c_110'*c_110+c_111'*c_111)*c_011 - c_011'*(c_110'*c_101+c_111'*c_100 ↩
           )*c_001 - c_001'*(c_101'*c_110+c_100'*c_111)*c_011+c_001'*(c_101'*c_101+ ↩
           c_100'*c_100)*c_001...
67       +(c_000'*c_000+c_001'*c_001)*(c_110'*c_110+c_111'*c_111)+(c_010'*c_010+c_011 ↩
           '*c_011)*(c_100'*c_100+c_101'*c_101);
68 if CNOT_op==1
69     delta_H_cnot=qo(epsilon*(c_000'*c_000+c_100'*c_100));
70 elseif CNOT_op==2
71     delta_H_cnot=qo(epsilon*(c_000'*c_000+c_101'*c_101));
72 elseif CNOT_op==3
73     delta_H_cnot=qo(epsilon*(c_001'*c_001+c_100'*c_100));
74 elseif CNOT_op==4
75      delta_H_cnot=qo(epsilon*(c_001'*c_001+c_101'*c_101));
76 end
77 H=H_cnot+delta_H_cnot;
78 H_trunc=truncate(H,{2:5,2:5});
79
80 %*************************************************************************
81 for a=1:length(amp_range)
82     amp_string=num2str(amp_range(a));
```

```
83      current_dir=strcat(save_dir,'\amp_pt',amp_string(3:end)); %save directory for ↩
            current noise amplitude
84
85      amp=amp_range(a)
86      for n=1:n_repeats
87
88          %Generate a set of noise matrices and their derivatives
89          h_init=amp.*wigner(levels,1);
90          h_init_vec=reshape(h_init,levels^2,1);
91          nu_vec=zeros(length(lambda),levels^2);
92          for k=1:length(lambda)
93              nu=amp.*wigner(levels,1);
94              nu_vec(k,:)=reshape(nu,1,levels^2);
95          end
96
97          h_vec=zeros(length(lambda),levels^2);
98          [lambda,h_vec]=ode23(@coloured_noise,lambda,h_init_vec);
99
100         dh_vec=zeros(length(lambda),levels^2);
101         for k=1:length(lambda)
102             dh_vec(k,:)=-tau*h_vec(k,:)+nu_vec((length(lambda)-round(lambda(k)/ ↩
                    lambda_step)),:);
103         end
104
105         %Solve generalised Pechukas equations to generate the energy spectrum
106         %for this noise instance
107         x_v_l_initial=generalised_perturb_initial(full(H_trunc(:,:)),z,Eb,h_init) ↩
                ;
108         [lambda_fine,x_v_l]=ode113(@generalised_pechukas_yukawa_system, ↩
                lambda_fine,x_v_l_initial);
109
110         %Save the data for this noise instance
111         file_name=strcat(current_dir,'\run_',num2str(n),'.mat');
112         save(file_name,'n','amp','x_v_l','h_vec','dh_vec')
113
114         disp(n)
115     end
116 end
```

```
1  function dh=coloured_noise(lambda,h)
2  %************************************************************************
3  %Coloured noise differential equation
4  %************************************************************************
5  %This function returns the vector form of the derivative of the random matrix
6  %noise term \deltah(\lambda) in the generalised Pechukas-Yukawa model.
7  %It's evolution is described the Ornstein-Uhlenbeck process.
8  %It returns the derivative in a form suitable for the ODE solver suite.
9  %************************************************************************
10
11 global levels nu_vec tau lambda_step lambda_length dh_vec;
12 dh=zeros(levels^2,1);
13 nu=zeros(1,length(levels^2));
14 %find values of white noise term \nu(\lambda) at \lambda using linear ↩
       interpolation
15 for k=1:levels^2
16     nu(k)=interp1([1:-lambda_step:0],nu_vec(:,k),lambda,'nearest');
17 end
18 %Ornstein-Uhlenbeck equation
```

```
for k=1:levels^2
    dh(k)=-tau*h(k)+nu(k);
end
```

```
function [ x_v_l_initial ] = generalised_perturb_initial(H_0,z,Eb,dh)
%*************************************************************************
%Perturbative initial conditions for generalised Pechukas-Yukawa equations
%*************************************************************************
%This function returns the initial conditions for the generalised Pechukas-
%Yukawa equations. These are calculated perturbatively to the 1st order in
%terms of Z^-1. The problem Hamiltonian, derivative of the noise term, z,
%and the energy spectrum of H_b are passed in.
%*************************************************************************

[levels,momenta]=size(H_0);
momenta=momenta^2;

%Calculate initial positions
x=zeros(levels,1);
for k=1:levels
    x(k)=z*Eb(k)+H_0(k,k)+dh(k,k);
end

%Calculate initial velocities
v=zeros(levels,1);
for k=1:levels
    v(k)=(z)*Eb(k);
end

%Calculate initial coupling strengths
l=zeros(momenta,1);
for k=1:momenta
    [r,c]=ind2sub(size(H_0),k);
    if (H_0(r,c)~=0||dh(r,c)~=0) && r~=c
        l(k)=z*(H_0(r,c)+dh(r,c))*(Eb(r)-Eb(c));
    end
end

x_v_l_initial=zeros(1,levels*2+momenta);
x_v_l_initial(1:levels)=x(:);
x_v_l_initial((levels+1):(2*levels))=v(:);
x_v_l_initial((2*levels+1):(2*levels+momenta))=l(:);
```

```
function [dx_dv_dl]=generalised_pechukas_yukawa_system(lambda,x_v_l)
%*************************************************************************
%Generalised Pechukas-Yukawa differential equation systems
%*************************************************************************
%Function to solve the extended Pechukas-Yukawa equation system for an
%arbitraray quantum system with n energy levels, for use with ode45. The
%derivatives of the noise term delta_h are passed in as global variable
%which is a cell array containing the delta_h_dot matrix for each point in
%time.
%*************************************************************************

global levels nu_vec tau lambda_step lambda_length dh_vec;

momenta=levels^2;
dx_dv_dl=zeros((levels*2+momenta),1);
```

```
16
17 %Extract current values of x, v, l and delta_h_dot to work with
18 x=zeros(levels,1);
19 x(:)=x_v_l(1:levels);
20 v=zeros(levels,1);
21 v(:)=x_v_l((levels+1):(2*levels));
22 l=zeros(levels,levels);
23 for p=1:1:levels
24     for q=1:1:levels
25         if p~=q
26             l(p,q)=x_v_l(2*levels+sub2ind(size(l),p,q));
27         end
28     end
29 end
30 dh=zeros(levels,levels);
31 dh_interp=zeros(1,levels^2);
32 for k=1:levels^2
33     dh_interp(k)=interp1([1:-lambda_step:0],dh_vec(:,k),lambda,'nearest');
34 end
35 dh=reshape(dh_interp,levels,levels);
36
37 %Calculate differential for position dx_n=v_n
38 dx=zeros(levels,1);
39 for n=1:1:levels
40     dx(n,1)=v(n)+dh(n,n);
41 end
42
43 %Calculate differential for velocity dv_n=2*sum(|l_nk|^2/(x_n-x_k)^3) where
44 %k~=n
45 dv=zeros(levels,1);
46 for n=1:1:levels
47     for k=1:1:levels
48         if n~=k
49             dv(n,1)=dv(n,1)+2*((abs(l(n,k))^2)/(x(n)-x(k))^3)+(l(n,k)*dh(k,n)-dh(↩
                   n,k)*l(k,n))/(x(n)-x(k))^2;
50         end
51     end
52 end
53
54 %Calculate differential for relative angular momentum
55 %dl_nm=sum(l_nk*l_km*(1/((x_n-x_k)^2)-1/((x_m-x_k)^2))) where k~=n,m
56 dl=zeros(levels,levels);
57 for n=1:1:levels
58     for m=1:1:levels
59         if n~=m
60             dl(n,m)=dh(n,m)*(v(m)-v(n))+(l(n,m)*(dh(n,n)-dh(m,m)))/(x(n)-x(m));
61             for k=1:1:levels
62                 if (k~=n)&&(k~=m)
63                     dl(n,m)=dl(n,m)+l(n,k)*l(k,m)*(1/((x(n)-x(k))^2)-1/((x(m)-x(k↩
                           ))^2))...
64                         +((x(n)-x(m))*(l(k,m)*dh(n,k)-l(n,k)*dh(k,m)))/((x(n)-x(k↩
                               ))*(x(k)-x(m)));
65                 end
66             end
67         end
68     end
69 end
```

```
70
71 %Construct dx_dv_dl
72 dx_dv_dl(1:levels)=dx(:);
73 dx_dv_dl((levels+1):(2*levels))=dv(:);
74 for p=1:1:levels
75     for q=1:1:levels
76         if p~=q
77             dx_dv_dl(2*levels+sub2ind(size(dl),p,q))=dl(p,q);
78         end
79     end
80 end
```

A.2 Analysis programs

The following MATLAB script is designed to calculate the level occupation statistics averaged over a large set of noise realisations by analysis of the eigenvalue gas spectrum;

```
1  %*************************************************************************
2  %Level occupation analysis
3  %*************************************************************************
4  %Script file to analyse the critical points (avoided crossings) in the
5  %energy spectra of the adiabatic CNOT gate and estimate the level occupations
6  %as the system moves through the critical points using the LZS eqn
7  %for a number of different noise instances and save all the results to a single
8  % .mat file. The average occupation values are also calculated.
9  %*************************************************************************
10
11 clc
12 clear
13
14 %Define constants and parameters
15 levels=16; %no. of energy levels in the system
16 momenta=levels^2; %no. of l_mn needed to describe the interactions in the ↩
       Pechukas gas
17 n_repeats=50; %no. of repeats at each given noise amplitude
18 amp_range=[0.025,0.05,0.075,0.1]; %noise amplitudes
19 lambda_step=0.005; %noise time step
20 lambda_fine_step=0.00001; %fine step to use when integrating for lambda(t) near 0
21 lambda=1:-lambda_step:0; %noise time interval
22 lambda_fine=[1:-lambda_step:0.1,0.1-lambda_fine_step:-lambda_fine_step:0]; %↩
       Pechukas integration time interval
23 lambda_length=length(lambda);
24
25 dlambda=logspace(0,-20,100); %range of sweep rates dlambda=1/computation time
26
27 %Select directories to analyse
28 dir_name=cell(1,3);
29 dir_name{1,1}='C:\Documents and Settings\phrdw2\My Documents\PhD work\1st year\↩
       CNOT Project\00to00_tDepNoise\amp_pt025';
30 dir_name{1,2}='C:\Documents and Settings\phrdw2\My Documents\PhD work\1st year\↩
       CNOT Project\00to00_tDepNoise\amp_pt05';
31 dir_name{1,3}='C:\Documents and Settings\phrdw2\My Documents\PhD work\1st year\↩
       CNOT Project\00to00_tDepNoise\amp_pt075';
```

```
32 dir_name{1,4}='C:\Documents and Settings\phrdw2\My Documents\PhD work\1st year\ ↩
       CNOT Project\00to00_tDepNoise\amp_pt1';
33
34
35 %occupation data will be stored in a cell array, each cell contains a
36 %table detailing the level occupation over time for that particular noise
37 %instance. Each row of the cell array contains occupations calculated for a
38 %different sweep rate
39 final_occupation=cell(length(dlambda),n_repeats);
40
41 for d=1:length(dir_name)
42     for n=1:n_repeats
43         file_name=strcat(dir_name{d},'\run_',num2str(n),'.mat');
44         load(file_name,'x_v_l');
45
46         n
47
48         xs=x_v_l(:,1:16);
49         if issorted(xs(1,:))==0 %check to make sure the energy eigenvalues are ↩
               sorted in ascending order
50             swap=1;
51             swap_count=levels;
52             while swap==1
53                 swap=0;
54                 for k=1:swap_count-1
55                     if xs(1,k)>xs(1,k+1)
56                         temp=xs(:,k+1);
57                         xs(:,k+1)=xs(:,k);
58                         xs(:,k)=temp;
59                         swap=1;
60                     end
61                 end
62                 swap_count=swap_count-1;
63             end
64         end
65
66         for s=1:length(dlambda)
67             avoided_crossings=zeros(5,1); %save in rows of level numbers m & n, ↩
                   gap width,lambda array index, gap centre point
68
69             for k=1:(levels-1)
70                 x_gap=(xs(:,k+1)-xs(:,k));
71                 g_min=0;
72                 lambda_index=0;
73                 for m=2:(length(lambda_fine)-1)
74                     if x_gap(m)<x_gap(m-1)&&x_gap(m)<x_gap(m+1)
75                         g_min=[g_min,x_gap(m)];
76                         lambda_index=[lambda_index,m];
77                     end
78                 end
79                 g_min=g_min(2:end);
80                 lambda_index=lambda_index(2:end);
81                 for l=1:length(g_min)
82                     avoided_crossings=[avoided_crossings,[k;k+1;g_min(l); ↩
                           lambda_index(l);(xs(lambda_index(l),k)+(g_min(l)/2))]];
83                 end
84             end
```

```
85              avoided_crossings=avoided_crossings(:,2:end);
86
87              if avoided_crossings(1,1)~=1&&avoided_crossings(2,1)~=2
88                  %if there are no distinct avoided crossings between the ground and
89                  %first excited states the limiting gap is simply the minimum at
90                  %lambda(t)=0
91                  ground_gap=xs(end,2)-xs(end,1);
92                  avoided_crossings=[[1;2;ground_gap;length(lambda_fine);(xs(end,1)+ground_gap)],avoided_crossings];
93              end
94
95              no_avoided_crossings=length(avoided_crossings);
96              start_point=avoided_crossings(4,1)-2;
97              occupation_length=length(lambda_fine(start_point:end));
98              occupation=zeros(16,occupation_length);
99              occupation(1,1)=1;
100
101             last_avoided_crossing=1;
102             current_top_level=1;
103             for k=2:occupation_length
104                 for l=1:no_avoided_crossings
105                     if avoided_crossings(1,l)<=current_top_level&&avoided_crossings(4,l)==(start_point+k)
106                         %anti-crossing has occured so recalulate level occupations
107                         l_mn=abs(x_v_l((start_point+k),sub2ind([levels,levels],avoided_crossings(1,l),avoided_crossings(2,l))));
108                         P_LZS=exp(-(avoided_crossings(3,l)^3)/(l_mn*dlambda(s)));
109                         occupation(:,k)=occupation(:,k-1);
110                         occupation(avoided_crossings(1,l),k)=occupation(avoided_crossings(1,l),k-1)-occupation(avoided_crossings(1,l),k-1)*P_LZS;
111                         occupation(avoided_crossings(2,l),k)=occupation(avoided_crossings(2,l),k-1)+occupation(avoided_crossings(1,l),k-1)*P_LZS;
112
113                         last_avoided_crossing=k;
114
115                         if current_top_level<avoided_crossings(2,l)
116                             current_top_level=avoided_crossings(2,l);
117                         end
118                     end
119                 end
120                 if last_avoided_crossing~=k
121                     %anti-crossing hasn't occured so level occupation stays the same
122                     occupation(:,k)=occupation(:,k-1);
123                 end
124
125                 [nanrow,nancol]=find(isnan(occupation(:,:)));
126                 occupation(nanrow,nancol)=0;
127                 [infrow,infcol]=find(isinf(occupation(:,:)));
128                 occupation(infrow,infcol)=0;
129
130                 %save the level occupation at lambda(t)=0
131                 final_occupation{s,n}=occupation(:,end);
```

```
132                 end
133             end
134         end
135
136         averaged_occupations=zeros(levels,length(dlambda));
137         var_occupations=zeros(levels,length(dlambda));
138         %average level occupations at t=0 over the 50 noise instances
139         for k=1:length(dlambda)
140             for l=1:levels
141                 l_occupation=zeros(1,n_repeats);
142                 for m=1:n_repeats
143                     l_occupation(1,m)=final_occupation{k,m}(l,1);
144                 end
145                 averaged_occupations(l,k)=mean(l_occupation);
146                 var_occupations(l,k)=var(l_occupation);
147             end
148         end
149
150
151         save_file_name=strcat(dir_name{d},'\final_occupation1.mat');
152         save(save_file_name,'dlambda','final_occupation','averaged_occupations');
153     end
```

Appendix B

Noise-enhanced performance of adiabatic quantum computing by lifting degeneracies

Noise enhanced performance of adiabatic quantum computing by lifting degeneracies

R.D. Wilson A.M. Zagoskin S. Savel'ev
Department of Physics, Loughborough University,
Loughborough, Leicestershire LE11 3TU, UK

Abstract

We investigate the symmetry breaking role of noise in adiabatic quantum computing using the example of the CNOT gate. In particular, we analyse situations where the choice of initial Hamiltonian produces symmetries in the Hamiltonian and degeneracies in the spectrum. We show that, in these situations, the conventional stipulation that the initial and problem Hamiltonians do not commute is unnecessary as noise will inherently play the role of a universal symmetry breaking perturbation and split any level crossings that may impede or obstruct the computation. The effects of an artificial noise source with a tailored time-dependent amplitude are also explored and it is found that such a scheme could offer a considerable performance enhancement. These results are found using a novel, generalised version of the Pechukas-Yukawa model of eigenvalue dynamics.

1 Introduction

Recently there has been a lot of interest in alternative paradigms to the standard approach to quantum computing (i.e. the quantum circuit model). Adiabatic quantum computing (AQC) is a promising example which is particularly suited to solving optimisation problems [1]. AQC involves slow adiabatic evolution from a configuration with an easily reachable ground state to one where the ground state encodes the solution to the hard computational problem in hand. This scheme is believed to have a number of advantages over the "standard" approach, namely, the precise time-dependent control of individual qubits is no longer required, and it benefits from an inherent robustness against some of the effects of decoherence by remaining in the instantaneous ground state at all times [2, 3, 4]. Crucially, AQC has been shown to be polynomially equivalent, under certain conditions, to the standard gate model of quantum computing [6, 7]. The effects of noise on AQC are generally considered to be detrimental but manageable [2, 3, 4]. It was nevertheless stated that its effect can increase the success probability of AQC in some situations by; providing an alternative evolution trajectory [2], or by thermal relaxation back to the ground state [5]. Here, we investigate a more general effect of noise on AQC.Namely, how noise inherently breaks any hidden symmetries in the Hamiltonian and, thus, splits any level crossings in the energy spectrum which could impede or even prevent the computation.

AQC can be described by the following Hamiltonian;

$$\mathcal{H}(\lambda(t)) = H_0 + \lambda(t) Z H_b, \tag{1}$$

where the ground state of the final Hamiltonian, H_0, encodes the desired solution, ZH_b is a large bias term (with $Z \gg 1$) and the initial configuration, $\mathcal{H}(\lambda = 1) = H_0 + ZH_b$, has an easily reachable, non-degenerate ground state. In order for there to be a high probability of the system remaining in the ground state as the bias is switched off, the rate of change of the control parameter $\lambda(t)$ must be sufficiently slow to suppress excitation via Landau-Zener-Stückelberg tunneling [8, 9, 10].

In AQC, the initial and final Hamiltonians are usually chosen such that no symmetries exist in $\mathcal{H}(\lambda(t))$ by ensuring that they do not commute. This is done to ensure that there are no degeneracies in the energy spectrum during the evolution. However, this restriction on the choice of initial Hamiltonian may prove practically impossible

to realise for generic problems. In [11] the example of the adiabatic equivalent of the CNOT gate is discussed as an example of a prototypical quantum algorithm. It was shown that, the choice of a generic H_b could lead to an abundance of level crossings in the energy spectrum for the $|00\rangle \rightarrow |00\rangle$ operation of the CNOT gate. The influence of these level-crossings on the performance of the adiabatic quantum algorithm was not considered there. However, the effects of level crossings in the spectrum were discussed in [1] and it was noted that the addition of an appropriate sort of perturbation to the system will break the symmetries and therefore split any level crossings. The question of how to provide an appropriate perturbation still remains open.

In this paper, we propose that noise will inherently fulfil the role of the crucial symmetry breaking perturbation in physical implementations of an AQC system and as a result of this, the condition that H_0 and H_b do not commute is no longer required. The CNOT gate algorithm is again used as an example of a prototypical quantum algorithm and we show that the performance of this generic algorithm is relatively resistant to the effects of noise, in agreement with [2, 3, 4]. As reported in [2], we find that in some situations the presence of noise increases the success probability, we then go on to explore the relationship between this increase in success probability and the fidelity of the final state. We also discuss the idea of using a tailored artificial noise signal to try and enhance the performance of the adiabatic quantum computation process. To do this, we derive and utilise a generalised stochastic version of the Pechukas-Yukawa equations [12, 13]; where the dynamics of the energy eigenvalues are mapped exactly on to the classical dynamics of a 1D gas of Brownian particles with a mutual repulsive force.

2 Generalised Pechukas-Yukawa model

The standard Pechukas-Yukawa model is derived from a Hamiltonian of the form (1). However, to incorporate a source of noise in to the model we start with the following Hamiltonian;

$$\mathcal{H}(\lambda(t)) = \mathcal{H}_0 + \lambda(t) Z H_b + \delta h(\lambda(t)), \qquad (2)$$

where the perturbation strength $\lambda(t)$ plays the role of 'time' and the new stochastic term $\delta h(\lambda)$ describes random fluctuations in the Hamiltonian due to an external noise source. The instantaneous eigenvalues and eigenfunctions of (2) are denoted $x_n(\lambda)$ and $|n(\lambda)\rangle$ respectively; $\mathcal{H}(\lambda)\,|n(\lambda)\rangle = x_n(\lambda)\,|n(\lambda)\rangle$. By following the same procedure as the derivation of the standard Pechukas-Yukawa model, as detailed in [14], we arrive at the following generalised system of equations;

$$\begin{aligned}
\dot{x}_n = \frac{\partial x_n}{\partial \lambda} &= v_n + \dot{\delta h}_{nn}, \\
\dot{v}_n = \frac{\partial v_n}{\partial \lambda} &= \sum_{k \neq n} \left[\frac{2\,|l_{nk}|^2}{(x_n - x_k)^3} + \frac{l_{nk}\dot{\delta h}_{kn} - \dot{\delta h}_{nk} l_{kn}}{(x_n - x_k)^2} \right], \\
\dot{l}_{nm} = \frac{\partial l_{nm}}{\partial \lambda} &= \sum_{k \neq m,n} \left[l_{nk} l_{km} \left(\frac{1}{(x_n - x_k)^2} - \frac{1}{(x_m - x_k)^2} \right) \right. \\
&\quad \left. + \frac{(x_n - x_m)(l_{nk}\dot{\delta h}_{km} - l_{km}\dot{\delta h}_{nk})}{(x_m - x_k)(x_n - x_k)} \right] \\
&\quad + \dot{\delta h}_{nm}(v_m - v_n) + \frac{l_{nm}(\dot{\delta h}_{nn} - \dot{\delta h}_{mm})}{(x_n - x_m)}.
\end{aligned} \qquad (3)$$

where $v_n(\lambda) = \langle n|\, Z H_b\, |n\rangle$ and $l_{nm} = (x_n - x_m)\,\langle n|\, Z H_b\, |m\rangle$ for $n \neq m$. These generalised equations can be used to describe a wider array of physical systems because of the inclusion of the $\delta h(\lambda)$ term without any additional assumptions or approximations. Note that if the noise term $\delta h(\lambda(t))$ is identically zero the system of equations (3) simply reduces to the standard Pechukas-Yukawa equations. The equations (3) describe the dynamics of the energy eigenvalues of the Hamiltonian (2), but also correspond to the classical dynamics of a 1D interacting gas, where the nth particle has position $x_n(\lambda)$ and velocity $v_n(\lambda)$ and the strength of the inter-particle force between the nth and the mth particles is described by $l_{nm}(\lambda)$.

In order to close the system of equations (3), we need to consider the nature of the noise term $\delta h(\lambda)$. In general, noise in any physical system arises from a number of independent sources and therefore as a consequence of the central-limit theorem it seems reasonable to assume that the sum of their effects will result in a random Hamiltonian with independent Gaussian distributed elements. Such a Hamiltonian will be drawn from one of the Gaussian ensembles of random matrix theory. Re-

cent measurements of the low frequency flux noise in superconducting flux qubits exhibit a coloured noise spectrum [15]. We therefore assume that the noise term, $\delta h(\lambda)$, evolves in time as a Ornstein-Uhlenbeck type process, which is a simple example of a random process with a coloured spectrum:

$$\dot{\delta h}(\lambda) = -\tau \delta h(\lambda) + \epsilon \eta(\lambda) \tag{4}$$

where τ is a correlation time, ϵ is the noise amplitude, and $\eta(\lambda)$ is a random matrix valued stochastic process where $\langle \eta(\lambda) \rangle = 0$ and $\langle \eta(\lambda)\eta(\lambda') \rangle = \delta(\lambda - \lambda')$.

3 The CNOT gate

As mentioned previously AQC has been shown to be polynomially equivalent to the circuit model of quantum computing.The 'ground state quantum computing' (GSQC) formalism, described in [7], offers the most practical method of constructing a H_0 that encodes an arbitrary M qubit, N step quantum circuit. In the GSQC formalism, each of the M qubits in the circuit is viewed as a single electron that can occupy the states in an array of $2 \times (N+1)$ quantum dots; where the rows in the array represents either the $|0\rangle$ or $|1\rangle$ states of the qubit. The state of the mth qubit during the nth step of the algorithm is given by the probability amplitude of the electron being found on the quantum dots denoted by the indices $(m, n, 0)$ and $(m, n, 1)$. This theoretical construction only incurs a polynomial overheard ($O(N)$) in hardware.

The CNOT gate is one of the simplest entangling quantum gates and when used in conjunction with single qubit rotations it forms a set of universal gates. Therefore, any quantum algorithm can be constructed using a combination of these gates, because of this property we assume that the adiabatic CNOT gate is a representative example of a prototypical adiabatic quantum algorithm. To construct H_0 for a CNOT gate using the GSQC formalism, we envisage an array of 8 quantum dots (as shown in the inset of Fig. 3), which corresponds to a system of 4 physical qubits. Following the procedure described in [7] we can then write;

$$\begin{aligned} H_{CNOT} = &\left(c^\dagger_{010} C^\dagger_{11} - c^\dagger_{000} C^\dagger_{10}\right)(C_{11} c_{010} - C_{10} c_{000}) \\ &+ \left(c^\dagger_{011} C^\dagger_{11} - c^\dagger_{001} C^\dagger_{10} \sigma_x\right)(C_{11} c_{011} - \sigma_x C_{10} c_{001}) \\ &+ C^\dagger_{00} C_{00} C^\dagger_{11} C_{11} + C^\dagger_{01} C_{01} C^\dagger_{10} C_{10}, \end{aligned} \tag{5}$$

where $c^\dagger_{mnj}$ is a fermionic creation operator that creates an electron on the corresponding quantum dot, $C^\dagger_{mn} = \left(c^\dagger_{mn0}, c^\dagger_{mn1}\right)$ and σ_x is a Pauli matrix. The ground state energy of the CNOT Hamiltonian (5) is zero. To specify the initial state of the qubits before the gate operation we add a small energy penalty to (5); e.g. of the form $H_{Init} = \mu \left(c^\dagger_{000} c_{000} + c^\dagger_{100} c_{100}\right)$ for the operation $|00\rangle \rightarrow |00\rangle$.

We numerically solve the equations (3) and (4). For stability reasons we use the multi-step Adams-Moulton method to solve (3). For the sake of generality, the initial conditions for the Pechukas gas, $x_n(\lambda = 1)$, $v_n(\lambda = 1)$ and $l_{nm}(\lambda = 1)$, are calculated using a perturbation theory expansion in terms of Z^{-1} as at $\lambda = 1$, $\mathcal{H}(1) = H_0 + Z H_b + \delta h(1) \equiv Z\left(H_b + Z^{-1} H_0 + Z^{-1} \delta h(1)\right)$. We assume that $\mathcal{H}(1)$ has a non-degenerate, well spaced energy spectrum. Note that the initial conditions contain all the information about the final Hamiltonian H_0. The initial noise term $\delta h(\lambda = 1)$ will be a random matrix drawn from the GOE with amplitude ϵ. Throughout the paper, we take $\mu = -0.1$, $Z^{-1} = 0.1$ and $\tau = 0.1$.

4 Energy spectra

Figure 1(a) shows the energy spectra of the CNOT gate acting on the $|00\rangle$ and $|11\rangle$ computational basis states. In both cases, the results from the eigenvalue dynamics simulations agree with the results of direct diagonalisation of H_0 to four significant figures. In both of the spectra, there is an abundance of level crossings which arise because of the symmetries of $\mathcal{H}(\lambda(t))$.

Degeneracies between the ground and first excited states occur in the $|11\rangle \rightarrow |10\rangle$ operation, which will result in a success probability of zero for this ideal case. This case can be viewed as an example of AQC with an "improper" choice of initial configuration, i.e. where $[H_0, H_b] = 0$. It is

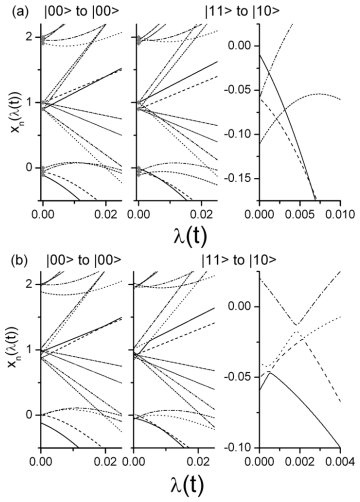

Figure 1: (a) The energy spectra of $|00\rangle \rightarrow |00\rangle$ and $|11\rangle \rightarrow |10\rangle$ operations of the adiabatic CNOT gate in the absence of noise. The solid grey diamonds show the results of direct diagonalisation of the H_0. (b) Examples of the spectra for $|00\rangle \rightarrow |00\rangle$ and $|11\rangle \rightarrow |10\rangle$ operations of the CNOT gate with a GOE random matrix noise term in the Hamiltonian with amplitude $\epsilon = 0.1$. For illustrative purposes, different line styles are used to denote the different energy levels and the third plot in each of the subfigures shows an enlarged view of a region of the $|11\rangle \rightarrow |10\rangle$ spectrum containing a number of crossings.

clear that the addition of any type of perturbation (e.g. noise) will break these symmetries, therefore splitting the degeneracies and resulting in a finite success probability. The results of the addition of noise are shown in plot Fig. 1(b) and it is evident that there are now no degeneracies in either of the spectra. The spectra for the $|01\rangle \rightarrow |01\rangle$ and $|10\rangle \rightarrow |11\rangle$ operations were found to show similar trends to the $|11\rangle \rightarrow |10\rangle$, in that they also exhibited a degeneracy between the ground and first excited states in the absence of noise.

5 The effects of noise on level occupation statistics

To properly characterise the effects of noise on the adiabatic quantum algorithm for the CNOT gate it is necessary to look at its effects on the probability of level occupation and in particular the success probability of the algorithm (i.e. $P(n = 0; \lambda(t) = 0 | n = 0; \lambda(t) = 1)$). During the evolution of an adiabatic quantum computer the main mechanism by which the system can tunnel from one state to another is Landau-Zener-Stückelberg tunneling [8, 9, 10]. This occurs when the separation of two adjacent energy levels is at a local minimum (i.e. at an avoided or level crossing) and the probability of excitation from $|n\rangle$ to $|n+1\rangle$ via this mechanism is given by

$$P_{LZS} = \exp\left(\frac{-\Delta_{min}^2}{|\langle n| ZH_b |n+1\rangle| \left|\dot{\lambda}(t)\right|}\right) \qquad (6)$$

, where Δ_{min} is the minimum separation between x_n and x_{n+1}. We assume that the system undergoes uniform evolution (i.e. $|\dot{\lambda}| = \frac{1}{T}$, where T is the computation time) and that the system can initially be found in the ground state with certainty (i.e. $P(n = 0; \lambda(t) = 1) = 1$). Given this information, it is possible to calculate the level occupations as a function of time by identifying all the avoided or level crossings in the spectrum and applying the LZS equation, (6) to them.

Figure 2 shows the dependence of the average success probability on the computation speed at a range of noise amplitudes for the $|00\rangle \rightarrow |00\rangle$ and $|11\rangle \rightarrow |10\rangle$ operations. In general, the success probability scales polynomially with the speed, i.e. $P \propto T^{-\gamma}$ with $\gamma \approx 1$, before approaching unity asymptotically. The exponent is different to those found in [11] for Hamiltonians drawn from the GUE, however there is no reason to expect a single exponent to hold universally for all choices of H_0. From a computational performance point of view, it is important to note that the scaling exponent is independent of the noise amplitude, i.e. only a prefactor change. This prefactor change could actually be viewed as being beneficial as we can see that the success probability at a given computation speed increases linearly with the noise amplitude (also shown in Fig. 3). This occurs as Δ_{min} increases proportionally with ϵ and hence this effect is more pronounced for the $|11\rangle \rightarrow |10\rangle$ operation where the existence of the ground state gap is purely due to noise-induced level splitting. As the $|01\rangle \rightarrow |01\rangle$ and $|10\rangle \rightarrow |11\rangle$ operations also have

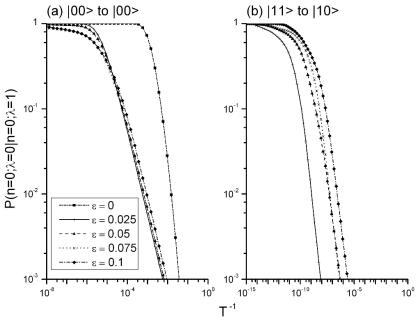

Figure 2: Plot of the success probability, averaged over a number of noise realisations, against computation speed for the $|00\rangle \rightarrow |00\rangle$ and $|11\rangle \rightarrow |10\rangle$ operations of the CNOT gate at various noise amplitudes. Fits to the polynomial regions, i.e. where $P \propto T^{-\gamma}$, of the curves yield exponents of; $\gamma = 4/3$ for the $\epsilon = 0$ case of the $|00\rangle \rightarrow |00\rangle$ operation, and $\gamma \approx 1$ for all other cases.

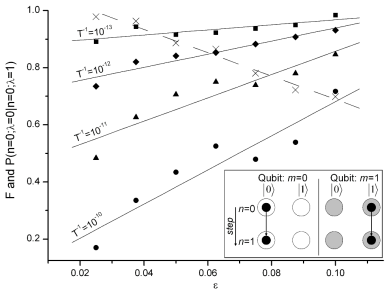

Figure 3: Plot showing the trade-off between the fidelity of the final state (dashed line and crosses) and the average success probability (solid lines and shapes) as functions of noise amplitude for the $|01\rangle \rightarrow |01\rangle$ operation. The inset schematic shows the GSQC representation of the $|01\rangle \rightarrow |01\rangle$ operation of the CNOT gate.

degenerate ground state gaps, their success probability curves behave in a very similar way to the plot shown in Fig. 2 for the $|11\rangle \rightarrow |10\rangle$ operation.

The increase in success probability with the noise amplitude (at a specific speed) may not be wholly beneficial though, as it will come at the cost of the fidelity of the final state (i.e. $F = |\langle 0_{ideal}(\lambda = 0)|0_{noise}(\lambda = 0)\rangle|$, where $0 \leq F \leq 1$). This is because the noise fluctuations will drive the state away from the ideal (i.e. in the absence of noise) path of evolution. The dependence of the fidelity on noise amplitude is shown in Fig. 3. The fidelity of the final state is an important quantity which needs to be maximised to ensure that readout will yield the desired solution. For the three operations where the existence of the ground state gap is due to noise-induced level splitting, there will be a noise amplitude that offers the optimal compromise between the success probability and the fidelity at a given speed and this is shown by the intersections of the curves in Fig. 3. These results suggest that the conventional stipulation that $[H_0, H_b] \neq 0$ is unnecessary in practical realisations, as when the effects of a generic noise source are taken in to consideration, any hidden symmetries in $\mathcal{H}(\lambda(t))$ will be broken naturally.

6 Effects of an artificial noise source

So far we have viewed $\delta h(\lambda)$ as the natural effect of a number of noise sources that are coupled to the system. If we now envisage a physical system with a negligible level of intrinsic noise. In this situation, it may be beneficial to add an artificial random perturbation to the system. This would be in order to break any degeneracies in the spectrum and offer an alternate, and possibly more efficient, path between the initial and final Hamiltonians. A perturbation term with a time-dependent amplitude, which is large enough to widen the energy gaps at avoided crossings throughout the majority of the computation process but then tends to 0 as $\lambda(t) \rightarrow 0$, would be preferable. For example we could take

$$\epsilon(\lambda) = \epsilon_0 \tanh(\alpha\lambda) \tag{7}$$

, where α is a constant determining the rate of decay at $\lambda(t) \gtrsim 0$. This would ensure that $\delta h(\lambda)_{ij}$ will not be significantly larger than H_{0ij} at $\lambda(t) \gtrsim 0$, where the bias term is small and the levels are densely packed. The results of simulations performed using a time-dependent amplitude of the form of (7) are shown in Fig. 4. On average, a given success probability can be achieved at a much faster computation speed, with an improvement of over 10^2 in some cases. In this idealised situation it is also clear to see that the fidelity of the final

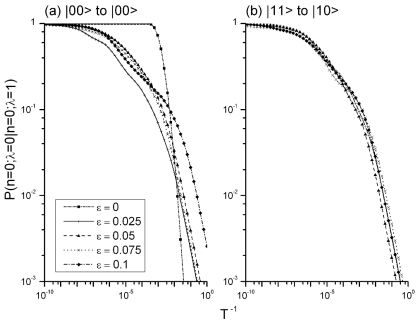

Figure 4: Plot of the success probability, averaged over a number of noise realisations, against computation speed for the $|00\rangle \rightarrow |00\rangle$ and $|11\rangle \rightarrow |10\rangle$ operations of the CNOT gate with an artificial noise source with a time-dependent amplitude and $\alpha = 10$.

solution state would be unaffected (i.e. $F = 1$) by this artifical noise signal as $\epsilon(\lambda = 0) = 0$.

7 Conclusions

We generalise the Pechukas-Yukawa equations to the stochastic case by including an additional noise term in the Hamiltonian. This was used in conjunction with a simple, yet generic, noise model, based on random matrices and a coloured stochastic process, to investigate the effects of noise on the adiabatic algorithm for the CNOT gate. We found that, in general, the success probability of the algorithm scaled polynomially as a function of computation speed and this scaling was independent of the amplitude of the noise. We demonstrate that when the effects of noise are taken in to account, the criteria used to select an initial configuration for the system may be relaxed and it is not necessary to avoid symmetries in the Hamiltonian. This is because, the presence of noise will break any degeneracies in the energy spectrum, crucially those that exist between the ground and first excited states. In these situations, the success probability at a given computation speed was found to increase linearly with noise amplitude. It was noted that this increase comes at the expense of the fidelity of the final state, but an optimal compromise between the two factors exists. The effects of an artificial noise source with a time-dependent noise amplitude were also investigated. This scheme was found to offer significantly higher success probabilities at relatively fast computation speeds and could be engineered in such a way that the fidelity of the solution state is unaffected.

References

[1] E. Farhi, J. Goldstone, S. Gutmann, and M. Sipser, arXiv:quant-ph/0001106 (2000)

[2] A. Childs, E. Farhi, and J. Preskill, Phys. Rev. A **65**, 012322 (2001)

[3] S. Ashhab, J. Johansson, and F. Nori, Phys. Rev. A **74**, 052330 (2006)

[4] J. Roland and N. J. Cerf, Phys. Rev. A **71**, 032330 (2005)

[5] M. H. S. Amin, P. J. Love, and C. J. S. Truncik, Phys. Rev. Lett. **100**, 060503 (2008)

[6] D. Aharonov, W. van Dam, J. Kempe, Z. Landau, S. Lloyd, and O. Regev, arXiv:quant-ph/0405098 (2004)

[7] A. Mizel, D. Lidar, and M. Mitchell, Phys. Rev. Lett. **99**, 070502 (2006)

[8] L. Landau, Phys. Z. Sowjetunion 2 **46** (1932)

[9] C. Zener, Proc. R. Soc. London **Ser. A 137** (1932)

[10] E. Stueckelberg, Helv. Phys. Acta. 5 **369** (1932)

[11] A. M. Zagoskin, S. Savel'ev, and F. Nori, Phys. Rev. Lett. **98**, 120503 (2007)

[12] P. Pechukas, Phys. Rev. Lett. **51**, 943 (1983)

[13] T. Yukawa, Phys. Rev. Lett. **54**, 1883 (1985)

[14] H.-J. Stöckman, *Quantum Chaos: an introduction* (Cambridge University Press, 1999) pp. 184–186

[15] T. Lanting, A. J. Berkley, B. Bumble, P. Bunyk, A. Fung, J. Johansson, A. Kaul, A. Kleinsasser, E. Ladizinsky, F. Maibaum, R. Harris, M. W. Johnson, E. Tolkacheva, and M. H. S. Amin, Phys. Rev. B **79**, 060509 (2009)

Appendix C

The relationship between minimum gap and success probability in adiabatic quantum computing

The relationship between minimum gap and success probability in adiabatic quantum computing

M. Cullimore M.J. Everitt M.A. Ormerod J.H. Samson
S. Savel'ev R.D. Wilson A.M. Zagoskin
Department of Physics, Loughborough University,
Loughborough, Leicestershire LE11 3TU, UK

Abstract

We explore the relationship between two figures of merit for an adiabatic quantum computation process: the success probability and the minimum gap between the ground and first excited states. We study a generic adiabatic algorithm and show that a rich structure exists in the distribution of these two important variables. In the case of two qubits, the success probability is to a good approximation a function of the minimum gap, the stage in the evolution at which the minimum occurs and the computation time. This structure persists in examples of larger systems and appears to be closely linked to the choice of initial and problem Hamiltonians.

1 Introduction

The promise of a qualitative advantage of quantum computers over classical ones in solving certain classes of problems has led to a massive effort in theoretical and experimental investigation of controlled, quantum-coherent systems. The standard model of quantum computing is analogous to classical computing in that it involves the precise manipulation of individual qubits in a register to apply logic gate operations. However, the requirement of precise time-dependent control of individual qubits has been found to be hard to achieve experimentally while still maintaining the quantum coherence of the system. A number of alternative approaches have been proposed, of which *adiabatic quantum computing* (AQC) is a promising example. It involves the evolution of a quantum system from a simple Hamiltonian with an easily-prepared ground state to a Hamiltonian that encodes the problem to be solved. If the system is initially prepared in the ground state and the time evolution occurs slowly enough to satisfy the adiabatic theorem, the final ground state that satisfies the problem at hand can be read out with a high probability [1].

The AQC process requires a Hamiltonian that interpolates from a simple initial configuration, H_i, to one that encodes the problem under consideration, H_f. A Hamiltonian for linear interpolation can be written

$$H(s) = (1-s)H_i + sH_f, \tag{1}$$

where $s \in [0,1]$ is the reduced time $s = t/T$, T being the computation time. The instantaneous eigenvalues and eigenstates of the Hamiltonian of an n-qubit system are given by

$$H(s)\,|\ell;s\rangle = E_\ell(s)\,|\ell;s\rangle\,,\ \text{with}\ E_0(s) \leqslant E_1(s) \leqslant \cdots \leqslant E_{2^n-1}(s). \tag{2}$$

The instantaneous state of the system is given by $|\psi(s)\rangle$, the solution of Schrödinger's equation, which in the reduced time reads

$$\frac{\mathrm{d}}{\mathrm{d}s}\,|\psi(s)\rangle = -iTH(s)\,|\psi(s)\rangle\,. \tag{3}$$

The system is initially in the ground state of H_i: $|\psi(0)\rangle = |0;s=0\rangle$.

At the end of the evolution we require a measure of how closely the state vector, $|\psi(1)\rangle$, corresponds to the desired result, $|0;s=1\rangle$. This is provided by the *success probability*

$$P = \big|\langle 0;s=1\,|\psi(1)\rangle\big|^2. \tag{4}$$

It was shown in [1] that for P to be arbitrarily close to 1, the following condition must be satisfied:

$$T \gg \frac{\mathcal{E}}{\Delta_{\min}^2} \tag{5}$$

where

$$\mathcal{E} = \max_{0\leqslant s\leqslant 1}\left|\left\langle 1;s\left|\frac{\mathrm{d}H}{\mathrm{d}s}\right|0;s\right\rangle\right| \tag{6}$$

is of the order of a typical eigenvalue of H and

$$\Delta_{\min} = \min_{0\leqslant s\leqslant 1}\big(E_1(s) - E_0(s)\big) \tag{7}$$

is the *minimum gap*, which occurs at reduced time(s) s^* : $E_1(s^*) - E_0(s^*) = \Delta_{\min}$. If $\mathcal{E}$ is considered constant, by (5) $\Delta_{\min}$ is the variable which determines the T that is required. It is clear that P will also be directly related to T and therefore $\Delta_{\min}$. These two variables, P and $\Delta_{\min}$, are used interchangeably throughout the literature to quantify the performance of a given computation (e.g. contrast [2] with [3]), and are assumed to increase monotonically with each other. The question of how either of these variables varies with system size, n, is an important one that is often addressed. However, the exact nature of the relationship between these two important figures of merit has not been adequately explored.

We explore the relationship between P and $\Delta_{\min}$ by looking at the statistical distributions of these two variables over a large set of generic problem Hamiltonians (H_f). We start by considering a simple two-qubit system and show that a rich structure arises in the scatter plots of success probability against $\Delta_{\min}$. We then go on to look at the scatter plots in three-, four- and five-qubit systems and find that, although some of the finer details of the structure are washed out, some remain. We propose that the structure in the distributions arises through our choice of Hamiltonians.

2 A generic adiabatic algorithm

We wish to look at the distribution of the success probability and $\Delta_{\min}$ over a large set of problem Hamiltonians. We use a simple, yet generic, model that is scalable and can be readily solved numerically. For H_i, we use a Hamiltonian that is easy to construct and whose ground state can be readily found:

$$H_i = -\sum_{i=1}^{n} \sigma_x^{(i)} = -\sum_{i=1}^{n} \mathbb{I} \otimes \cdots \otimes \sigma_x \otimes \cdots \otimes \mathbb{I}, \tag{8}$$

where σ_a, with $a = x$, y or z, denote the usual Pauli matrices, n is the number of qubits in the system and the index i denotes which qubit the operator is applied to. This H_i is simply a transverse field acting on all the qubits and its ground state is an equal superposition of all 2^n computational basis states.

For H_f, we use a Hamiltonian where all possible couplings between the n qubits are realised in the z-direction, with random strengths:

$$H_f = \sum_{x=0}^{2^n-1} J_x \bigotimes_{i=1}^{n} (\sigma_z)^{x_i} = \sum_{y=0}^{2^n-1} f_y \left|y\right\rangle\left\langle y\right| \tag{9}$$

where x_i is the ith digit in the binary representation of x and J_x are the coupling coefficients. These will be selected from a given random distribution. H_f is diagonal in the computational basis so that the binary-ordered set of states $|y\rangle$ is a permutation of the energy-ordered set of states $|l; s = 1\rangle$ defined in eq 2. A Hamiltonian of this type can easily be used to encode any finite computational optimisation problem (minimisation of a function $f : \{0,1\}^n \to \mathbb{R}$) by choice of the $\{J_x\}$, including NP-hard problems such as the travelling salesman problem (TSP). It is important to note that, at present, only one- and two-qubit interactions are experimentally feasible, although the TSP can be implemented with this restriction [4].

For each sample in the scatter plots, we solve the Schrödinger equation numerically over the parameterised time, s, for a given computation time, T, using the Dormand-Prince method [5]. This is an adaptive step-size algorithm; solutions accurate to fourth- and fifth-order in Δs are used to estimate the local error in the former. If it is less than the desired tolerance, then the fifth-order solution is used for the integration. Otherwise the step-size Δs is decreased.

3 Two-qubit simulations

Fig. 1 is a scatter plot of success probability against minimum gap for a large set of problem instances, with the coupling coefficients drawn from the uniform distribution $\mathcal{U}(-3, 3)$. The computation time is $T = 5$. Observe the sharp upper and lower edges. The lower bound of the success probability is always $1/4$ for infinitesimally small $\Delta_{\min}$. This arises when $J_1 = J_2 = J_3 = 0$, which means there is four-fold degeneracy at $s = 1$ and the system remains in its original ground state.

It is important to verify that this structure is independent of our choice of random distribution of coupling coefficients and that is also not an artifact of the pseudo-random number generators used. Fig. 2 also shows scatter plots of

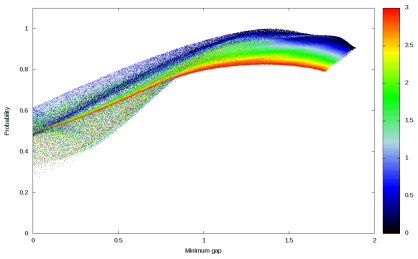

Figure 1: Success probability against minimum gap for a two-qubit system at a computation time of $T = 5$. The J_i have been chosen from the uniform distribution $\mathcal{U}(-3, 3)$ for the $500,000$ random problem instances. The data points are coloured by $|J_3|$.

success probability and minimum gap, but in this case the coupling coefficients are drawn from a Gaussian distribution, $\mathcal{N}(0, 1^2)$ (mean $\mu = 0$, standard deviation $\sigma = 1$). The trends and structure in the distributions are similar to those shown in Fig. 1. However, there are some subtle differences in sharpness between the Gaussian and uniform cases. For a large minimum gap, the lowest probability occurs for large $|J_3|$, so we see a sharp cutoff in the uniform case and a rougher, more sparsely populated edge in the Gaussian case. In general though, this shows that the results are independent of our choice of coupling coefficients and, as a different psuedo-random number generator routine was used, we can say that the results are not a numerical artifact.

Four computation times are shown: $T = 5$, 10, 20 and 40. As this increases, the distribution shifts and tends towards a success probability of 1, as expected from the adiabatic theorem.

The two interesting features of these scatter plots are the well-defined sharp edges and the densely-populated bands. It is clear that the bands correspond to groups of Hamiltonians with similar $|J_3|$. The bands where $J_3 = 0$ can be seen as two separable one-qubit evolutions for J_1 and J_2, so the total success probability is simply the product of the one-qubit success probabilities. Another interesting point to note is that the bands of similar H_f gradually reverse in order in the distribution as the computation time T is changed.

We have supplemented the uniform random data with sets of J_i chosen on a rectangular grid with the same cut-offs. These have the advantage that all problem Hamiltonians with a given value of J_3 can be plotted in the (J_1, J_2)-plane and coloured by their minimum gap or success probability; see Fig. 3. These two plots can be considered first- and second-order stability diagrams respectively.

The first part of Fig. 3 (minimum gap) can be explained as follows: dark

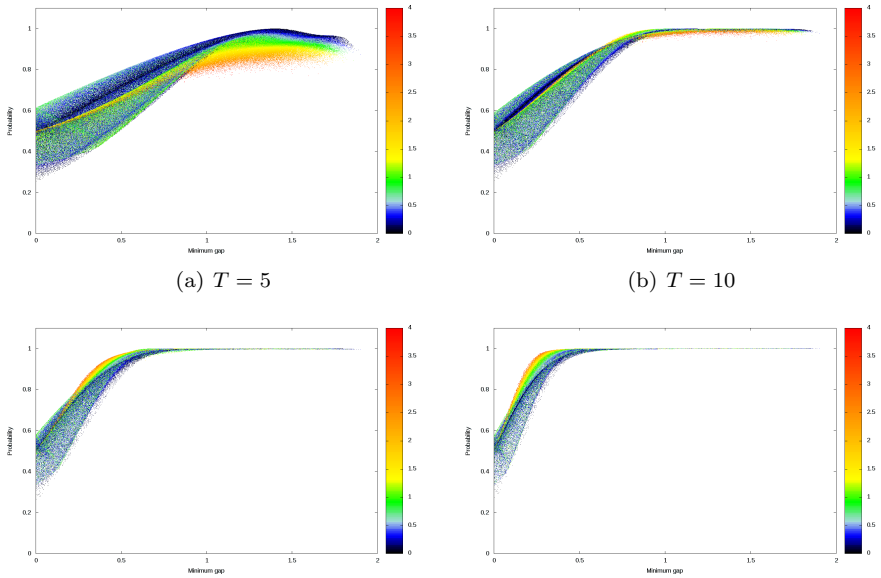

(a) $T = 5$ (b) $T = 10$

(c) $T = 20$ (d) $T = 40$

Figure 2: Success probability against minimum gap for a two-qubit system at computation times of $T = 5$, 10, 20 and 40. The J_i have been chosen from the Gaussian distribution $\mathcal{N}(0, 1^2)$ for the 500,000 random problem instances. The data points are coloured by $|J_3|$.

lines correspond to problem Hamiltonians with a degenerate ground state.

$$\text{triply-degenerate} \begin{cases} J_1 = J_2 = J_3 \\ J_1 = J_2 = -J_3 \end{cases}$$

$$\text{doubly-degenerate} \begin{cases} J_1 = J_2 \text{ and } J_1, J_2 \in (-J_3, J_3) \\ J_1 = J_3 \text{ and } J_2 > J_3 \\ J_2 = J_3 \text{ and } J_1 > J_3 \\ J_1 = -J_3 \text{ and } J_2 < -J_3 \\ J_2 = -J_3 \text{ and } J_1 < -J_3 \end{cases}$$

These lines separate H_f with different ground states: those in the top-right have $|11\rangle$; working clockwise, the others have $|10\rangle$, $|00\rangle$ and $|01\rangle$.

The second part of Fig. 3 (success probability) is harder to interpret. As expected, there is a broad correspondence between lines of low P and those of low $\Delta_{\min}$. The difference, due to second-order corrections, is not presently understood. Nor is the interesting observation that H_f with high P are gathered around the points of triple degeneracy.

These plots suggest a projection of a surface onto the $(\Delta_{\min}, P)$ plane; we seek to find a suitable parameterisation of the set of Hamiltonians to collapse it onto a low-dimensional surface. We find that a plot of P against the minimum gap $\Delta_{\min}$ and the position s^* of the gap indeed shows that all points lie close to a curved surface (which rises with increasing T). This is understandable, since those two parameters largely determine the shape of the lowest two energy levels.

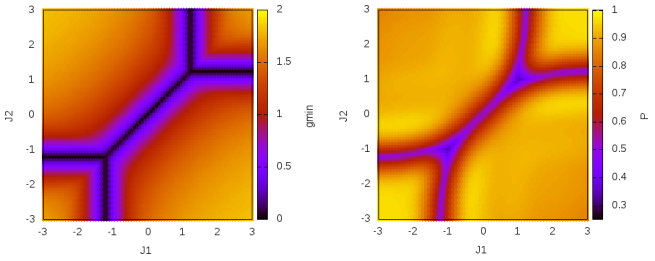

Figure 3: Minimum gap (left) and success probability (right) as a function of (J_1, J_2) at fixed $J_3 \approx 1.22$, $T = 5$. Each coloured point in the plane is a problem Hamiltonian. Observe that points with high success probability (yellow) are nested around the points of triple degeneracy.

Figure 4 shows a projection of this surface onto the $(\Delta_{\min}, s^*)$ plane. Visual inspection shows that the colour is to a good approximation a function only of position in the plane. Note that the position of the points depends only on the Hamiltonian parameters, while the probability depends also on the computation time.

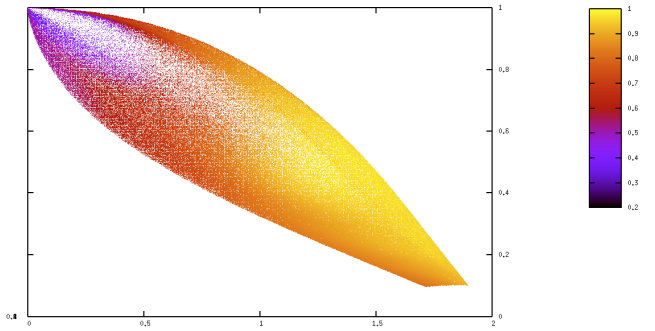

Figure 4: Scatter plot of position s^* of minimum gap against minimum gap $\Delta_{\min}$. The J_i have been chosen from the uniform distribution $\mathcal{U}(-3, 3)$ for the $50,000$ random problem instances. Points are coloured by the success probability P at $T = 5$.

4 Larger systems

We have shown that the relationship between the success probability and $\Delta_{\min}$ is not just a case of trivial proportionality for simple two-qubit systems. However, it is important to determine whether the interesting structure in this relationship remains in larger systems. To determine whether these densely-populated bands represent groups of problem instances that have followed similar evolution paths for the state vector (e.g. the system remaining mostly in the ground state, then being excited at a single avoided crossing), we calculated the average overlap

with the ground state:

$$\delta = \int_0^1 ds \left| \langle 0; s \, | \psi(s) \rangle \right|^2. \tag{10}$$

The points in Fig. 5 are coloured with respect to this average overlap value, δ, and we can see a smooth graduation across the figures, with the average overlap with the ground state increasing with the success probability. The exception to the smooth graduation of δ is the densely populated band where $\delta \approx 1$. This band must consist of cases with a degenerate or near-degenerate ground state at $s = 1$, as it includes cases which remain close to the instantaneous ground state throughout the majority of the evolution but have a low success probability. These results also lends credence to the idea that the structure is closely linked to the choice of Hamiltonians.

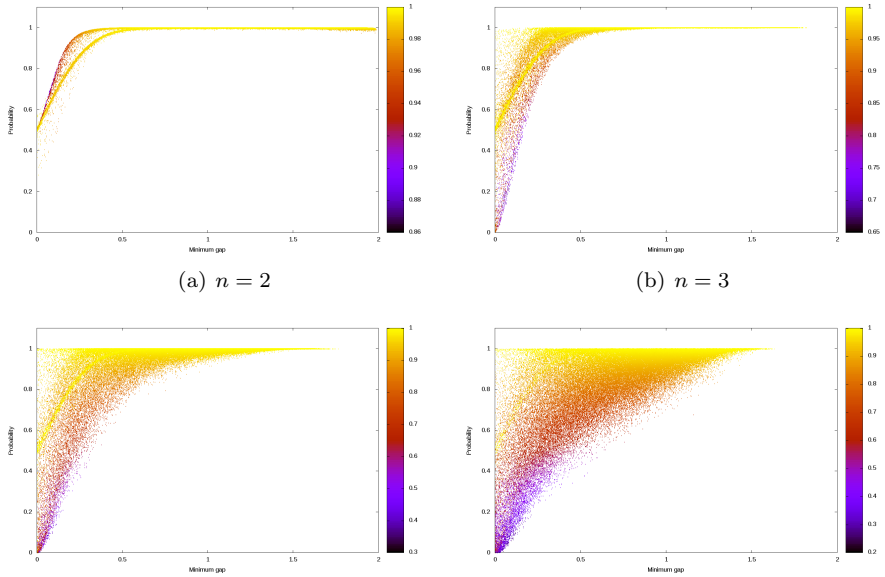

(a) $n = 2$ (b) $n = 3$

(c) $n = 4$ (d) $n = 5$

Figure 5: Distributions of success probability against $\Delta_{\min}$ for two-, three-, four- and five-qubit systems over a set of 100,000 random problem instances, with $T = 40$. The colouring of the points denotes δ, average overlap of the state vector with the instantaneous ground state.

We note that these distributions are reminiscent of the 2D projections of the higher-dimensional equilibrium surfaces seen in catastrophe theory [6]. In this case success probability, $\Delta_{\min}$ and δ are all internal variables of the system and not independent control parameters, so we are looking at a different situation to those usually studied in catastrophe theory. Identifying the nature of this surface and the dimensions of the phase space that it exists in is an important task, as it could have a major impact on adiabatic algorithm design. At this point we can conjecture that the constraint originates from an adiabatic invariant of the Hamiltonian. We find it strange that, to the best of our knowledge, there has been no research on adiabatic invariants of adiabatic quantum computers.A systematic investigation of adiabatic invariants of quantum computers espe-

cially adiabatic and approximately adiabatic computers could yield important information about their behaviour and make a major impact on the adiabatic algorithm design.

5 Conclusion

We have shown that the relationship between the success probability and the minimum ground state gap may not be as straightforward as is often assumed. There is a rich structure of distinct sharp edges and densely-populated bands in the distribution, particularly in smaller systems. A partial explanation has been proposed, whereby this is the projection of a higher-dimensional surface; identification of the parameters governing this surface will guide understanding of the set of problems amenable to adiabatic quantum computing. We do not propose a definitive explanation of the origin of this rich structure: this remains an open question. However, we do suggest that there is some evidence that some of this structure could arise by our choice of Hamiltonians. We speculate that a systematic investigation of adiabatic invariants of quantum computers — especially adiabatic and approximately adiabatic computers — could yield important information about their behaviour and have a major impact on adiabatic algorithm design.

References

[1] E. Farhi, J. Goldstone, S. Gutmann, and M. Sipser. Quantum computation by adiabatic evolution. *quant-ph/0001106*, 2000.

[2] A. M. Childs, E. Farhi, and J. Preskill. Robustness of adiabatic quantum computation. *Phys. Rev. A*, 65:012322, 2001.

[3] E. Farhi, J. Goldstone, S. Gutmann, J. Lapan, A. Lundgren, and D. Preda. A Quantum Adiabatic Evolution Algorithm Applied to Random Instances of an NP-Complete Problem. *Science*, 292(5516):472–475, 2001.

[4] Arnab Das and Bikas K. Chakrabarti Quantum annealing and analog quantum computation, *Rev. Mod. Phys.* 80:1061-1081, 2008.

[5] J. R. Dormand and P. J. Prince. A family of embedded Runge-Kutta formulae. *Journal of Computational and Applied Mathematics*, 6(1):19–26, 1980.

[6] P. T. Saunders. *An introduction to catastrophe theory.* Cambridge University Press, 1980.

Bibliography

[1] Richard P. Feynman. Simulating physics with computers. *International Journal of Theoretical Physics*, VoL 21, Nos. 6/7, 1982.

[2] Peter W. Shor. Polynomial-time algorithms for prime factorization and discrete logarithms on a quantum computer. *SIAM J.Sci.Statist.Comput.*, 26:1484, 1997.

[3] Lov K. Grover. A fast quantum mechanical algorithm for database search. *Proceedings, 28th Annual ACM Symposium on the Theory of Computing (STOC)*, pages 212–219, 1996.

[4] David Deutsch. Quantum theory, the church-turing principle and the universal quantum computer. *Proceedings of the Royal Society of London A*, 400:97–117, 1985.

[5] D Deutsch and R Jozsa. Rapid solution of problems by quantum computation. *Proc Roy Soc Lond A*, 439:553–558, October 1992.

[6] Edward Farhi, Jeffrey Goldstone, Sam Gutmann, and Michael Sipser. Quantum computation by adiabatic evolution. *quant-ph/0001106*, 2000.

[7] A.M. Childs, E. Farhi, and J. Preskill. Robustness of adiabatic quantum computation. *Phys. Rev. A*, 65:012322, 2001.

[8] S. Ashhab, JR Johansson, and F. Nori. Decoherence in a scalable adiabatic quantum computer. *Phys. Rev. A*, 74:052330, 2006.

[9] Jeremie Roland and Nicolas J. Cerf. Noise resistance of adiabatic quantum computation using random matrix theory. *Phys. Rev. A*, 71:032330, 2005.

[10] D. Aharonov, W. van Dam, J. Kempe, Z. Landau, S. Lloyd, and O. Regev. Adiabatic Quantum Computation is Equivalent to Standard Quantum Computation. *quant-ph/0405098*, 2004.

[11] A. Mizel, D.A. Lidar, and M. Mitchell. Simple proof of equivalence between adiabatic quantum computation and the circuit model. *Phys. Rev. Lett.*, 99:070502, 2007.

[12] M. H. S. Amin, Peter J. Love, and C. J. S. Truncik. Thermally assisted adiabatic quantum computation. *Phys. Rev. Lett.*, 100(6):060503, 2008.

[13] A. M. Turing. On computable numbers, with an application to the entscheidungsproblem. *Proc. London Math. Soc.*, 2(42):230–265, 1936.

[14] David P. DiVincenzo. The physical implementation of quantum computation. *Arxiv preprint quant-ph/0002077*, 2000.

[15] Michael A. Nielsen and Isaac L. Chuang. *Quantum Computation and Quantum Information*. Cambridge University Press, 2000.

[16] B.H. Bransden and C.J. Joachain. *Introduction To Quantum Mechanics*. Longman Scientific & Technical, 1989.

[17] D.R. Mitchell, C. Adami, W. Lue, and C.P. Williams. Random matrix model of adiabatic quantum computing. *Physical Review A*, 71(5):52324, 2005.

[18] M. Žnidarič. Eigenlevel statistics of the quantum adiabatic algorithm. *Physical review. A*, 72(5):52336–52336, 2005.

[19] W. Van Dam, M. Mosca, and U. Vazirani. How powerful is adiabatic quantum computation? *Foundations of Computer Science, Annual IEEE Symposium on*, 0:279, 2001.

[20] E. Farhi, J. Goldstone, and S. Gutmann. Quantum Adiabatic Evolution Algorithms with Different Paths. *ArXiv Quantum Physics e-prints*, aug 2002.

[21] B. Altshuler, H. Krovi, and J. Roland. Adiabatic quantum optimization fails for random instances of NP-complete problems. *ArXiv e-prints*, August 2009.

[22] Neil G. Dickson and M. H. S. Amin. Does adiabatic quantum optimization fail for np-complete problems? *Phys. Rev. Lett.*, 106(5):050502, Feb 2011.

[23] X. Peng, Z. Liao, N. Xu, G. Qin, X. Zhou, D. Suter, and J. Du. Quantum Adiabatic Algorithm for Factorization and Its Experimental Implementation. *Physical Review Letters*, 101(22):220405–+, November 2008.

[24] Jérémie Roland and Nicolas J. Cerf. Quantum search by local adiabatic evolution. *Phys. Rev. A*, 65(4):042308, Mar 2002.

[25] Jérémie Roland and Nicolas J. Cerf. Adiabatic quantum search algorithm for structured problems. *Phys. Rev. A*, 68(6):062312, Dec 2003.

[26] Matthias Steffen, Wim van Dam, Tad Hogg, Greg Breyta, and Isaac Chuang. Experimental implementation of an adiabatic quantum optimization algorithm. *Phys. Rev. Lett.*, 90(6):067903, Feb 2003.

[27] Warren S. Warren. The usefulness of nmr quantum computing. *Science*, 277(5332):1688–1690, 1997.

[28] I. Chiorescu, Y. Nakamura, C. J. P. M. Harmans, and J. E. Mooij. Coherent quantum dynamics of a superconducting flux qubit. *Science*, 299(5614):1869–1871, 2003.

[29] E. Il'ichev, A. Yu Smirnov, M. Grajcar, A. Izmalkov, D. Born, N. Oukhanski, Th Wagner, W. Krech, H. G. Meyer, and A. M. Zagoskin. Radio-frequency method for investigation of quantum properties of superconducting structures. *FIZIKA NIZKIKH TEMPERATUR*, 30:823, 2004.

[30] V. T. Petrashov, K. G. Chua, K. M. Marshall, R. Sh. Shaikhaidarov, and J. T. Nicholls. Andreev probe of persistent current states in superconducting quantum circuits. *Phys. Rev. Lett.*, 95(14):147001, Sep 2005.

[31] S. H. W. van der Ploeg, A. Izmalkov, Alec Maassen van den Brink, U. Hübner, M. Grajcar, E. Il'ichev, H.-G. Meyer, and A. M. Zagoskin. Controllable coupling of superconducting flux qubits. *Phys. Rev. Lett.*, 98(5):057004, Feb 2007.

[32] J. E. Mooij, T. P. Orlando, L. Levitov, Lin Tian, Caspar H. van der Wal, and Seth Lloyd. Josephson persistent-current qubit. *Science*, 285(5430):1036–1039, 1999.

[33] S.H.W. van der Ploeg, A. Izmalkov, M. Grajcar, U. Hubner, S. Linzen, S. Uchaikin, T. Wagner, A.Yu. Smirnov, A.M. van den Brink, M.H.S. Amin, A.M. Zagoskin, E. Il'ichev, and H.-G. Meyer. Adiabatic quantum computation with flux qubits, first experimental results. *Applied Superconductivity, IEEE Transactions on*, 17(2):113 –119, june 2007.

[34] T. Lanting, A. J. Berkley, B. Bumble, P. Bunyk, A. Fung, J. Johansson, A. Kaul, A. Kleinsasser, E. Ladizinsky, F. Maibaum, R. Harris, M. W. Johnson, E. Tolkacheva, and M. H. S. Amin. Geometrical dependence of low frequency noise in superconducting flux qubits. *Phys. Rev. B*, 79:060509, 2009.

[35] R. Harris, J. Johansson, A. J. Berkley, M. W. Johnson, T. Lanting, Siyuan Han, P. Bunyk, E. Ladizinsky, T. Oh, I. Perminov, E. Tolkacheva, S. Uchaikin, E. M. Chapple, C. Enderud, C. Rich, M. Thom, J. Wang, B. Wilson, and G. Rose. Experimental demonstration of a robust and scalable flux qubit. *Phys. Rev. B*, 81(13):134510, Apr 2010.

[36] S.; Yan F.; Yoshihara F.; Harrabi K.; Fitch G.; Cory D. G.; Nakamura Y.; Tsai J.-S.; Oliver W.D. Bylander, J.; Gustavsson. Noise spectroscopy through dynamical decoupling with a superconducting flux qubit. *Nature Physics*, 7:565570, 2011.

[37] Amin M.H.S. Gildert S. Lanting T. Hamze F. Dickson N. Harris R. Berkley A.J. Johansson J. Bunyk-P. Chapple E.M. Enderud C. Hilton J.P. Karimi K. Ladizinsky E. Ladizinsky N. Oh T. Perminov I. Rich C. Thom M.C. Tolkacheva E. Truncik C.J.S. Uchaikin S. Wang J. Wilson B. Rose G. Johnson, M.W. Quantum annealing with manufactured spins. *Nature*, 473(7346):194–198, 2011. cited By (since 1996) 1.

[38] P. Pechukas. Distribution of energy eigenvalues in the irregular spectrum. *Phys. Rev. Lett.*, 51:943, 1983.

[39] T. Yukawa. New approach to the statistical properties of energy levels. *Phys. Rev. Lett.*, 54:1883, 1985.

[40] A. M. Zagoskin, S. Savel'ev, and Franco Nori. Modeling an adiabatic quantum computer via an exact map to a gas of particles. *Phys. Rev. Lett.*, 98(12):120503, 2007.

[41] Giuseppe E. Santoro, Roman Martoňak, Erio Tosatti, and Roberto Car. Theory of Quantum Annealing of an Ising Spin Glass. *Science*, 295(5564):2427–2430, 2002.

[42] L.D. Landau. *Phys. Z. Sowjetunion 2*, 46, 1932.

[43] C. Zener. *Proc. R. Soc. London*, Ser. A 137(696):696–702, 1932.

[44] E.C.G. Stueckelberg. *Helv. Phys. Acta. 5*, 369:369–422, 1932.

[45] M.L. Mehta. *Random matrices*. Academic Press, 2004.

[46] Hans-Jürgen Stöckman. *Quantum Chaos: an introduction*. Cambridge University Press, 1999.

[47] G. E. Uhlenbeck and L. S. Ornstein. On the theory of the brownian motion. *Phys. Rev.*, 36(5):823–841, Sep 1930.

[48] C.F. Gerald and P.O. Wheatley. *Applied Numerical Analaysis (fifth edition).* Addison-Wesley, 1994.

[49] J. F. Shriner and G. E. Mitchell. Small sample size effects in statistical analyses of eigenvalue distributions. *Zeitschrift fr Physik A Hadrons and Nuclei*, 342:53–60, 1992. 10.1007/BF01294488.

[50] M Cullimore, M. Everitt, M. Ormerod, J. Samson, S Savel'ev, R. Wilson, and A. Zagoskin. The relationship between minimum gap and success probability in adiabatic quantum computing. *ArXiv e-prints*, 1107.4034, July 2011.

[51] A.M. Zagoskin. *Quantum Engineering: Theory and Design of Quantum Coherent Structures.* Cambridge University Press, 2011.

[52] R. D. Wilson, A. M. Zagoskin, and S. Savel'ev. Noise-enhanced performance of adiabatic quantum computing by lifting degeneracies. *Phys. Rev. A*, 82(5):052328, Nov 2010.

[53] Yu. L. Klimontovich. *Statistical Physics.* Harwood, 1986.

[54] B.R. Young W.Y. Svrcek, D.P. Mahoney. *A real-time approach to process control.* Wiley, 2000.

[55] E.M. Lifshitz L.D. Landau. *Mechanics.* Butterworth-Heinemann, 1976.